



**زانكۆی پۆلیتیه كنیکی هه ولیر**  
**ERBIL POLYTECHNIC UNIVERSITY**

**THERMAL PERFORMANCE ANALYSIS OF A FLAT PLATE  
SOLAR COLLECTOR SYSTEM FOR HEATING  
GREENHOUSE USING NANO-FLUID**

A Thesis

Submitted to the Council of the Erbil Technical Engineering College at Erbil  
Polytechnic University in Partial Fulfillment of the Requirements for the Degree  
of Master of Science in Mechanical and Energy Engineering

By

**Zhyan Faeaq Hassan**

B.Sc. in Refrigeration and Air-Conditioning Engineering

Supervised by

**Dr. Banipal Nanno Yaqob**

Erbil-Kurdistan

September 2022

## DECLARATION

I declare that the Master Thesis entitled: "*THERMAL PERFORMANCE ANALYSIS OF A FLAT PLATE SOLAR COLLECTOR SYSTEM FOR HEATING GREENHOUSE USING NANO-FLUID*" is my own original work, and hereby I certify that unless stated, all work contained within this thesis is my own independent research and has not been submitted for the award of any other degree at any institution, except where due acknowledgement is made in the text.

Signature:



Student Name: Zhyan Faeaq Hassan

Date: 27/10/2022

## LINGUISTIC REVIEW

I confirm that I have reviewed the thesis titled “*THERMAL PERFORMANCE ANALYSIS OF A FLAT PLATE SOLAR COLLECTOR SYSTEM FOR HEATING GREENHOUSE USING NANO-FLUID*” from the English linguistic point of view, and I can confirm that it is free of grammatical and spelling errors.

Signature:

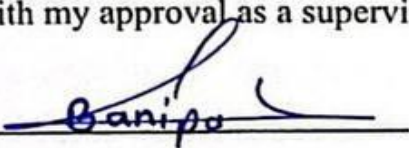


Name of Reviewer: Jack C Wynker

Date: 12/9/2022

## SUPERVISOR CERTIFICATE

This thesis has been written under my supervision and has been submitted for the award of the degree of Master of Science in Mechanical and Energy Engineering with my approval as a supervisor.



Signature

Dr. Banipal Nanno Yaqob


Name

27/10/2022

Date

**I confirm that all requirements have been fulfilled.**

Signature:



Name: Asst. Prof. Dr. Ahmed Mohammed Adham

Head of the Department of Technical Mechanical and Energy Engineering

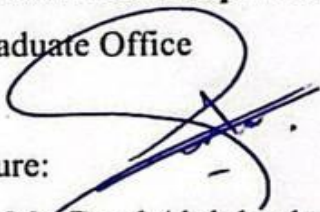
Date:



**I confirm that all requirements have been fulfilled.**

Postgraduate Office

Signature:



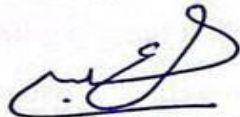
Name: Mr. Byad Abdulqader Ahmed

Date: 30/10/2022

## EXAMINING COMMITTEE CERTIFICATION

We certify that we have read this thesis: *"THERMAL PERFORMANCE ANALYSIS OF A FLAT PLATE SOLAR COLLECTOR SYSTEM FOR HEATING GREENHOUSE USING NANO-FLUID"* and as an examining committee, examined the student (*Zhyan Faeaq Hassan*) in its content and what related to it. We approve that it meets the standards of a thesis for the degree of Master in Mechanical and Energy Engineering.

Signature:



Name: Asst. Prof. Dr. Ranj Sirwan Abdullah

Member

Date: 27/10/2022

Signature:



Name: Asst. Prof. Dr. Arkan Fawzi Saeed

Member

Date: 27/10/2022

Signature:



Name: Dr. Banipal Nanno Yaqob

Supervisor

Date: 27/10/2022

Signature:



Name: Asst. Prof. Dr. Rizgar Bakr Weli

Chairman

Date: 27/10/2022

Signature:



Name: Prof. Dr. Ayad Zaki Saber Agha

Dean of Erbil Technical Engineering College

Date: 30-10-2022

## DEDICATION

This thesis is dedicated to my beloved family, who has been a constant source of support and encouragement during the challenges of my studies. I wholeheartedly thank my loving parents, who have always loved me unconditionally and whose good examples have taught me to work hard for the things I aspire to achieve.

My beloved siblings, particularly my dearest brother, (*Zana*), stand by me and help me in all things, great and small.

I dedicate this work and give special thanks to all my friends who supported me until my research was fully finished.

I am genuinely thankful to have you all in my life.

## AKNOWLEDGMENT

In the name of ALLAH, Most Gracious, Most Merciful. All praise is due to ALLAH, the Lord of the worlds.

Foremost, I am thankful to almighty ALLAH for giving me the strength, knowledge, ability, and opportunity to undertake and complete this research successfully.

I would like to express my deep and sincere gratitude to my research supervisor, *Dr. Banipal Nanno Yaqob*, for the continuous support of this master's thesis and his patience, motivation, and immense knowledge. He consistently allowed this thesis to be my own work but steered me whenever he thought I needed it. I am really thankful for your help and support.

I would like to express my wholehearted thanks and appreciation to the General Director of the Scientific Research Center at Erbil Polytechnic University, *Asst. Prof. Dr. Hayman Kakakhan Awla*, and his colleagues for their technical support and help.

I would like to give my special thanks to *Asst. Prof. Dr. Ranj S. Abdullah and Asst. Prof. Dr. Nazar Faraj Antwan* for their helpful comments regarding the numerical aspects of my study.

My wholehearted thanks go to late *Asst. Prof. Dr. Idres I.A. Hamakhan* for his comments, support, and for sharing his knowledge.

This thesis would not have been possible without the support of my family. I am forever thankful for their love, understanding, prayers, and support. My accomplishments and success are because they believed in me.

Lastly, my special thanks go to all my friends and those who have supported me in completing the research work directly or indirectly.

## ABSTRACT

Plants are grown in commercial greenhouses to enhance their quality and protect them from the effects of the natural environment, such as cold, wind and rain. In temperate climates, energy is the highest overhead expense in the production of greenhouse production. Also, the cost of fossil fuels and other traditional energy forms continues to rise. A suitable heating system at a reasonable price is essential for heating the greenhouse to provide optimum indoor conditions throughout the colder months. Flat plate solar collectors (FPSC) are one of the most environmentally friendly and energy-efficient heating solutions. In this work, the thermal performance of the FPSC for the greenhouse heating system was experimentally and numerically investigated by firstly utilizing distilled water as a working fluid and secondly using  $\text{Al}_2\text{O}_3$ -water nanofluid with different nanoparticle concentrations of (0.2wt.%, 0.5wt.%, 1wt.%, and 1.5wt.%) with a mean diameter of 50 nm. The simulation model was conducted using TRNSYS 18. The outcome was validated with experimental results. All configurations were fully modeled in TRNSYS, and experimental tests evaluated the inputs of the model software. As a first step, the study estimates the maximum amount of energy needed, which was 12.8 kW on the coldest day of winter (12<sup>th</sup> January 2022) according to the Erbil's weather data, for a greenhouse located in the Scientific Research Center in Erbil, Iraq. A temperature of 23°C was selected as the set point temperature in the greenhouse, which is essential for the experiments needed to develop several plants. This investigation followed the ASHRAE standard. The most interesting finding was that when nanofluids were used as a working fluid, the efficiency gain was larger than using water only, even with a low concentration of nanoparticles. The experimental results illustrated that using  $\text{Al}_2\text{O}_3$ -water nanofluid at a



concentration of 0.2wt.% increase the collector efficiency by 7.9% compared to water. Furthermore, the simulation results indicate that the maximum collector efficiency was attained, which was 83.6%, when 1wt.% nanofluid was used in the FPSC, which increased the collector efficiency by 26.1% over the water case. Any additional increase in the percentage of nanoparticles reduces collector efficiency. In summary, results show that during the coldest months of the year, the system could raise the inner air temperature of the greenhouse, which is ideal for farming applications and does not pollute the environment. It was also shown that utilizing nanofluid is a profitable working fluid that decreases the cost of heating system. Additionally, adding nanofluid to the system as HTFs could produce and store more energy, which in turn increase energy produced by about 22% over the case of using water only.

# TABLE OF CONTENTS

DECLARATION .....	I
LINGUISTIC REVIEW .....	II
SUPERVISOR CERTIFICATE.....	III
EXAMINING COMMITTEE CERTIFICATION.....	IV
DEDICATION .....	V
ACKNOWLEDGMENT.....	VI
ABSTRACT .....	VII
TABLE OF CONTENTS .....	IX
LIST OF FIGURES.....	XIV
LIST OF TABLES .....	XIX
NOMENCLATURE.....	XX
LIST OF SYMBOLS .....	XX
GREEK LETTERS .....	XXI
SUBSCRIPTS .....	XXI
LIST OF ABBREVIATIONS .....	XXII
CHAPTER 1.....	1
INTRODUCTION.....	1
1.1 General .....	1
1.2 Solar Energy .....	4

1.3 Solar Water Heating System .....	5
1.4 Solar Water Heating System Component Design .....	6
1.4.1 Solar Collector.....	6
1.4.2 Storage Tank .....	8
1.4.3 Heat Transfer Fluids.....	9
1.5 Greenhouse.....	10
1.6 Research Problem Statement.....	11
1.7 Research Objectives .....	12
1.8 Research Methodology.....	12
1.9 Thesis Layout .....	13
1.10 Overview .....	13
CHAPTER 2.....	14
LITERATURE REVIEW.....	14
2.1 Introduction .....	14
2.2 Thermal Performance of FPSC.....	14
2.3 Enhancing the Thermal Performance of FPSC Using Nanofluids .....	16
2.4 Greenhouse Heating System .....	20
2.5 Overview .....	23
CHAPTER 3.....	26
MATHEMATICAL MODEL .....	26
3.1 Introduction .....	26
3.2 Heat Load Calculation.....	26

3.3 Thermal Performance of the FPSC .....	28
3.4 Thermophysical Properties of Nanofluids .....	29
3.4.1 Thermal Conductivity .....	30
3.4.2 Density .....	31
3.4.3 Specific heat .....	31
3.4.4 Viscosity .....	32
3.5 Pressure Drop and Pumping Power Analysis .....	32
3.6 Economic Analysis.....	34
CHAPTER 4.....	36
EXPERIMENTAL SETUP .....	36
4.1 Introduction .....	36
4.2 Components of System Design .....	38
4.2.1 Heating Load .....	38
4.2.2 Flat Plate Solar Collector (FPSC) .....	39
4.2.3 Storage Tanks .....	40
4.2.4 Pumps .....	42
4.2.5 Temperature Sensors .....	43
4.2.6 Pressure Sensor .....	44
4.2.7 Flow Meter .....	45
4.2.8 Piping System.....	46
4.2.9 Pyranometer .....	47
4.3 Material .....	47

4.4 Preparation Method of the Nanofluid .....	48
4.5 Operating methods .....	49
4.6 Uncertainty Analysis.....	54
CHAPTER 5.....	55
NUMERICAL SIMULATION MODEL.....	55
5.1 Introduction .....	55
5.2 The TRNSYS Simulation Program's Components .....	56
5.2.1 Weather Data (Type 15-2) .....	56
5.2.2 Solar Collector (Type 1b).....	56
5.2.3 Storage Tank (Type 156) .....	58
5.2.4 Pump (Type 114).....	58
5.2.5 Controller (Type 165) .....	59
5.2.6 Buried Pipe Model (Type 952) .....	59
5.2.7 Building Load (Type 56).....	59
5.2.8 Forcing Function (Type 14h) .....	60
5.2.9 Psychrometrics (Type 33e) .....	60
5.2.10 Output (Type 65a).....	60
5.2.11 Equation Tool (Equa).....	61
CHAPTER 6.....	62
RESULTS AND DISCUSSIONS .....	62
6.1 Introduction .....	62
6.2 Experimental Results .....	62

6.2.1 Water as Working Fluid .....	63
6.2.2 Nanofluid as Working Fluid.....	67
6.2.3 Comparisons between Different Working Fluids .....	73
6.3 Simulation Studies.....	75
6.3.1 TRNSYS Model Validation .....	75
6.3.2 Comparisons between the Working Fluids .....	77
6.3.3 Greenhouse Heating Load.....	88
CHAPTER 7.....	98
CONCLUSION AND RECOMMENDATIONS .....	98
7.1 Summary .....	98
7.2 Conclusion.....	98
7.3 Recommendation for Further Study.....	100
REFERENCES.....	R <sub>1</sub>
APPENDIX (A).....	A <sub>1</sub>
SAMPLE OF CALCULATIONS .....	A <sub>1</sub>
APPENDIX (B).....	A <sub>12</sub>
TECHNICAL SPECIFICATION AND CALIBRATION.....	A <sub>12</sub>
APPENDIX (C).....	A <sub>15</sub>
SAMPLE OF TRNSYS SIMULATION RESULTS .....	A <sub>15</sub>
APPENDIX (D).....	A <sub>16</sub>
EXPERIMENTAL RESULTS.....	A <sub>16</sub>

## LIST OF FIGURES

Figure 1.1 A schematic representation of the greenhouse effect (Dincer, 2000).	1
Figure 1.2 The worldwide primary energy consumption from 1978 to 2018 (Kober <i>et al.</i> , 2020).	2
Figure 1.3 Kurdistan's energy resources (Morad, 2018).	3
Figure 1.4 A schematic representation of the different forms of solar energy.	4
Figure 1.5 Types of solar water heating systems.	5
Figure 1.6 Classification of solar collectors (Naderi, 2016; Joardder <i>et al.</i> , 2017)	7
Figure 1.7 A schematic diagram of FPSC.	8
Figure 1.8 Storage tank model (indirect back-up).	9
Figure 2.1 FPSC size reductions for different kinds of nanofluids (Faizal <i>et al.</i> , 2013).	18
Figure 4.1 Experimental setup of SWHS.	37
Figure 4.2 Schematic of the test greenhouse external view.	38
Figure 4.3 Tubular heat exchanger buried under the greenhouse.	39
Figure 4.4 Photograph of the FPSC.	40
Figure 4.5 Photograph of the storage tanks.	41
Figure 4.6 Water circulation pumps type of (a) SPERONI; and (b) DAB.	43
Figure 4.7 Temperature sensors (a) QAP21.2; (b) QAE26.9; and (c) QAA25.	44
Figure 4.8 Pressure sensor.	45
Figure 4.9 Flow rate measuring sensor.	46
Figure 4.11 Piping System.	46

Figure 4.12 LP02 pyranometer with LI19 read-out unit/data-logger. ....	47
Figure 4.13 SEM images of Al <sub>2</sub> O <sub>3</sub> nanoparticles (Skyspring Company).....	48
Figure 4.14 Nanofluid preparation diagram.....	49
Figure 4.15 Magnetic stirrer and ultrasonic homogenizer. ....	49
Figure 4.16 A screen shoot of the computer program software (DESIGO INSIGHT).....	52
Figure 4.17 A 3D design diagram of a solar water heating system. ....	53
Figure 5.1 TRNSYS modeling of the SWHS. ....	57
Figure 5.2 Yearly ambient temperatures for the city of Erbil.....	58
Figure 6.1 Inlet and the outlet collector water temperature of the FPSC on 8 <sup>th</sup> March.....	64
Figure 6.2 Efficiency of the collector and solar irradiance as a function of day times on 8 <sup>th</sup> March.....	65
Figure 6.3 Efficiency of FPSC as a function of reduced temperature parameters on 8 <sup>th</sup> March.....	66
Figure 6.4 Greenhouse heating load versus energy provided (heat supply) during the day times on 8 <sup>th</sup> March. ....	67
Figure 6.5 Inlet and outlet nanofluid temperature with respect to day time for 29 <sup>th</sup> March.....	68
Figure 6.6 Inlet and outlet nanofluid temperature with respect to day time for 31 <sup>st</sup> March.....	68
Figure 6.7 Collector efficiency and solar irradiance as a function of the day time for 29 <sup>th</sup> March using Al <sub>2</sub> O <sub>3</sub> as nanofluid.....	69



Figure 6.8 Collector efficiency and solar irradiance as a function of the day time for 31 <sup>st</sup> March using Al <sub>2</sub> O <sub>3</sub> as nanofluid. ....	70
Figure 6.9 Efficiency of FPSC using Al <sub>2</sub> O <sub>3</sub> -water nanofluid for 29 <sup>th</sup> March. ....	71
Figure 6.10 Efficiency of FPSC using Al <sub>2</sub> O <sub>3</sub> -water nanofluid for 31 <sup>st</sup> March. ...	71
Figure 6.11 Greenhouse heating load versus energy provided (heat supply) as a function of day times for 29 <sup>th</sup> March.....	72
Figure 6.12 Collector difference temperature at different working fluids (DW and 0.2wt.% Al <sub>2</sub> O <sub>3</sub> -water nanofluid). ....	74
Figure 6.13 Collector efficiency at different working fluids (DW and 0.2wt.% Al <sub>2</sub> O <sub>3</sub> -water nanofluid).....	74
Figure 6.14 Comparison between the simulation and experimental results for FPSC water temperature.....	76
Figure 6.15 Comparison between experimental and simulation temperatures of the collectors nanofluid for 0.2wt.% concentration. ....	76
Figure 6.16 Solar irradiance verification between experimental and simulation results.....	77
Figure 6.17 Collector efficiency at different working fluids DW and nanofluid with concentration of (0.2wt.%, 0.5wt.%, 1wt.%, and 1.5wt.%). ....	78
Figure 6.18 System pressure drop for water and different concentration of Al <sub>2</sub> O <sub>3</sub> -water nanofluid.....	80
Figure 6.19 Pump power for water and different concentration of Al <sub>2</sub> O <sub>3</sub> -water nanofluid.....	80
Figure 6.20 Efficiency versus solar irradiance for DW and for nanofluid with different concentration. ....	81
Figure 6.21 FPSC efficiency for DW and for Al <sub>2</sub> O <sub>3</sub> -water nanofluid with different concentrations.....	82

Figure 6.22 Collector outlet temperatures for different working fluids. ....	84
Figure 6.23 Average collector outlet temperatures for different working fluid for November. ....	85
Figure 6.24 Average collector outlet temperatures for different working fluid for December.....	85
Figure 6.25 Average collector outlet temperatures for different working fluid for January.....	86
Figure 6.26 Average collector outlet temperatures for different working fluid for February.....	86
Figure 6.27 Average collector outlet temperatures for different working fluid for March.....	87
Figure 6.28 Average collector outlet temperatures for different working fluid for April.....	87
Figure 6.29 Greenhouse heating load value on 12 <sup>th</sup> January. ....	88
Figure 6.30 Greenhouse heating load required and energy provided (heat supply) with non-set-point temperature for 12 <sup>th</sup> January. ....	90
Figure 6.31 Greenhouse heating load required and energy provided (heat supply) with set-point temperature for 12 <sup>th</sup> January. ....	90
Figure 6.32 Greenhouse heating load required and energy provided (heat supply) with non-set-point temperature for 30 <sup>th</sup> November. ....	91
Figure 6.33 Greenhouse heating load required and energy provided (heat supply) with non-set-point temperature for 28 <sup>th</sup> December. ....	92
Figure 6.34 Greenhouse heating load required and energy provided (heat supply) with non-set-point temperature for 4 <sup>th</sup> February. ....	92
Figure 6.35 Greenhouse heating load required and energy provided (heat supply) with non-set-point temperature for 4 <sup>th</sup> March. ....	93

Figure 6.36 Greenhouse heating load required and energy provided (heat supply) with non-set-point temperature for 3 <sup>th</sup> April. ....	93
Figure 6.37 Greenhouse heating load required and energy provided (heat supply) with set-point temperature for 30 <sup>th</sup> November. ....	94
Figure 6.38 Greenhouse heating load required and energy provided (heat supply) with set-point temperature for 28 <sup>th</sup> December. ....	94
Figure 6.39 Greenhouse heating load required and energy provided (heat supply) with set-point temperature for 4 <sup>th</sup> February. ....	95
Figure 6.40 Greenhouse heating load required and energy provided (heat supply) with non-set-point temperature for 4 <sup>th</sup> March. ....	95
Figure 6.41 Greenhouse heating load required and energy provided (heat supply) with set-point temperature for 3 <sup>th</sup> April. ....	96
Figure 6.42 Monthly average solar irradiance. ....	97
Figure B.1 Calibration curve for flow meter type QVE3100. ....	A <sub>14</sub>
Figure C.1 TRNSYS inlet and the outlet collector water temperature of the FPSC. ....	A <sub>15</sub>
Figure C.2 TRNSYS inlet and the outlet collector water temperature of the FPSC. ....	A <sub>15</sub>

## LIST OF TABLES

Table 1.1 Comparisons between concentrate and non-concentrate collectors. ....	6
Table 2.1 Development of FPSC performance employing various nanofluids. ..	24
Table 3.1 Thermo physical properties of the working fluids.....	30
Table 3.2 The values of $Kl$ for several types of valves and fittings. ....	34
Table 3.3 The costs and payback period of the SWHS.....	35
Table 4.1 Technical Specification of FPSC.....	40
Table 4.2 Specifications of the heat exchanger.....	42
Table 4.3 The uncertainty of the measuring devices. ....	54
Table 6.1 Values of $F_R(\tau\alpha)$ and $F_R(U_L)$ for $Al_2O_3$ -water nanofluid. ....	71
Table 6.2 Values of $F_R(\tau\alpha)$ and $F_R(U_L)$ for different working fluids.....	82
Table 6.3: Average monthly greenhouse useful heat in (kWh). ....	97
B.1.1 Technical Specification of Temperature Sensors.....	A <sub>12</sub>
B.2.1 Technical Specification of Flow Meter.....	A <sub>13</sub>
B.2.2 Calibration of Flow Meter Type QVE3100 .....	A <sub>13</sub>
C.1 Inlet and Outlet Temperature ( $^{\circ}C$ ) of the FPSC.....	A <sub>16</sub>
C.2 Efficiency (%) of the collector and solar irradiance ( $W/m^2$ ) .....	A <sub>17</sub>
C.3 Greenhouse Heating Load (kW) and Heat Supply (kW) .....	A <sub>18</sub>
C.4 Values of $F_R(\tau\alpha)$ , $F_R(U_L)$ , and $R^2$ .....	A <sub>19</sub>

# NOMENCLATURE

## LIST OF SYMBOLS

$A$	Surface area ( $\text{m}^2$ )
$C_p$	Heat capacity ( $\text{J/kg}\cdot^\circ\text{C}$ )
$D$	Diameter (m)
$f$	Friction factor
$F_R$	Collector heat removal factor
$F_R(\tau\alpha)$	Absorbed energy
$F_R(U_L)$	Removed energy ( $\text{W/m}^2\cdot^\circ\text{C}$ )
$G_T$	Solar irradiance ( $\text{W/m}^2$ )
$h_i$	Inside surface convective ( $\text{W/m}^2\cdot^\circ\text{C}$ )
$h_o$	Outside surface convective ( $\text{W/m}^2\cdot^\circ\text{C}$ )
$k_m$	Thermal conductivity ( $\text{W/m}\cdot^\circ\text{C}$ )
$K_l$	Loss coefficient
$\Delta l$	Pipe length (m)
$\dot{m}$	Mass flow rate (kg/s)
$\Delta P$	Pressure drop (kPa)
$Q_{loss}$	Overall heat losses (W)
$Q_u$	Supplied heat transfer (W)
$R^2$	Root mean square error
$Re$	Reynolds number
$R_{total}$	Total thermal resistance ( $^\circ\text{C/W}$ )
$T$	Temperature ( $^\circ\text{C}$ )
$U$	Energy loss coefficient ( $\text{W/m}^2\cdot^\circ\text{C}$ )
$U_L$	Overall heat transfer coefficient ( $\text{W/m}^2\cdot^\circ\text{C}$ )
$U_x$	Measurement uncertainty (%)

$V$	Mean flow velocity (m/s)
$\dot{V}$	Volume flow rate (m <sup>3</sup> /s)
$\bar{x}_n$	Mean measured parameters

### **GREEK LETTERS**

$\varphi$	Particle concentration by weight
$\eta_{th}$	Collector Efficiency (%)
$\mu$	Viscosity (mPa.s)
$\rho$	Density (kg/m <sup>3</sup> )
$\sigma$	standard deviation
$\tau\alpha$	Absorptance–transmittance

### **SUBSCRIPTS**

a	Ambient
bf	Base fluid
C	Collector
G	Greenhouse
H	Heat exchanger
i	Inlet
np	Nanoparticle
o	Outlet
p	pipe

## LIST OF ABBREVIATIONS

Al <sub>2</sub> O <sub>3</sub>	Aluminium Oxide
APS	Annual Payment Saving
ASHRAE	American Society Of Heating, Refrigerating, And Air-Conditioning Engineers
DW	Distilled Water
EC	Electricity Cost
FPSC	Flat Plate Solar Collector
GE	Gain Of Energy
HTF	Heat Transfer Fluid
PD	Payback Duration
SEM	Scanning Electron Microscopes
SWHS	Solar Water Heating Systems
TC	Total Cost
TRNSYS	Transient Systems Simulation

# CHAPTER 1

## INTRODUCTION

### 1.1 General

Population expansion and industrial development are raising the world's energy needs dramatically. Fossil fuels, wind, solar energy, and nuclear resources are the four primary energy sources. The global energy industry is experiencing significant challenges today because of the depletion of fossil fuel reserves due to fossil fuel usage. Due to the absence of the world's fossil fuel reserves due to the usage of fossil fuels, the energy industry throughout the globe is now experiencing significant issues. For a long time, it has been known that the excessive use of fossil fuels accelerates the depletion of fossil fuel sources, harms the environment, and increases health concerns and the danger of global climate change. Figure 1.1 is a schematic illustration of the challenge of global climate change.

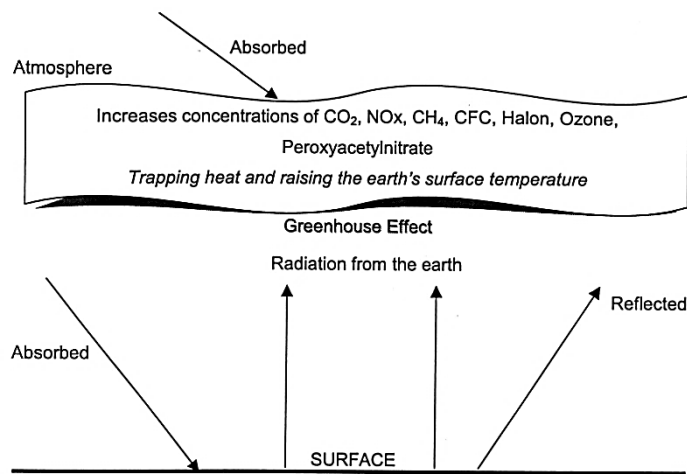


Figure 1.1 A schematic representation of the greenhouse effect (Dincer, 2000).



The development of renewable energy (RE), which is energy produced from natural sources such as sunshine and is a significant energy source, is one of the most incredible ways to reduce climate change. An effective strategy for slowing the pace of climate change is to encourage renewable energy (RE), which includes solar power and other natural resources like wind and water. Primary, domestic, pure, or unlimited renewable energy resources are called renewable. Biomass, hydropower, geothermal, wind, marine, and solar energy are all examples of renewable energy sources (RES). Figure 1.2 depicts the evolution of world energy consumption during the last 40 years.

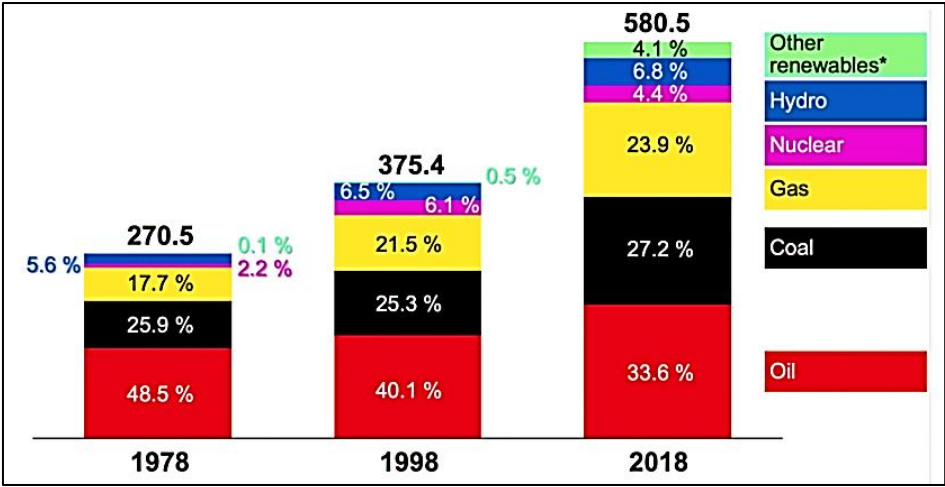


Figure 1.2 The worldwide primary energy consumption from 1978 to 2018 (Kober *et al.*, 2020).

As seen in the above graph, in 1978, fossil fuels (coal, oil, and gas) accounted for 92.1 percent of the world's total energy consumption, but by 2018, this ratio had dropped to 84.7 percent. All kinds of renewable energy (RE) consumption grew from 5.7% in 1978 to 11.1% by 2018 (Kober *et al.*, 2020).

Reduced carbon dioxide emissions are among the most significant characteristics of renewable energy sources, which go a long way toward protecting the environment. Because fossil fuels are being depleted at rates that may lead to their depletion shortly, they are not considered renewable. Concerns about fossil fuel pricing, climate change effects, and the environmental ramifications of greenhouse gases have led to an increase in renewable energy sources.

The majority of Kurdistan's energy comes from fossil fuels, with gasoline and natural gas accounting for around 85% of the country's total energy production. The remaining 15% is covered by hydroelectric plants and solar energy, accounting for less than 1%, as illustrated in Figure 1.3.

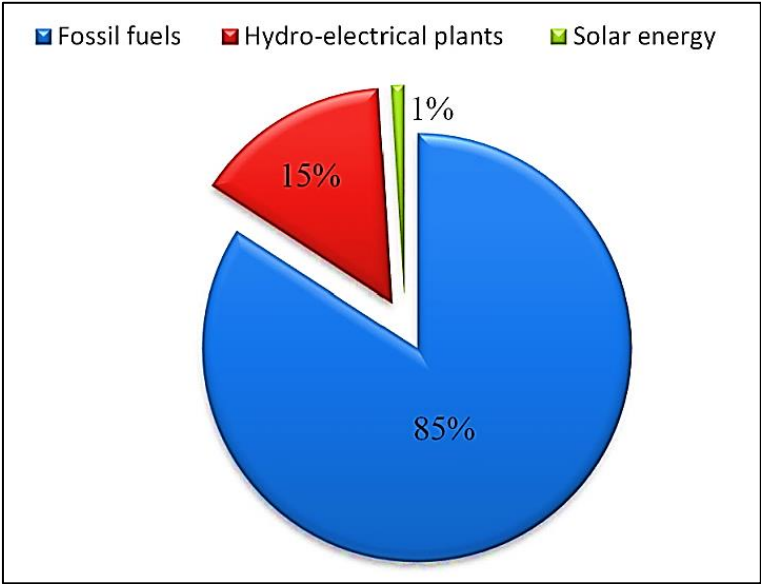


Figure 1.3 Kurdistan's energy resources (Morad, 2018).

## 1.2 Solar Energy

Worldwide, conventional energy sources and electricity have become more limited resources. All governments are compelled to embrace renewable energy sources to fulfill their rising needs. Compared to other renewable energy sources, solar energy is one of the cleanest because it is free, abundant, cheap, easy to access, efficient, and has a negligible impact on the environment. It can also provide energy independence in the most remote rural areas (Kannan and Vakeesan, 2016). Village systems, industrial operations, agriculture, and residences may benefit from this technology. As illustrated in Figure 1.4, there are two general methods for collecting solar energy, each with its advantages and disadvantages. These are: (i) solar electric conversion (converting solar energy into electrical energy via a photovoltaic solar cell or concentrated solar power) and (ii) solar thermal transformation (changing solar energy into thermal energy using a solar collector).

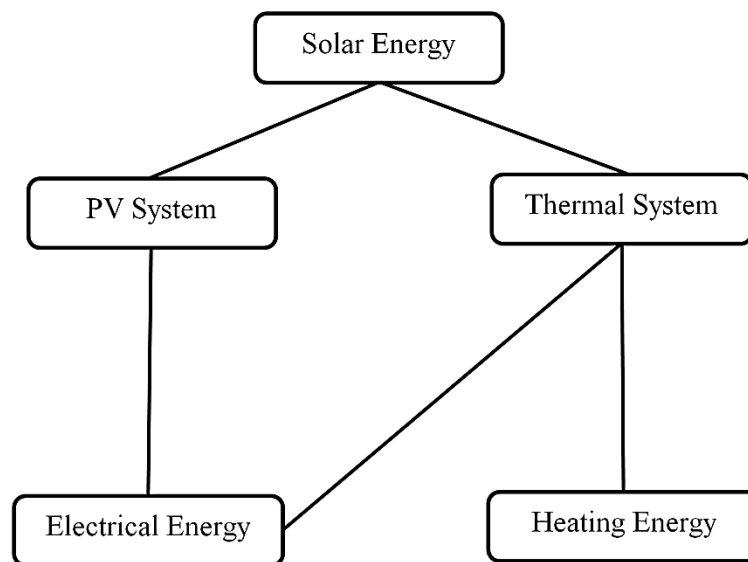


Figure 1.4 A schematic representation of the different forms of solar energy.

### 1.3 Solar Water Heating System

In the last decade, solar thermal energy has been extensively researched by scientists throughout the world. Solar water heating systems (SWHS), often known as solar domestic hot water systems, are one of the most common uses of solar thermal energy. In a solar water heating system, the sun's rays are transformed into heat and transported via a medium such as water, fluid, or air. Solar heating systems have sparked the most intense interest due to their significant benefits in resource conservation, lower equipment investment and operating costs, and long-term application. The system is relatively simple since only sunlight is required to heat the water. As seen in Figure 1.5, there are two domestic solar water heating system types: active and passive systems. The main difference between active and passive systems is that active systems use circulating pumps to move water around; this is called a forced circulation system. On the other hand, passive systems use gravity to circulate water; this system uses natural convection heat transfer and does not have any mechanical devices to carry water or fluids between a collector and an elevated storage tank (Jamar *et al.*, 2016).

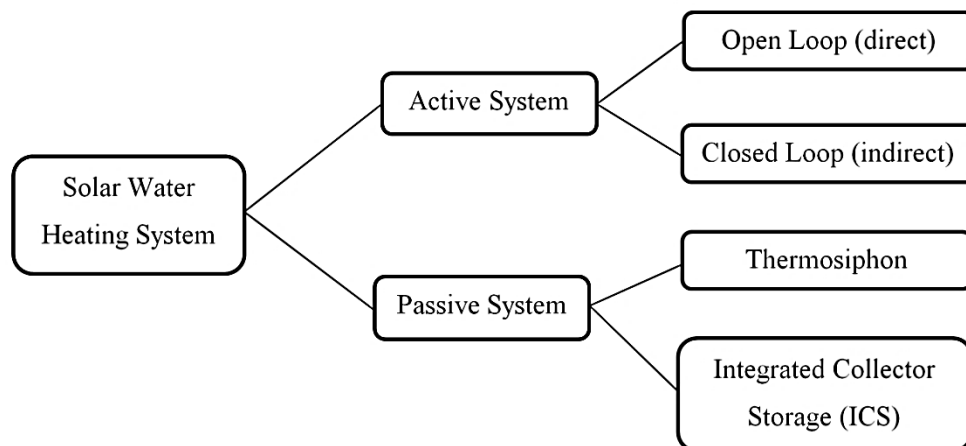


Figure 1.5 Types of solar water heating systems.

## 1.4 Solar Water Heating System Component Design

The design of solar system components has been the focus of many researchers in recent years to enhance the efficiency of solar systems and maintain their market share. Solar water heating systems have three primary components: solar collectors, thermal storage tanks, and heat transmission fluids. Additionally, the design of the system also includes a pump, heat exchanger, auxiliary heating, and piping units.

### 1.4.1 Solar Collector

A heat exchanger known as the solar collector is an essential part of any solar energy system since it converts solar energy into thermal energy. Solar collectors are typically intended to absorb and collect solar energy. These collector devices transform the absorbed solar energy into heat, which is ultimately transferred to the working fluid of a system, generally water, air, or oil. Table 1.1 depicts the distinction between concentrating and non-concentrating solar collectors. In addition, there are primarily a few kinds of collectors whose temperature ranges are shown in Figure 1.6.

Table 1.1 Comparisons between concentrate and non-concentrate collectors.

Parameter	Non-Concentrate collectors	Concentrate collectors
Absorber area	Same as collector area	Much smaller than collector area
Efficiency	Good	Better
Obtained Temperature	Less	More
Steam Pressure	Low	Medium

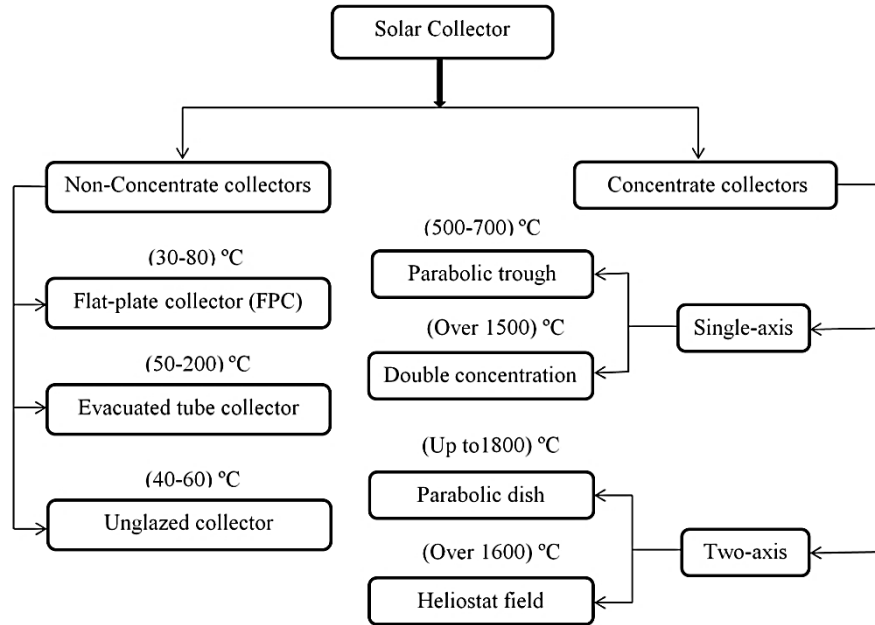


Figure 1.6 Classification of solar collectors (Naderi, 2016; Joardder *et al.*, 2017)

#### 1.4.1.1 Flat Plate Solar Collector (FPSC)

A flat plate solar collector (FPSC) is one of the most popular and productive forms of solar collector. It is one of the best ways to use solar energy; also it is a type of stationary collector utilized in many domestic and industrial applications. In addition, there is no need for the sun monitoring system since it is fixed. An appropriate working fluid such as water, oil, or ethylene glycol was used to transfer the heat generated by solar radiation (Zayed *et al.*, 2019). As seen in Figure 1.7, a system of flat plate solar collectors includes an absorber, glass, insulation, back sheet, riser and header pipes, and aluminum rails. Accumulated energy is maximized using an absorber plate composed of aluminum or copper coated with a perfect selective coating. Furthermore, toughened and clear glass is used to shield and cover the absorber from the outside environment, and creating a greenhouse effect and limiting top heat

losses while allowing more than 90% of sunlight to pass through (Muhammad *et al.*, 2016). Compared to other solar collectors, flat plate collectors are more affordable, easier to construct and install, also require less maintenance. Due to high radiation and convection losses from its surface, the FPSC has low thermal efficiency, but this is not the only drawback of FPSCs. The low convective heat transfer coefficient between the absorber and the working fluid is another drawback of this type (Li *et al.*, 2017).

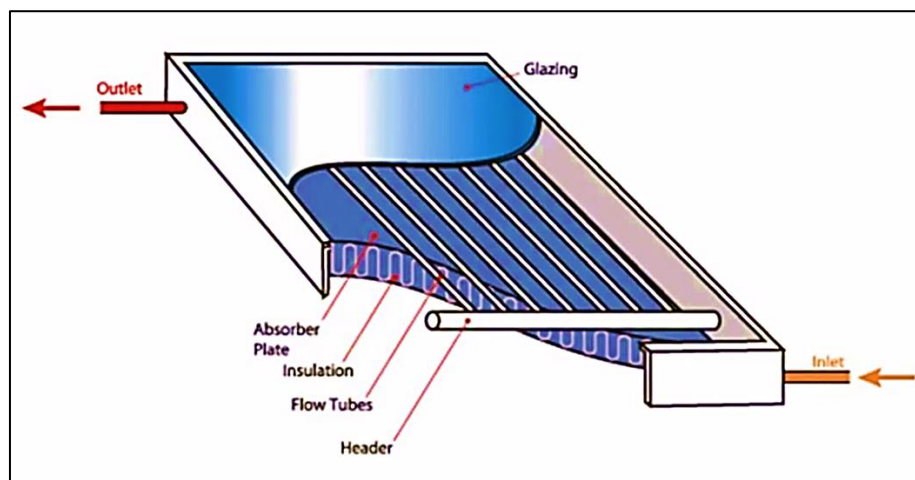


Figure 1.7 A schematic diagram of FPSC.

### 1.4.2 Storage Tank

When using a solar water heating system, the gathered solar thermal energy is stored in a tank known as a "thermal storage tank". This tank provides the necessary temperature of hot water to be utilized. The solar water tank behaves similar to an electric battery, except that it stores heat energy in the form of hot water. Steel, concrete, plastic, fiberglass, and other appropriate materials are often utilized to construct hot water storage tanks. Steel tanks are the most frequently used because of the ease of installation compared to the other forms (Shukla *et al.*, 2013). Optimizing the construction of the hot water tank and increasing the efficiency of the immersed heat exchange is one of the most

excellent methods to enhance the performance of SWHS. Tanks with built-in heat exchangers fall into three categories: (i) storage-only with no back-up, (ii) direct back-up and (iii) indirect back-up. The model of the storage tank prototype used in this work was illustrated in Figure 1.8.

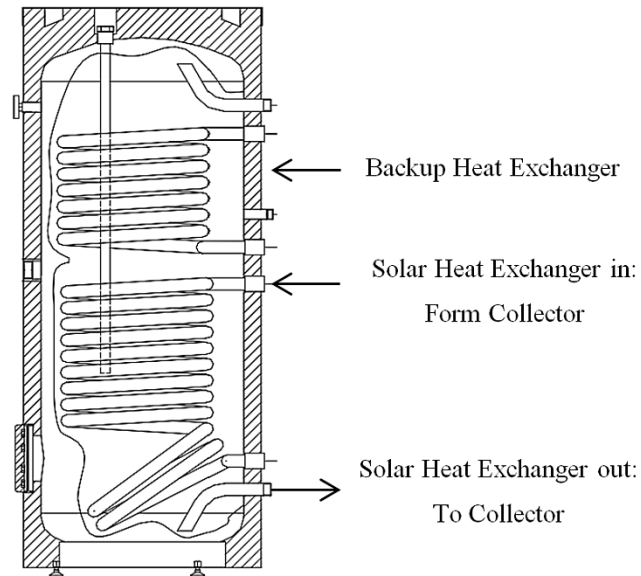


Figure 1.8 Storage tank model (indirect back-up).

### 1.4.3 Heat Transfer Fluids

Thermal energy is transferred from the collector to the tank by using heat transfer fluid. Increasing heat flow and reducing the size of heat transfer equipment are two of the most pressing concerns in heat transfer in today's world. Low viscosity, low thermal expansion coefficient, anti-corrosive, high specific heat capacity, high thermal conductivity, and a reasonable price are required for heat transfer fluids. Nano-fluids, which are stable suspensions of nanofibers and solid nanoparticles, have recently been recommended as a new technique in heat transfer activities (Jamar *et al.*, 2016).



The suspension of nanoparticles in a standard heat transfer fluid, known as base fluid, produces nanofluid, an advanced fluid containing tiny quantities of nanoparticles (typically less than 100 nm in size). Choi and Eastman in 1995 were the first to introduce the concept of "nanofluid", which has since been demonstrated to be more effective at transferring heat than traditional fluids. Nanoparticles dispersing in this fluid change its thermophysical properties, such as its thermal conductivity, viscosity, density, and specific heat. Heat transfer can be increased by increasing the thermal conductivity of the working fluid utilized in the applications. Due to the nanoparticles' Brownian motion, the nanofluid's thermal conductivity is higher than the base fluid. The thermal conductivity of nanofluids is also impacted by various other parameters, including the type of nanoparticles, the base fluid, the shape, size, concentration, and temperature of the nanoparticles (Zayed *et al.*, 2019). However, increases the density and viscosity of nanofluids, resulting in an increase in pressure drop and pumping power in a conventional forced heat transfer system (Hawwash *et al.*, 2021).

## **1.5 Greenhouse**

The greenhouse is a controlled-environment system that protects plants from extreme weather conditions. Under adverse weather conditions, it is possible to manage the interior climatic parameters of the greenhouse to establish a favorable environment for crop development, both in terms of quality and quantity. Because the need for agricultural resources is expanding, greenhouse farming is a developing industry in any country. As a result, greenhouse food production offers an additional option for addressing year-round increased food demand. The first concern for the greenhouse is to install a suitable heating

system that can maintain a comfortable temperature while conserving energy outside of the cultivation season. So, it is important to have a low-cost heating system to keep the greenhouse at the needed temperature during the winter. There is also a significant increase in the initial cost of fossil fuels and conventional energy sources. Several researchers have investigated solar thermal energy to heat greenhouses during the winter seasons throughout the last decade. There has been an increase in demand for solar energy as a green and sustainable option because of the negative environmental repercussions, limited fossil fuel supplies, and high consumption of energy and food.

## **1.6 Research Problem Statement**

An appropriate environment for plant development must be maintained in greenhouses throughout the cold winter months. Growing crop yields and mechanized agricultural production processes have increased the need for energy in agriculture. A heating system must be installed in greenhouses to provide a suitable environment for plant development throughout the winter months (Xu, Song and Ma, 2020). Due to the rising cost of heating a greenhouse with natural gas or oil, many producers have started using other energy sources. Consequently, a greenhouse must use a low-cost and renewable heating system to ensure optimal inside conditions throughout the winter months. A solar heating system that uses a flat plate collector in a greenhouse is a cost-effective option that does not pollute the environment and decreases the heating costs.

Using a solar water heating system to heat a greenhouse in Iraq, particularly in Kurdistan, is still unfamiliar and a relatively new concept. Many people are unaware of the practical advantages of employing SWHS for greenhouse heating. Solar heating greenhouses might be an option in Kurdistan because of

the region's sunny climate, which means decreasing heating costs and less gas pollution. Much reported researches have been done on FPSC for greenhouse heating systems. However, as yet, no research has been done on utilizing nanofluid as a working fluid for that purpose.

### **1.7 Research Objectives**

The primary purpose of this thesis is to investigate the possibility of using SWHS for heating greenhouse using  $\text{Al}_2\text{O}_3$ -water nanofluid as a working fluid for Erbil, Kurdistan-Iraq, on reaching maximum energy saving and, therefore, minimal gas emission. Additionally, to encourage the ministry of agriculture and farmers to adopt this system.

### **1.8 Research Methodology**

To achieve the aim of this work, two different methods are used including experimental prototype system and numerical simulation model using (TRNSYS 18). The following steps are implemented:

- SWHS are investigated experimentally and numerically, including efficiency, the temperatures at its inlet and outlet, heating load, and the amount of heat supplied to the greenhouse.
- Distilled water (DW) is used in this study as a working fluid and then replaced with nanofluid for the system's thermal performance enhancement.
- Developing solar water heating system using TRNSYS simulation software, the SWHS consisting of flat plate collectors, pumps, storage tank, and heating load.

- The results of TRNSYS are validated firstly with the experimental results. Then the TRNSYS simulation results are discussed to highlight the outcome of the research. Then conclusions and recommendations are discussed accordingly.

## **1.9 Thesis Layout**

The overall structure of the study takes the form of seven chapters, including:

- In Chapter 2, which is the foundation of the work, the literature relevant to the study topic is discussed.
- In Chapter 3, the study's mathematical model is depicted in detail.
- In Chapter 4, an overview of the system's overall procedure and operating conditions is demonstrated.
- In Chapter 5, the TRNSYS software that was used to develop and simulate the solar water heating system is discussed. Furthermore, the parts of the TRNSYS library and how they fit into the TRNSYS models were clarified.
- In Chapter 6, the results and discussion are explained.
- Finally, the conclusions and recommendation of the research are outlined in Chapter 7.

## **1.10 Overview**

This chapter presented background information and a problem statement. The work also described the nature of the study, as did the research method, and further complicated the research problem and objectives. The purpose of the research was also discussed.

The next chapter gives an overview of the literature that underlies this study.

## **CHAPTER 2**

### **LITERATURE REVIEW**

#### **2.1 Introduction**

The main objective of this chapter is to identify the various experimental and simulation methodologies utilized in solar water greenhouse heating systems and improve the collectors' performance. The majority of the chapter was devoted to evaluating the many approaches used in this field to choose the most effective method for answering the research objectives. Solar thermal systems and nanofluids have been extensively studied. Some of the results of these investigations are detailed in this chapter.

#### **2.2 Thermal Performance of FPSC**

William Bailey developed the first flat plate collectors for solar energy in 1909. The earliest published publications on this subject were outlined in Hottel and Willer's research in the 1950s (Florschuetz, 1979; Saffarian, Moravej and Doranehgard, 2020), later many researchers investigated this type of collector. Flat plate solar collectors have several advantages; however, their thermal efficiency and output temperatures are lower than other collectors. Since then, different methods to improve their efficiency and thermal performance have been presented. Several factors influence the performance of flat plate solar collectors including design, operational climate, and environmental parameters (Raj and Subudhi, 2018). For example, the size may be reduced, or the glazing materials can be changed, although these changes might be inconvenient. One of the best ways to improve efficiency is to change the working fluid from pure

water to a fluid with a higher thermal conductivity. The thermal performance enhancement of FPSC using different methods is presented as follows:

The flat plate collectors are investigated by (Giovannetti *et al.*, 2014) for the performance of highly transmitting and spectrally selective glass coatings based on transparent conductive oxides (TCO). Uncovered single-glazed and double-glazed collectors are utilized in these types of construction. Tin-doped indium oxide and aluminum-doped zinc oxide have also been analyzed as potential functional layers. This method enhanced thermal efficiency by combining single-glazed collectors with low or non-selective absorbers and double-glazed collectors with highly selective absorbers.

(Pandya and Behura, 2017) studied the thermal efficiency performance of V-Through SWH and the influence of tilt angle and dust particles on the glass cover. The thermal efficiency of SWH was increased from 27% to 30% by raising the tilt angle from 15° to 25°. At a tilt angle of 25°, the thermal efficiency of the transparent glass collector was reduced from 30% to 20% due to the collection of dust particles.

A new sort of superhydrophobic (SH) solar selective absorber (SSA) utilized in a low-temperature FPSC was studied by (Zhu *et al.*, 2017). The simple sol-gel process is used to create the SH-coated selective absorber. The water contact angle of SH-SSA may reach as much as 157° even when the sliding angle is less than 2°. Without corrosion, the selective absorber can resist outside circumstances with a solar absorption of 89.46%. The absorber can keep the water temperature below 83.8°C even without a glass cover or with a glass cover. The borosilicate glass cover on the selective absorber may improve thermal performance.

(Bhowmik and Amin, 2017) examined the efficiency of flat plate solar collectors using solar reflectors to improve collector reflectivity. The angle of the reflector was permitted to shift during the day to increase radiation intensity. The sun's energy was transformed into heat and then transmitted to a fluid in the collector. Consequently, a prototype of a solar water heating system was built, and a 10% increase in collector efficiency was achieved by employing a reflector. The researchers found that a solar collector with a solar reflector would have better thermal performance than a collector without a solar reflector.

(Zhou, Wang and Huang, 2019) performed tests on a three-dimensional numerical method of a FPSC using transparent insulating materials (TIM). The purpose of this study was to examine how the TIM improved the thermal performance of the FPSC in cold weather. A numerical investigation was performed using computational fluid dynamics (CFD). Under low ambient temperatures, the results demonstrated that the collector with TIM is more efficient, and when the transmittance is below 80%, the collector has no the advantage of being good value, also the optimum mass flow rate is 0.06 kg/s under corresponding conditions. The transmittance of TIM is a crucial performance improvement parameter for the collector.

### **2.3 Enhancing the Thermal Performance of FPSC Using Nanofluids**

One of the critical objectives in industrial applications is to increase the heat transfer rate. The low thermal conductivity of common heat transfer fluids, including water, oil, and ethylene glycol, may be improved by adding nanoparticles. There are three main types of nanoparticles: metal-based, carbon-based, and nanocomposites (Das, Choi and Patel, 2006; Suman, Khan and Pathak, 2015; Bellos, Said and Tzivanidis, 2018). Since 2012, the use of

nanofluid in flat plate solar collectors to improve heat transfer performance has been a principle of research for several researchers.

(Yousefi *et al.*, 2012) investigated the efficiency enhancement of a flat plate solar collector using MWCNT-H<sub>2</sub>O nanofluid and the effect of the surfactant Triton X-100 on nanofluid stability. The efficiency of the collector was calculated using mass flow rates of 0.0167, 0.033, and 0.05 kg/s. Experimental results observed that thermal efficiency increased with increasing mass flow rate by around 57%. In addition, they analyzed the efficiency of solar collectors containing 0.2wt% MWCNT with and without surfactant. As a result, they were able to show that adding surfactants could enhance the collector's efficiency.

CuO, Al<sub>2</sub>O<sub>3</sub>, SiO<sub>2</sub>, and TiO<sub>2</sub> based water nanofluids were studied by (Faizal *et al.*, 2013) to determine their effect on the performance of an FPSC. According to the results, it was determined that the higher density and lower specific heat of nanoparticles result in greater thermal efficiency and that CuO nanofluid was the best option for achieving maximum efficiency and had the highest value in comparison to the other three nanofluids. As shown in Figure 2.1, the size of the collector was reduced by 25.6%, 22.1%, 21.6%, and 21.4% when 3wt% was used at a mass rate of 3.8 L/min for CuO-H<sub>2</sub>O, SiO<sub>2</sub>-H<sub>2</sub>O, TiO<sub>2</sub>-H<sub>2</sub>O, and Al<sub>2</sub>O<sub>3</sub>-H<sub>2</sub>O, respectively.

(Said, Sabiha, *et al.*, 2015) experimentally investigated the use of TiO<sub>2</sub> nanoparticles and polyethylene glycol disperser to improve the efficiency of a flat plate solar collector. The nanofluid mass ranged from 0.5 to 1.5 kg/min, and they employed two volume fractions of nanoparticles: 0.1% and 0.3%, respectively. Polyethylene glycol (PEG 400) dispersant was used to improve the thermophysical characteristics and minimize sedimentation of TiO<sub>2</sub>-nanofluid. According to the findings, the maximum energy efficiency increased to 76.6% at



a volumetric fraction of 0.1% and a mass flow rate of 0.5 kg/min, while the exergy efficiency reached a maximum of 16.9%. For the volumetric fractions investigated, the pressure drop and pumping power of this nanofluid were about the same as those of the base fluid.

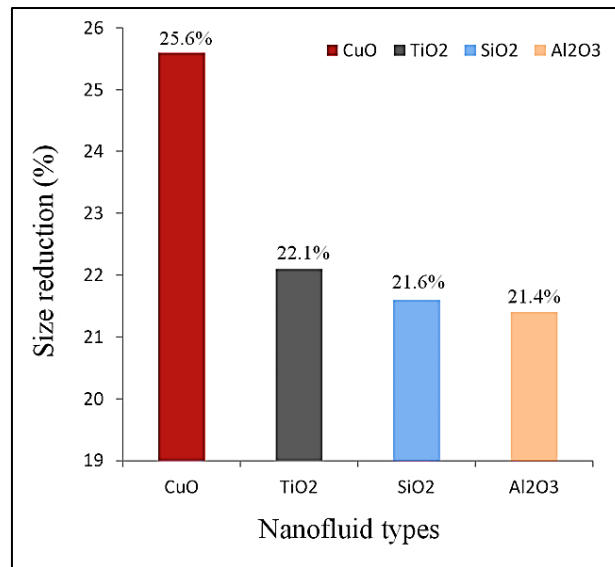


Figure 2.1 FPSC size reductions for different kinds of nanofluids (Faizal *et al.*, 2013).

The FPSC efficiency of CuO–water nanofluid under a laminar flow regime was theoretically studied by (Sint *et al.*, 2017). They used a mathematical model and a MATLAB coded program also calculated the maximum solar energy available for the FPSC, the convective heat transfer coefficient of the nanofluid, and the total heat loss coefficient of the collector. Their investigation was based on the computation of the thermal efficiency as a function of the nanoparticles' size and volume concentration. According to their study, energy efficiency can be improved by up to 2%, while nanoparticle size has no significant impact on thermal efficiency. As a result, they discovered that using a

2wt% CuO-water nanofluid at a mass rate of 1.2 kg/min increased collectors' efficiency up to 5%.

The performance of the FPSC utilizing Al<sub>2</sub>O<sub>3</sub>/DDW nanofluid with six different volume fractions varying from 0.1% to 3% and a mass flow rate of 5.4 kg/min has been theoretically and experimentally investigated by (Hawwash *et al.*, 2018). At low and high-temperature differences, the results reveal that utilizing alumina nanofluid enhances collector thermal efficiency by around 3% and 18% compared to water. Researchers in this investigation used ANSYS 17 software to simulate and verify their experimental results. Alumina nanoparticle concentrations until 0.5% weight fraction positively influence the collector's efficiency; further, after that point, any additional increase in concentration negatively affects collector performance and increases pumping power.

Using CeO<sub>2</sub>-H<sub>2</sub>O nanofluid to enhance the efficiency of flat plate solar collector was examined experimentally by (Sharafeldin and Gróf, 2018), and the average particle size used was 25 nm. In their experiment, volume fractions of 0.0167%, 0.0333%, and 0.0666% were evaluated for different mass fluxes of 0.015, 0.018, and 0.019 kg/s.m<sup>2</sup>. As a result, they found that nanofluid had the maximum collector efficiency at volume fractions of 0.066% and a mass flow of 0.019 kg/s.m<sup>2</sup>. It was also shown that nanofluid can improve the collector efficiency by 10.74% to a zero value of reduced temperature parameters  $\left(\frac{T_i - T_a}{G_T}\right)$ .

(Hawwash *et al.*, 2021) studied the thermal performance improvement of a flat plate solar collector experimentally and theoretically utilizing various working fluids (water, Al<sub>2</sub>O<sub>3</sub>, and CuO). Furthermore, the analysis was carried out using the computational fluid dynamic model (CFD) according to Egypt's

weather, and its outcome was validated with experimental results. Copper oxide nanoparticles with a volume fraction of 0.5% were found to have the highest thermal efficiency in the collector. They indicated that employing CuO-water nanofluid is more efficient than alumina oxide-water nanofluid under the same circumstances. Additionally, it was discovered that the FPSC's thermal performance and pressure drop improved when nanofluids were used as the working fluid.

There are several studies on the use of nanofluids to improve the performance of FPSC, as illustrated in Table 2.1.

## **2.4 Greenhouse Heating System**

Greenhouses are often used in agriculture to grow plants that need a lot of attention to maximize yields. Many researchers were provided a concise overview of greenhouses (Ahmed, Mustafa and Hasan, 2013). Due to the massive heating loads and the relatively high cost of fossil fuels, there is a significant interest in alternative or renewable energy sources for greenhouse heating. Various renewable energy including solar, geothermal, and biomass energy could be utilized for heating greenhouse instead of fossil fuels (Chau *et al.*, 2009; Cuce, Harjunowibowo and Cuce, 2016; Taki, Rohani and Rahmati-Joneidabad, 2018).

(Resources and All, 2012) experimentally studied the greenhouse heating systems in Japan and observed that the hourly energy consumption for heating a greenhouse with heat pumps varied from 0.22 to 0.56 MJ/m<sup>2</sup> from January to March, while heating using a kerosene heater ranged from 0.42 to 0.76 MJ/m<sup>2</sup>. Moreover, in the heat pump greenhouse, hourly CO<sub>2</sub> emissions varied from 9.5–24 g/m<sup>2</sup>, while in the kerosene heating greenhouse, they varied from 31–55 g/m<sup>2</sup>.

(Esen and Yuksel, 2013) experimentally investigated three different heating methods for greenhouse heating, (i) a solar system, (ii) biogas, and (iii) ground energy. Tests were performed over the winter season according to Elazig, Turkey climatic conditions from November 2009 to March 2010. A hybrid greenhouse heating system that uses biogas, solar power, and a ground source heat pump (BSGSHPGHS) has been developed and constructed. The greenhouse (6 m x 4 m x 2.10 m) was constructed and heated by alternative energy sources, and the greenhouse heating demand was estimated. Their findings revealed that many energy sources could be employed for greenhouse heating and that developed systems have successfully achieved the required value, which was 23°C, and many plants prefer this temperature for better growth.

An experimental investigation was conducted by (Joudi and Farhan, 2014) into the usage of a solar air heater (SAH) system to heat an innovative greenhouse installed in Baghdad, Iraq. The modern greenhouse is a hybrid structure with a conventional greenhouse and a collection of solar air heaters on the roof. They established six solar air heaters on the greenhouse roof with a single glass cover. A "V" corrugated absorber plate is joined in parallel, which differs from the previous conventional approach in that soil heat storage was not included. Furthermore, they determined that the sum of the stored energy from the SAHs and the stored free solar heat inside the greenhouse could exceed the daily heating needs by approximately 46%.

A thermal model was developed by (Attar *et al.*, 2013) to evaluate the performance of a solar water heating system (SWHS) used for greenhouses based on the Tunisian climate. This system was based on a capillary polypropylene heat exchanger built into the greenhouse. The SWHS was primarily made up of two solar collectors, with a total surface area of 4m<sup>2</sup>

connected to a 200-liter storage tank. TRNSYS16 was used to analyze all the design factors that affect the greenhouse solar heating system. The system's efficiency has improved due to the reduced stratification caused by the higher flow rates. However, they notice that reducing the intake flow rate of the heat exchanger is a viable method of reducing heating losses. They also showed that increasing the capacity of the tank decreases the temperature at the collector's output and that using a flat plate collector can raise the temperature of the air inside a greenhouse by 5°C.

(Bazgaou *et al.*, 2021) examined an active solar heating system (ASHS) comprised of two solar water heaters with flat collectors, two storage tanks, and exchanger pipes for its performance. They compared the climatic and agricultural conditions of two similar greenhouses to evaluate the active solar heating system (ASHS) performance and its influence on crop quality and quantity. One greenhouse had an ASHS heater installed, while the other did not. Consequently, the experiment reveals that ASHS can enhance nighttime environmental conditions inside the greenhouse. Tomato fruit quality is improved externally (color, weight, and firmness) and internally (sugar, acidity, and flavor) by the thermal comfort provided by ASHS in the root zone, which enhances the absorption of nutrients. They also noted that ASHS was a cost-effective solution in terms of investment and energy savings. In addition, they found that winter tomato yields increased by 55% due to this enhancement. However, this work will focus on using FPSC for heating greenhouse using  $\text{Al}_2\text{O}_3$ -water nanofluid as a working fluid to reach maximum energy saving and, therefore, minimal gas emission.

## **2.5 Overview**

During the last decade, extensive theoretical and experimental research has been conducted to increase the heat transfer performance of flat plate solar collectors. Even with small particle fractions, nanofluids were able to have high thermal conductivity, which indicated a promising improvement in the collector's efficiency. Moreover, most of the experiments revealed that employing nanoparticle suspensions enhanced thermal conductivity much more than utilizing traditional fluids. According to a brief review of greenhouse heating systems conducted by many researchers, using a flat plate solar collector makes the greenhouse solar heating system a beneficial system that does not pollute the environment and lowers the cost of heating.

The next chapter is concerned with the methodology used for this study.

Table 2.1 Development of FPSC performance employing various nanofluids.

Author	Process	Base fluid	Type	Size (nm)	Concentration (%)	Mass flow rate	Surfactant	Increased energy efficiency by (%)
(Yousefi <i>et al.</i> , 2012)	Exp.	water	Al <sub>2</sub> O <sub>3</sub>	15	0.2 vol.% and 0.4vol.%	1-3 L/min	Triton X-100	28.3%
(He, Zeng and Wang, 2014)	Exp.	water	Cu	25	0.1wt.%	140 L/h	SDBS	23.83%
(Moghadam <i>et al.</i> , 2014)	Exp.	Water	CuO	40	0.4vol.%	1 to 3 kg/min	-	16.7%
(Salavati Meibodi <i>et al.</i> , 2015)	Exp.	EG- water	SiO <sub>2</sub>	40	(0.5,0.75,1)vol. %	(0.018,0.03 2,0.045) kg/s	-	4 and 8%
(Verma, Tiwari and Chauhan, 2016)	Exp.	Water	MgO	40	0.25-1.5vol.%	0.5-2.5L/min	Cetyl Trimethyl Ammonium Bromide	9.34%
(Kiliç, Menlik and Sözen, 2018)	Exp.	Water	TiO <sub>2</sub>	44	2wt.%	0.033kg/s	Triton X-100	0.345%

(Tong <i>et al.</i> , 2019)	Exp.	water	Al <sub>2</sub> O <sub>3</sub> CuO	20 40	1vol.% 0.5vol.%	0.033 kg/s to 0.047 kg/s	-	3.4% -3.7%
(Michael Joseph Stalin <i>et al.</i> , 2020)	Exp.	water	CeO <sub>2</sub>	-	0.01vol.% to 0.1vol. %	1 to 3 L/m	-	28.07%



## CHAPTER 3

### MATHEMATICAL MODEL

#### 3.1 Introduction

Using greenhouses to protect farmed plants from unfavorable growing conditions may affect their early-stage development and may lead to enhancing production. In addition, it faces overheating problems during the day and extreme cold at night. These issues have an impact on both the product's quality and its production. A greenhouse with heated soil and/or air can therefore assist in overcoming these issues. It is required to determine the amount of energy lost in each part of the greenhouse to analyze how the heating system affects the greenhouse. When evaluating a heating system, a number of benefits were taken into account, such as lowering heating costs, improving the quality and quantity of production, and having a good average installation mean life.

#### 3.2 Heat Load Calculation

Analysis of the heating load is the first stage in establishing the heating system capacity of a greenhouse before selecting the elements of a system when constructing a heating system for a greenhouse. The quantity of heat lost from a greenhouse depends on the structure heat loss. Conduction, convection, and radiation are the most common heat transfers from a greenhouse. In a heat loss equation, all three losses are usually added together as a coefficient to figure out how much heat a greenhouse needs. The maximum greenhouse heating load required is calculated based on the minimum ambient air temperature which is

the coldest day during the year. The greenhouse overall thermal losses ( $Q_{G\_loss}$ ) is calculated as follows (Holman, 1999):

$$Q_{Gloss} = U A_G (T_{room} - T_a) \quad (3.1)$$

where:

$A_G$  shows the greenhouse surface area,  $T_{room}$  is the room design temperature,  $T_a$  is ambient temperatures, and  $U$  refers to the energy loss coefficient that can be found as:

$$U = \frac{1}{R_{total}} \quad (3.2)$$

where:

$R_{total}$  is the total thermal resistance of the material, calculated from the following equation:

$$R_{total} = \frac{1}{h_i} + \frac{x}{k_m} + \frac{1}{h_o} \quad (3.3)$$

where:

$h_i$  and  $h_o$  are interior and exterior wall surface convective heat transfer coefficient, respectively,  $x$  shows the thickness of the material, and  $k_m$  is the material thermal conductivity. Sample of calculations are presented in **Appendix A**.

The amount of heat supply from the storage tank to the greenhouse depended on the amount of greenhouse heat required which is varied with time. The following expression gives the heat transfer rate ( $Q_{Hu}$ ) supplied by the heat exchanger to the greenhouse (Holman, 1999):

$$Q_{Hu} = \dot{m}_H C_p (T_{Hi} - T_{Ho}) \quad (3.4)$$

where:

$\dot{m}_H$  states the total mass flow rate through the heat exchanger,  $C_p$  shows the heat capacity of working fluid,  $T_{Ho}$  and  $T_{Hi}$  are the temperatures of the water exiting and entering the heat exchanger, respectively.

### 3.3 Thermal Performance of the FPSC

Hottel and Woertz in 1942 provided the first experimental analysis of the performance of FPSCs, which was later expanded by ASHRAE to provide a standard for assessing the performance of FPSCs. Exposing the functioning collector to solar radiation and measuring the fluid inlet and outlet temperatures and the fluid flow rate is the most basic method of determining collector performance. To calculate the thermal performance of FPSCs, the useful heat gain ( $Q_{Cu}$ ) from FPSC's must first be calculated as follows (Deceased and Beckman, 1982):

$$Q_{Cu} = \dot{m}_C C_p (T_{Co} - T_{Ci}) \quad (3.5)$$

where:

$\dot{m}_C$  specifies the collector fluid mass flow rate,  $T_{Co}$  and  $T_{Ci}$  are collector exiting and entering fluid temperatures.

On the other hand, to show the effect of the collector optical properties and heat losses, the usable energy gained by the working fluid can also be represented in terms of the overall loss coefficient  $U_L$ , absorbed solar radiation  $S$

and the heat removal factor  $F_R$ . The following formulae are used to determine the usable energy (Deceased and Beckman, 1982):

$$Q_{Cu} = F_R A_c [G_T (\tau\alpha) - U_L (T_{Ci} - T_a)] \quad (3.6)$$

where:

$F_R$  is the collector heat removal factor,  $A_c$  specifies the gross area of the collector,  $G_T$  indicates the intensity of solar radiation,  $\tau\alpha$  shows the effective absorptance–transmittance product,  $U_L$  indicates the overall heat transfer coefficient,  $T_{Ci}$  is the input fluid temperature, and  $T_a$  is the ambient temperature.

The flat plate solar collector thermal efficiency  $\eta_{th}$  can be estimated as:

$$\eta_{th} = \frac{Q_{Cu}}{G_T A_c} \quad (3.7)$$

Substituting Eq. (3.6) into Eq. (3.7) gives:

$$\eta_{th} = F_R (\tau\alpha) - F_R (U_L) \left( \frac{T_{Ci} - T_a}{G_T} \right) \quad (3.8)$$

Instantaneous efficiency is determined from Eq. (3.7) and is planned as a result of reduced temperature parameters  $\left( \frac{T_{Ci} - T_a}{G_T} \right)$ . Based on Eq. (3.8), assuming  $U_L$ ,  $F_R$ , and  $(\tau\alpha)$  all remained the same, the plots of  $\eta_{th}$  versus  $\left( \frac{T_{Ci} - T_a}{G_T} \right)$  would be straight lines with intercept  $F_R (\tau\alpha)$  and slope  $(-F_R U_L)$ .

### 3.4 Thermophysical Properties of Nanofluids

Compared to standard fluids, nanofluids have much better thermal and physical properties. For example, their physical phenomena, thermal diffusivity, and

convective heat transfer coefficients are much higher than standard fluids. Dispersing nanoparticles into the base fluid has a strong impact on the thermophysical properties of nanofluids (Angayarkanni and Philip, 2015), Water and Al<sub>2</sub>O<sub>3</sub>-nanoparticles thermophysical properties are presented in Table 3.1. Various nanomaterials can change their properties for different periods of time. Some of the most critical parameters that may significantly affect a material's thermophysical properties are the concentration of nanoparticles, purity level, form, and size of nanomaterials. Nanofluid thermophysical properties are discussed in this section.

Table 3.1 Thermo physical properties of the working fluids.

Particle & base fluid	particle size (nm)	$k$ (W/m.K)	$C_p$ (J/kg.K)	$\rho$ (kg/m <sup>3</sup> )	$\mu$ (mPa.s)
Al <sub>2</sub> O <sub>3</sub>	50	40	773	3960	-
Water	-	0.605	4179	997.1	0.89

### 3.4.1 Thermal Conductivity

One of the most specific characteristics of the nanofluid is an improvement in thermal conductivity over the base fluid, even at small particle fractions. Thermal conductivity is a property of any material responsible mainly for heat transfer. Thus, if needed to enhance the heat transfer rate, it must concentrate on thermal conductivity. The addition of nanoparticles raises the thermal conductivity of a standard fluid due to Brownian motion, which is a crucial process governing the thermal behavior of nanoparticles–fluid

suspensions. The mixture's thermal conductivity ( $k$ ) can be calculated using the following formula (Yu and Choi, 2003):

$$k_{nf} = k_{bf} \left[ \frac{k_p + 2k_{bf} - 2\varphi(k_{bf} - k_p)}{k_p + 2k_{bf} + \varphi(k_{bf} - k_p)} \right] \quad (3.9)$$

where:

$\varphi$  is particle percentage concentration by weight,  $bf$  specifies the base fluid,  $np$  indicates the nanoparticle, and  $nf$  shows the nanofluid.

### 3.4.2 Density

Density is another crucial factor in figuring out how well heat transfer works in nanofluids. It directly affects the Nusselt and Reynolds numbers, pressure loss, and friction factor. The nanofluid density ( $\rho$ ) is determined by applying the following equation (Buonomo *et al.*, 2018):

$$\rho_{nf} = (1 - \varphi)\rho_{bf} + \varphi\rho_{np} \quad (3.10)$$

### 3.4.3 Specific heat

The specific heat of a nanofluid is an essential parameter that is used to describe the nanofluid because of the crucial role it plays in the processes of heat transfer and heat storage. Based on the base fluid, nanofluids may either increase or reduce their specific heat ( $C_p$ ); it depends on the kinds and concentrations of nanoparticles, temperatures, and types of base fluids. Moreover, the nanofluid's heat capacity ( $C_p$ ) is calculated as follows (Xuan and Roetzel, 2000):

$$C_{p,nf} = \frac{(C_p\rho)_{bf}(1-\varphi)+(C_p\rho)_{np}(\varphi)}{\rho_{nf}} \quad (3.11)$$

### 3.4.4 Viscosity

The use of nanoparticles increases the viscosity, which improves the material's thermal properties. With more nanoparticles, the viscosity of the nanofluid goes up because the friction between nanoparticles and adjacent layers of the base fluid and between nanoparticles themselves goes up as intermolecular layers form. The nanofluids viscosity increased with an increase in concentration and a high volume fraction of particles. When viscosity rises, the Prandtl number increases while reducing the Reynolds number, which affects the amount of heat transferred and the pumping power (Ganvir, Walke and Kriplani, 2017). Additionally, the viscosity ( $\mu$ ) of the nanofluid is found as follows (Sarkar, 2011):

$$\mu_{nf} = \mu_{bf}(1 + 2.5\varphi) \quad (3.12)$$

### 3.5 Pressure Drop and Pumping Power Analysis

A forced convection electric pump maintains a steady fluid flow in a flat plate solar collector system. However, pumping power can be estimated based on the pressure drop. The pressure drop  $\Delta P$  that occurs in process piping systems is an essential consideration in evaluating pipe flow since it significantly affects the amount of power required by the pump to maintain the flow. The friction created by fluids rubbing against pipe components and the internal walls of a piping system results in a pressure drop. The working fluids density and friction factor

are the two most important determinants of pressure drop. The total pressure drop is determined by applying the following equation (Alim *et al.*, 2013):

$$\Delta P = f \frac{\rho V^2}{2} \frac{\Delta l}{D_i} + \sum K_l \frac{\rho V^2}{2} \quad (3.13)$$

where

$f$  indicates the friction factor,  $\rho$  shows the density of the fluid,  $V$  is the mean flow velocity,  $\Delta l$  indicates the pipe length,  $D_i$  represents the pipe inside diameter,  $K_l$  is the loss coefficient of valves or fittings. Table 3.2 illustrates the values of  $K_l$  for several types of valves and fittings.

The frictional factor for laminar and turbulent flow, respectively, is calculated by using the following formulas:

$$f = \frac{64}{Re} \quad \{\text{Laminar flow}\} \quad (3.14)$$

$$f = \frac{0.079}{(Re)^{1/4}} \quad \{\text{Turbulent flow}\} \quad (3.15)$$

The Reynolds number  $Re$  is determined using the following equations (Alim *et al.*, 2013):

$$Re = \frac{\rho V D_i}{\mu} \quad (3.16)$$

The mean flow velocity  $V$  can be calculated using the following formula:

$$V = \frac{\dot{V}}{A_p} \quad (3.17)$$



where

$\dot{V}$  indicated the total volume flow rate,  $A_p$  shows the cross-section area of the pipe.

Finally, the pumping power is calculated as follows (Bezaatpour and Rostamzadeh, 2021):

$$\text{pumping power} = \dot{V} \times \Delta P \quad (3.18)$$

Table 3.2 The values of  $K_l$  for several types of valves and fittings.

Valve or Fitting	Type	Loss Coefficient ( $K_l$ )
Global valve	Fully open	10
	½ open	12.5
Gate valve	Fully open	0.19
	½ open	4.5
	¼ open	24
Ball valve	Open	0
Elbow	45°	0.4
	90°	0.75
Tee	Line flow	0.4
	Branch flow	1.5

### 3.6 Economic Analysis

In this section, the SWHS cost, energy cost, and payback time are compared with the price of a water heating system with electricity to conduct an economic analysis of the water heaters. The payback period refers to the time it takes for an

investment to earn back its initial cost or the time it takes for an investor to break even. The SWHS used in this investigation cost a total of \$50,400; in Erbil city, the cost of one kWh of electricity is \$0.23 according to the Ministry of Electricity in Kurdistan region. The SWHS costs and payback period are reported in Table 3.3. Interestingly, the data in this table is that the system payback duration is about 6 years when using nanofluid as a working fluid, while when using water, it is about 7 years. The following formulas are used to determine the Annual payment saving (*APS*):

$$APS = GE \times EC \quad (3.19)$$

where:

*GE* indicates the Gain of energy, *EC* shows the electricity cost.

Additionally, the payback duration (*PD*) can be written as follows:

$$PD = \frac{TC}{APS} \quad (3.20)$$

where:

*TC* is the total cost of the SWHS

Table 3.3 The costs and payback period of the SWHS.

	Water	Nanofluid
Gain of energy (kWh/year)	30685.56	37506.25
Annual payment saving (\$/year)	7057.68	8626.44
Payback of SWHS (year)	7.14	5.84

## CHAPTER 4

### EXPERIMENTAL SETUP

#### 4.1 Introduction

The experimental setup is performed and reported in detail in this chapter. The experimental prototype was set up in the Scientific Research Center in Erbil, Kurdistan, Iraq (36.2 °N latitude and 44 °E longitude). This region has a high rate of sunlight in the summer, and a high frequency of bad weather days throughout the winter, Figure 4.1 depicts the current setup of the system. Additionally, a technique that used for nanofluid preparation was explained in detail. There are the main components of system design:

- Greenhouse
- Flat plate solar collectors
- Hot water storage tanks
- Circulation pumps
- Temperature sensors
- Pressure sensors
- Flow sensors
- Energy meter
- Piping System
- Residential water softener
- Expansion vessel
- Controllers
- Pyranometer

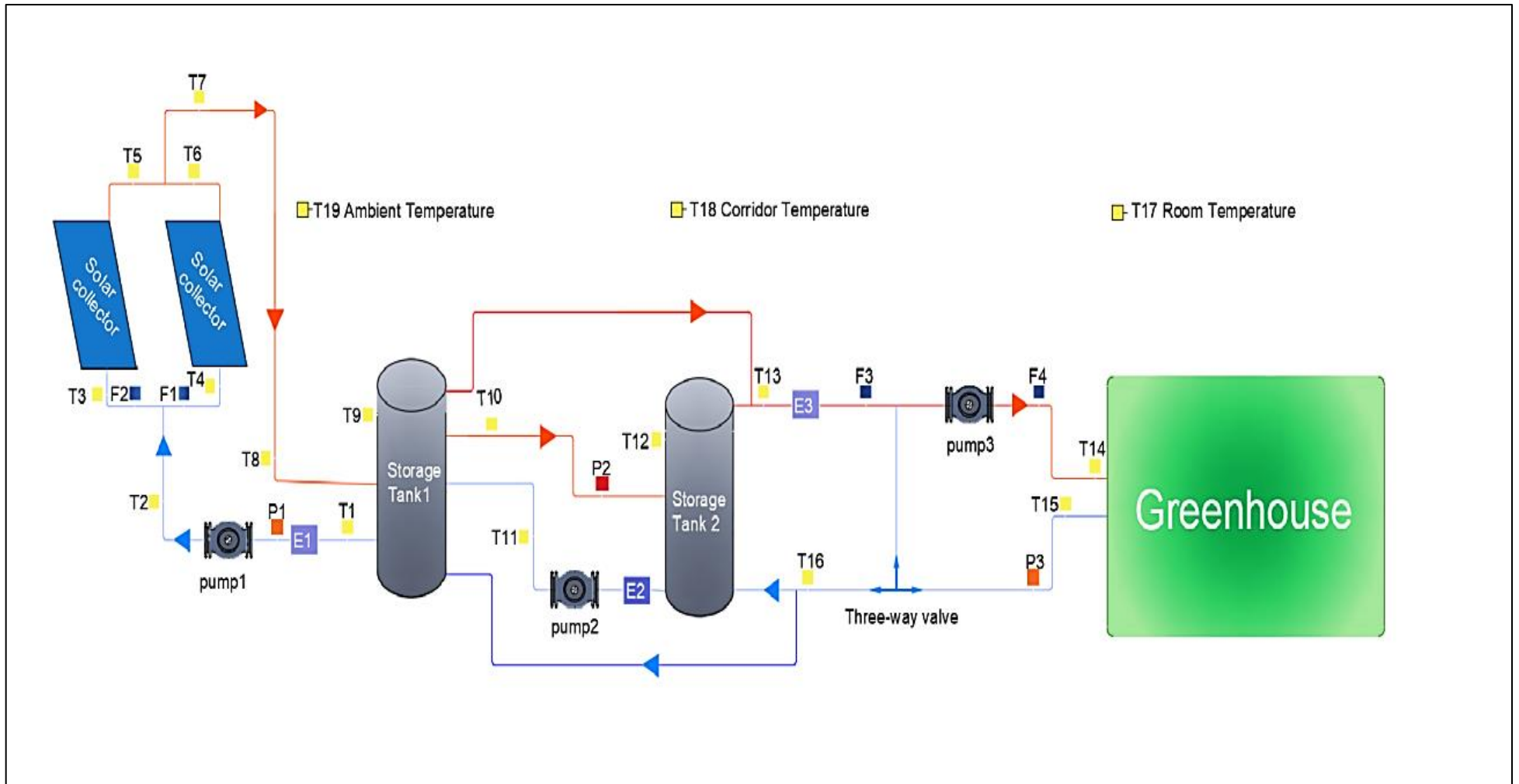


Figure 4.1 Experimental setup of SWHS.

## 4.2 Components of System Design

All the major individual components that were used in the experiment are described as follows:

### 4.2.1 Heating Load

Greenhouses come in various shapes, sizes, and materials that are utilized for the frame and the covering. A greenhouse's structure is often made of wood, aluminum, or steel, while most of the typical covering materials include polyethylene and glass. Climate, technical advancement, economic factors, and product type in each region or country are the factors that affect the type of greenhouse that is utilized.

A greenhouse with  $85.8 \text{ m}^3$  in volume was installed in the backyard of the Research Center Building with the dimensions of (5.25 m length, 4.95 m width, and 3.6 m height) as shown in Figure 4.2, with a horizontal buried heat exchanger type (**PE-XC EVOH**) with 1-inch in diameter placed at 10 cm underground, as shown in Figure 4.3. The walls and the roof were all made of a single glass with 1 cm thickness.

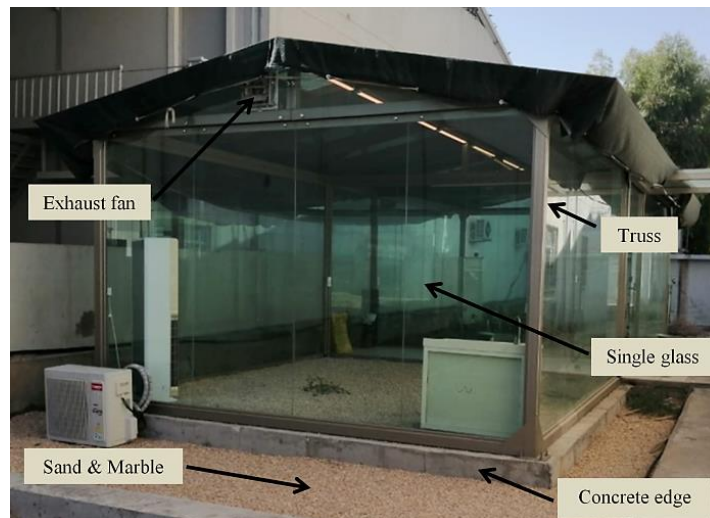


Figure 4.2 Schematic of the test greenhouse external view.

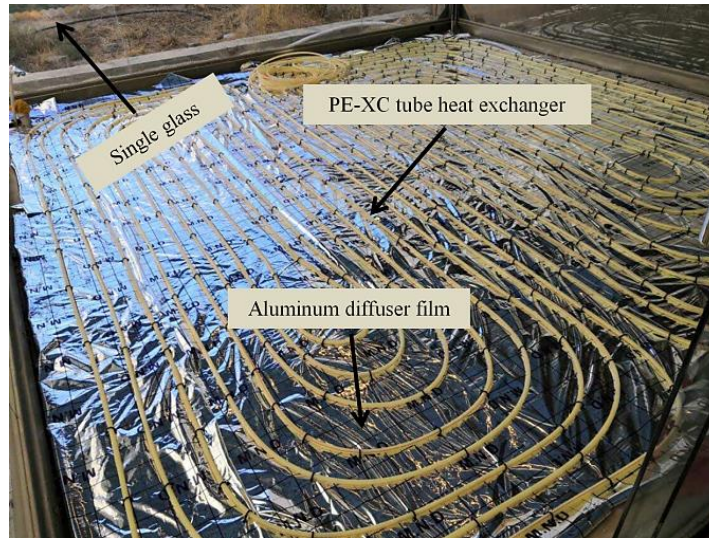


Figure 4.3 Tubular heat exchanger buried under the greenhouse.

#### 4.2.2 Flat Plate Solar Collector (FPSC)

The model of the flat plate solar collectors used in this work is **Wikosun 2020-Mi/2340-Ti**, which is installed on the top of the Scientific Research Center Building. The system consists of ten flat plate solar collector panels, with an area of  $2 \text{ m}^2$  each, set in two parallel rows (five by five) tilted southward in an angle of  $60^\circ$  (which is the optimum angle in winter season), as shown in Figure 4.4. This kind of FPSC has robust characteristics, and the copper plate absorber is covered with a specific selective Tinox surface. The collector design is made up of four copper parallel tubes joined at each end by two pipes, the intake and exit manifolds, with a 22 mm outer diameter. This collector has a maximum working pressure of 10 bar, a stagnation temperature of  $208 \text{ }^\circ\text{C}$ , and an efficiency of 80.1%. The technical specification of the FPSC is given in Table 4.1.



Figure 4.4 Photograph of the FPSC.

Table 4.1 Technical Specification of FPSC.

Content	Description
Collector gross surface	2.353 m <sup>2</sup>
Absorber surface	2.138 m <sup>2</sup>
Weight	44 kg
Length x width x depth	2150 x 1090 x 100 mm
Cover	3.2 mm protection glass, super transparent, hailstone secure
Absorber material	Copper on copper plate
Insulation rear wall	40 mm mineral wool 70 kg/m <sup>3</sup> with glass fiber
Insulation side wall	30 mm mineral wool
Peak power	1713 Watt / collector

### 4.2.3 Storage Tanks

In this study, two indirect and no-backup storage tanks of **WBO 1005 UNO/DUO** type with a maximum working pressure and temperature of 16 bar

and 130°C, respectively, were employed as shown in Figure 4.5. Each of these tanks has a 1000-liter in capacity, is filled with water, and contains two helically coiled heat exchangers, one at the lower level and one at the top level of the storage tank. The lower heat exchanger in the first storage tank is linked to the solar collectors, while the upper heat exchanger is connected to the heat exchanger at the lower level of the second storage tank. Table 4.2 displays the heat exchanger's technical specifications. The tank has a diameter of 0.79 m, a height of 2 m, and an insulating layer of 0.1 m thick fleece. In addition, there are two electrical heater plugs. Two additional pipe plugs are placed on these storage tanks to supply hot water to the load zone (greenhouse in this case) and return cold water from the load zone. A temperature sensor, a flange, a sensor gauge, and an external current node on the top of the tanks are also connected.

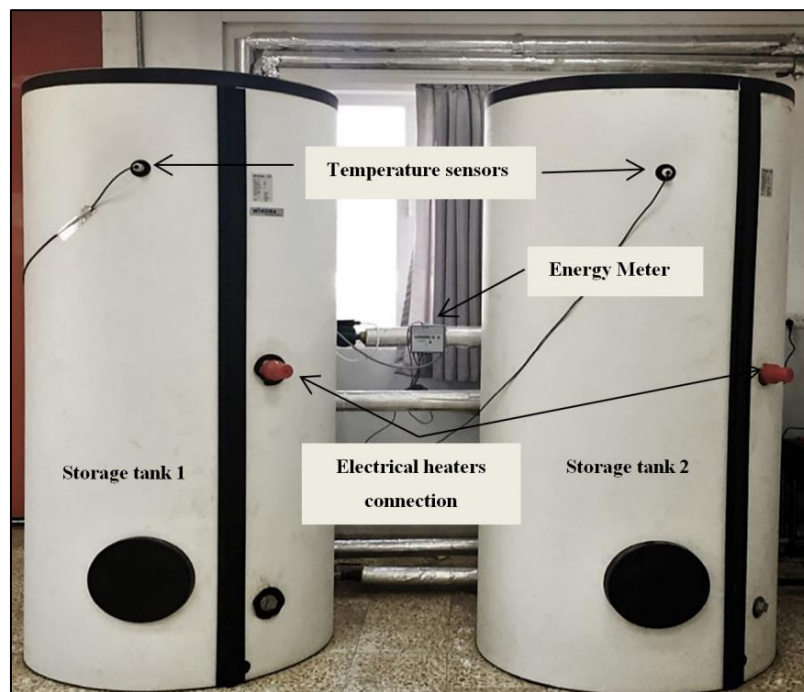


Figure 4.5 Photograph of the storage tanks.



Table 4.2 Specifications of the heat exchanger.

Content	Description
Capacity of heat exchanger lower-upper	19.8 liter- 13.3 liter
Surface of heat exchanger lower-upper	3 m <sup>2</sup> - 2 m <sup>2</sup>
Flow rate of heat exchanger lower-upper	2.4 m <sup>3</sup> /h- 2.4 m <sup>3</sup> /h
Pressure loss of heat exchanger lower-upper	158 mbar- 108 mbar

#### 4.2.4 Pumps

A total of three pumps were used in this experiment to circulate fluid. The first pump is connected between the collectors and the first storage tank, while the second pump is connected between the first and second storage tanks, as shown in Figure 4.6 (a). Their types are Speroni **SCR 25/80–180–230 V–3** with rotation speeds of (low, medium, and high), with a power of (122, 159, and 170) watt, respectively. Furthermore, the maximum operating pressure and temperature range are 10 bar and (5 to 110)°C, respectively. The third pump type is **DAB VS 35/150 M (EVO)** with 56 watts and 0.25 amps, which is utilized to circulate water from the storage tank to the greenhouse, as indicated in Figure 4.6 (b).



(a)



(b)

Figure 4.6 Water circulation pumps type of (a) SPERONI; and (b) DAB.

#### 4.2.5 Temperature Sensors

This work employs three different kinds of temperature sensors. The first temperature sensor used is a cable temperature sensor from **SIEMENS** and its type is **QAP21.2**. This kind of sensor is made of nickel and is fixed to the outside wall of the pipe using a cable tie made of stainless steel. The second temperature sensor type is **QAE26.9** which is immersion temperature sensor made by **SIEMENS**. This sort of sensor is constructed from stainless steel and has a submerged stem inside the pipe. Figures 4.7 (a) and (b) display these two kinds of sensors. The third temperature sensor type used is **QAA25**, as shown in Figure 4.7 (c), which is a room temperature sensor and set-point temperature adjuster installed inside the greenhouse zoon. Technical specification of these temperature sensors are presented in **Appendix B**.

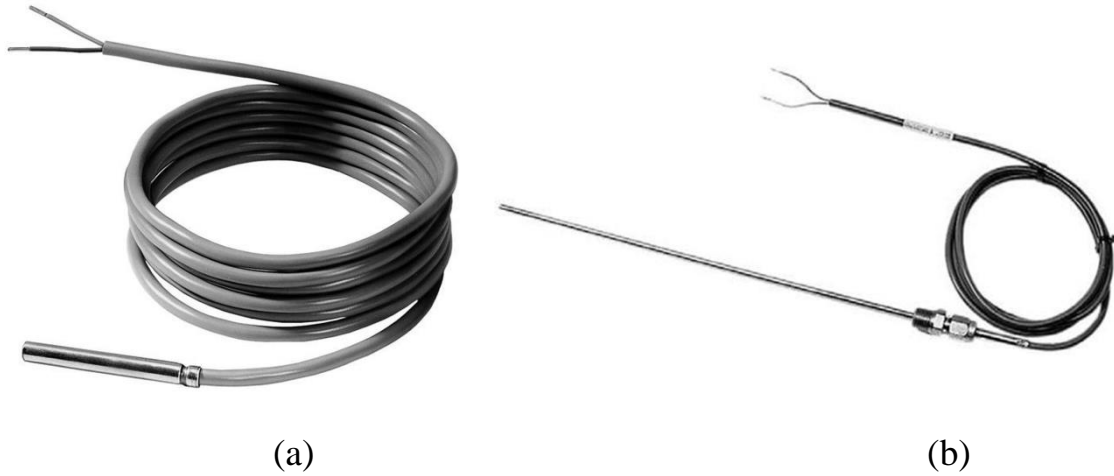


Figure 4.7 Temperature sensors (a) QAP21.2; (b) QAE26.9; and (c) QAA25.

#### 4.2.6 Pressure Sensor

A pressure sensor is used to determine the pressure inside the piping system at different locations. Three main locations for the pressure sensors were chosen: before the solar collectors, between the storage tanks, and before the greenhouse. This pressure sensor model is **QBE2002-P10** from **SIEMENS**,

having a pressure range of (0–10) bar, and measuring accuracy of 0.4% of full scale. Figure 4.8 illustrates the pressure sensor used in this work.



Figure 4.8 Pressure sensor.

#### 4.2.7 Flow Meter

In this study, the water flow rate through the piping system was measured using a flow meter model of **QVE3100** from **SIEMENS**, as illustrated in Figure 4.9. This flow meter is an automatic flow sensor that continuously measures the flow. It is constructed of brass, has a connection attached to the controller, and displays data on the computer. The specifications and calibration of this kind of flow meter are shown in **Appendix B**.



Figure 4.9 Flow rate measuring sensor.

#### 4.2.8 Piping System

As illustrated in Figure 4.11, this system used black steel pipes with a diameter of 25.4 mm that were insulated with fiberglass insulation to reduce heat loss. Also, the external pipes were insulated with fiberglass and covered with an aluminum sheet to protect them from the weather.



Figure 4.11 Piping System.

### 4.2.9 Pyranometer

In this work, the pyranometer type (**LP02**), which measures the solar radiation over the complete solar spectrum range of (285 to 3000 nm) and maximum irradiance of ( $2000 \text{ W/m}^2$ ), was used to record total solar irradiance and performance data was obtained using a high-accuracy handheld read-out device/data-logger (**LI19**), as shown in Figure 4.12.



Figure 4.12 LP02 pyranometer with LI19 read-out unit/data-logger.

### 4.3 Material

The working fluid used in this study is distilled water (DW) as a first run and water-based  $\text{Al}_2\text{O}_3$  nanoparticles as a second run. Reagent grade chemicals were used in the experimental investigation.  $\text{Al}_2\text{O}_3$  white powders with a purity of +99.9% and a mean diameter of 50 nm average diameter produced by (Skyspring nanomaterials, USA) Company were used for the experimental investigation. A **SEM** image of nanoparticles is indicated in Figure 4.13.

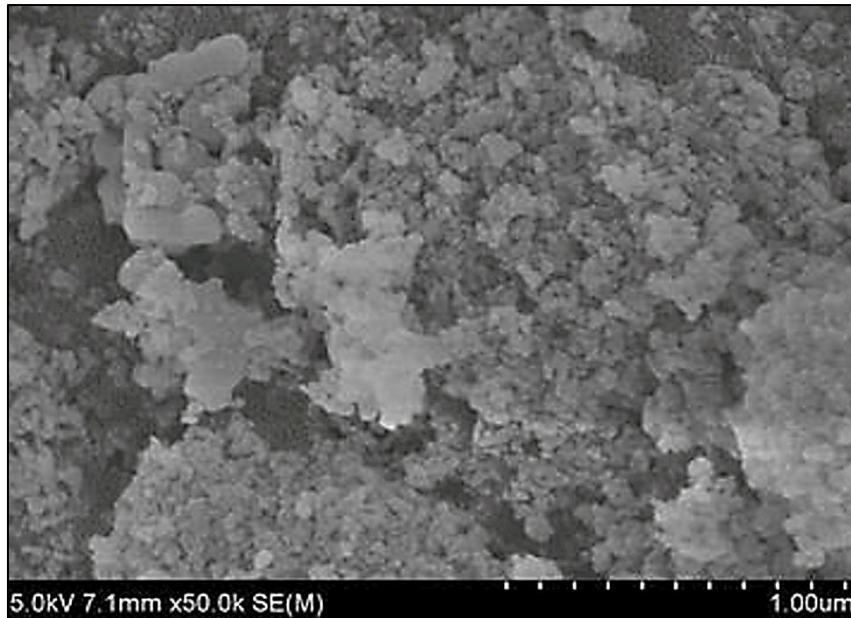


Figure 4.13 SEM images of Al<sub>2</sub>O<sub>3</sub> nanoparticles (Skyspring Company).

#### 4.4 Preparation Method of the Nanofluid

Nanoparticles are dispersed in a base fluid to create nanofluid. The properties of Al<sub>2</sub>O<sub>3</sub> nanoparticles are simple to make, inexpensive compared to other metal oxides nanoparticles (Arthur and Karim, 2016), and have excellent thermal conductivity. A technique has been used to minimize Al<sub>2</sub>O<sub>3</sub> agglomeration and rising dispersion behavior by dispersing Al<sub>2</sub>O<sub>3</sub> powder nanoparticles in distilled water as the base fluid. Figure 4.14 illustrates the procedure of nanofluid preparation. First, the nanoparticles were added to distilled water and dissolved by magnetic stirrer for 10 minutes. Second, an ultrasonic homogenizer (40 kHz) frequency was utilized for approximately 15 minutes to disseminate the nanoparticle mixture and decrease agglomeration. Figure 4.15 shows the magnetic stirrer and the ultrasonic homogenizer used for nanofluid preparation, where this entire process was performed in the laboratory of the Scientific Research Center at Erbil Polytechnic University.

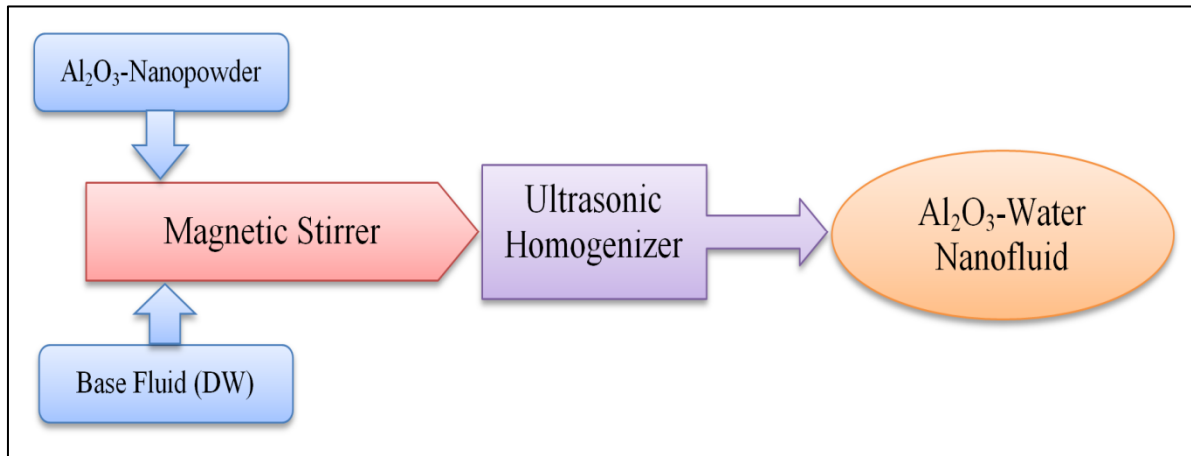


Figure 4.14 Nanofluid preparation diagram.



Figure 4.15 Magnetic stirrer and ultrasonic homogenizer.

#### 4.5 Operating methods

This work is a preparation to an experiment whose primary aim is to determine the most appropriate heating system characteristics for each type of agricultural production. A secondary aim is to reach a temperature of 23°C,



which is appropriate temperature for many vegetable products. The solar water heating system operated in this study is a closed system. In the first test, distilled water was used as a working fluid to transfer heat from the solar collectors to the storage tank. In the second test, nanofluid was used in the closed loop connecting the solar collectors with the storage tank instead of distilled water to increase the thermal efficiency of the system. The system was run as demonstrated in the process below:

First, switch on the water softener and control pump. Once the steel tank has filled with water from the water softener, switch on all the pumps to fill the system until reaching to the setup system pressure. To vent the system, ensure there is no air in the system by opening all the safety valves on the collectors, storage tanks, greenhouse, and piping system. After that, close all the safety pressure valves. Then, cold working fluid from the lower heat exchanger inside the storage tank is pumped to the collectors. Using the absorber plate, these collectors absorbed solar radiation and convert into usable heat energy, which is subsequently and returned to the heat exchanger; after that, the heated fluid will exchange its heat with the cold water that is stored inside the tank, and then it will be pumped back to the solar collectors. The circulating pump between the storage tank and the solar collectors will operate automatically under two conditions. First, during cloudy days, the circulating pump between the storage tank and the solar collectors will automatically turn on when the water temperature exit from the collectors is 2°C higher than the water temperature inlet to the collectors. Second, it turns on automatically to prevent water freezing overnight when the outside air temperature becomes lower than 4°C. Each measuring signal has been transferred to a computer monitor using the (DESIGO INSIGHT) program as shown in Figure 4.16.

When the water temperature in the storage tanks increases, the circulation pump connecting the storage tank with the greenhouse will turn on. The stored heat in the tank will be transferred through the buried heat exchanger where it heats the greenhouse space till reaching the set point temperature (23°C in this case). The exit water from the greenhouse heat exchanger will be allowed to return through the cold line to the storage tank to reheat it again and recirculate it through this loop. A 3D design diagram of a solar water heating system is shown in Figure 4.17.

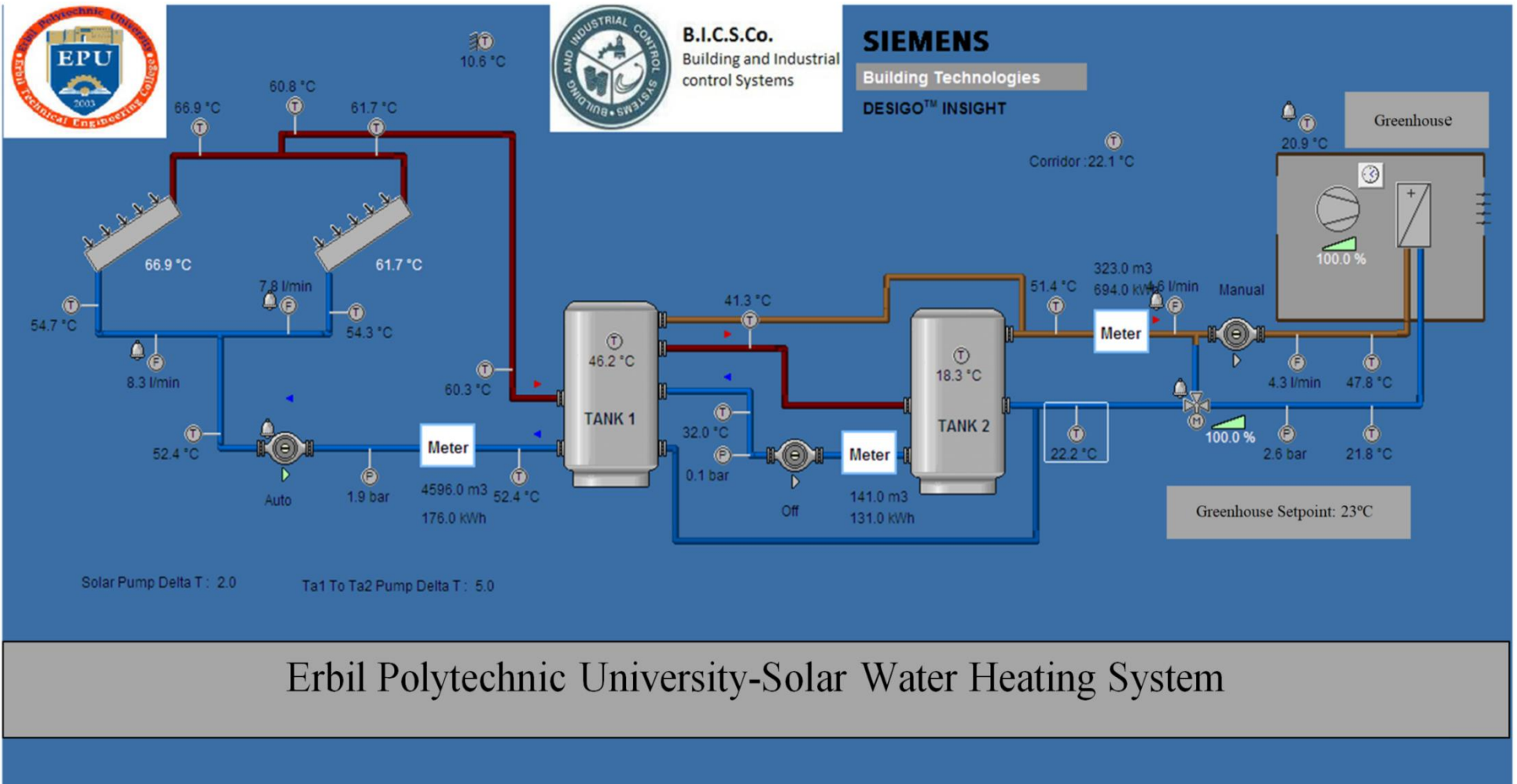


Figure 4.16 A screen shot of the computer program software (DESIGO INSIGHT).

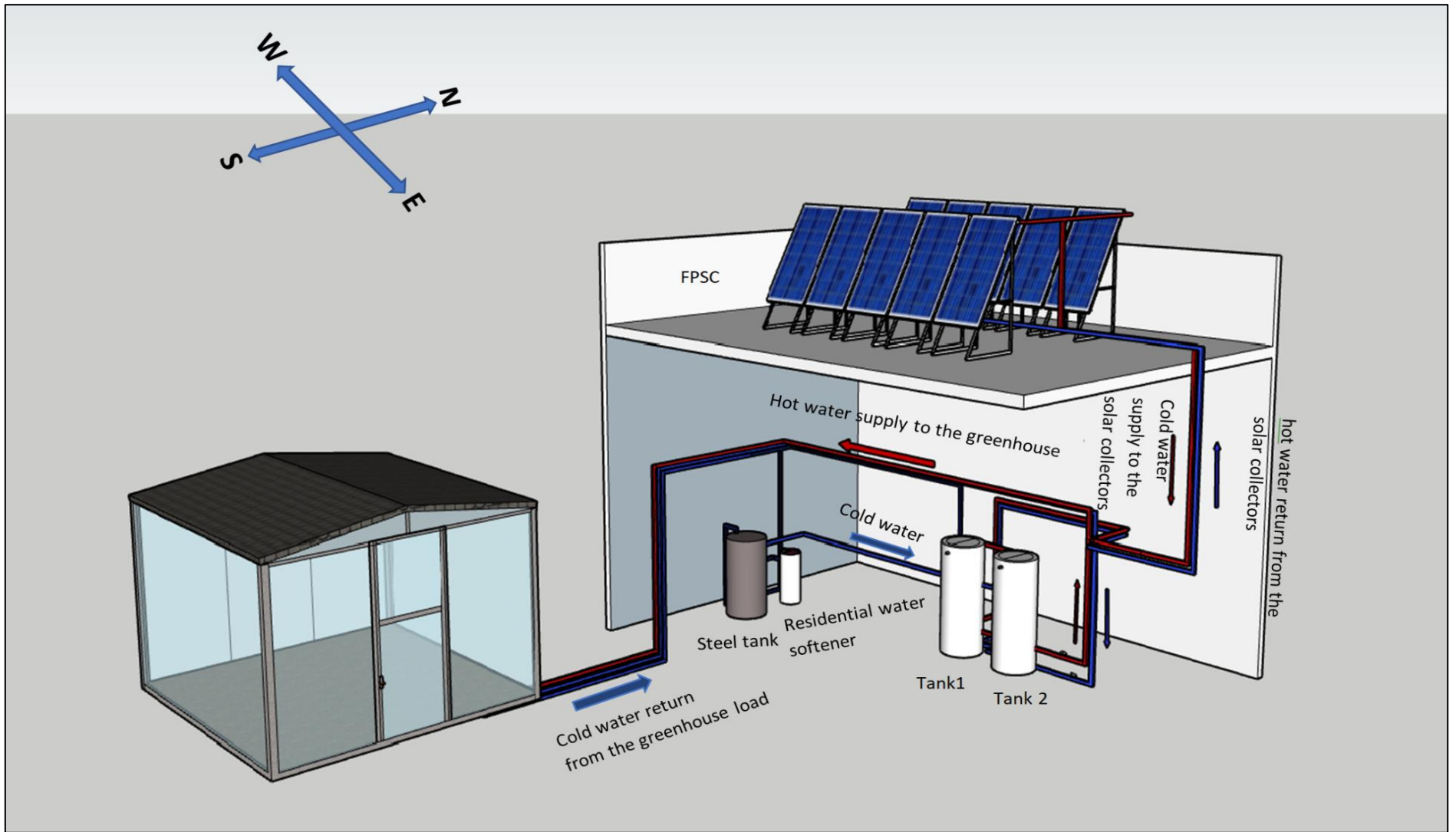


Figure 4.17 A 3D design diagram of a solar water heating system.

## 4.6 Uncertainty Analysis

The precision of results obtained are determined by uncertainty analysis. Because of the inaccuracies generated by data reading, instrument selection, test circumstances, surroundings, observance, and other factors, uncertainty analysis should be performed regardless of how appropriate the instruments are. The primary causes of uncertainty in collector efficiency estimation include errors in solar irradiance, mass flow rate, and temperature measurements. The standard deviation and mean of different measurements are included in the Gaussian distribution approach and are given as (Mukherjee *et al.*, 2020):

$$U_x = \pm \left( 2 \frac{\sigma_n}{x_n} \right) \times 100 \quad (4.1)$$

where:

$U_x$  represents measurement uncertainty,  $\sigma$  signifies the measured data standard deviation, and  $x_n$  symbolizes the mean measured parameters. The number of measurements are indicated by the suffix  $n$ . The uncertainties of the primary apparatuses utilized in this investigation are shown in Table 4.3.

Table 4.3 The uncertainty of the measuring devices.

Measuring device	Uncertainty (%)
Pyranometer	$\pm 1.08$
Flow meter	$\pm 0.85$
Thermometer	$\pm 2.3$
Useful heat gain	$\pm 3.36$

## CHAPTER 5

### NUMERICAL SIMULATION MODEL

#### 5.1 Introduction

TRNSYS (TRaNsient System Simulation) is a program that has been available since 1975. It is a commercially accessible application that is often used to study and simulate the performance and behavior of systems as a function of time (Jani *et al.*, 2020). TRNSYS is a comprehensive and extensible simulation program for the transient simulation of multi-zone systems such as greenhouses, among other modeling software. It is used to test the energy concepts of systems, from simple domestic hot water systems to the design and modeling of buildings and their equipment, including control techniques, occupant behavior, and alternative energy systems (wind, solar, photovoltaic, hydrogen systems, etc.).

The software has several subroutines that represent subsystem components. Ordinary differential or algebraic equations are used to describe the mathematical models of the different subsystems. As a first step in simulating the whole system, it is necessary to identify the individual components whose combined performance best defines the overall system performance (Kalogirou, 2001). There are several constant parameters and time-dependent INPUTS and OUTPUTS for each element, represented by boxes.

## **5.2 The TRNSYS Simulation Program's Components**

In TRNSYS, the system model consists of the essential components that make the system run. Each part is identified by its UNIT number, which identifies a FORTRAN procedure that models the component. The schematic layout of the SWHS model using the TRNSYS program is displayed in Figure 5.1. This section describes the major individual component model used to simulate the system as follows:

### **5.2.1 Weather Data (Type 15-2)**

This type was used to input the weather data into the TRNSYS simulation program. It includes hourly data on solar radiation, temperature, and other meteorological parameters. The typical meteorological year (TMY2) data files of Erbil's weather data with latitude and longitude (36.2°N, 44°E) were used. The ambient temperature variation for the whole year is shown in Figure 5.2. An example of the TRNSYS simulation results are shown in **Appendix C**. Nevertheless, it is connected to Type 56, which represents a greenhouse load; moreover, it is connected to the flat plate collector Type 1b.

### **5.2.2 Solar Collector (Type 1b)**

This component was used to model and analyze FPSC's thermal performance. User specified parameters include the number of collectors in series, collector area, intercept efficiency, fluid specific heat, etc. Series and parallel configurations are possible for the array of solar collectors. This research was conducted using two different fluids, distilled water and nanofluid. A Type 156 water tank is connected to the solar collector.

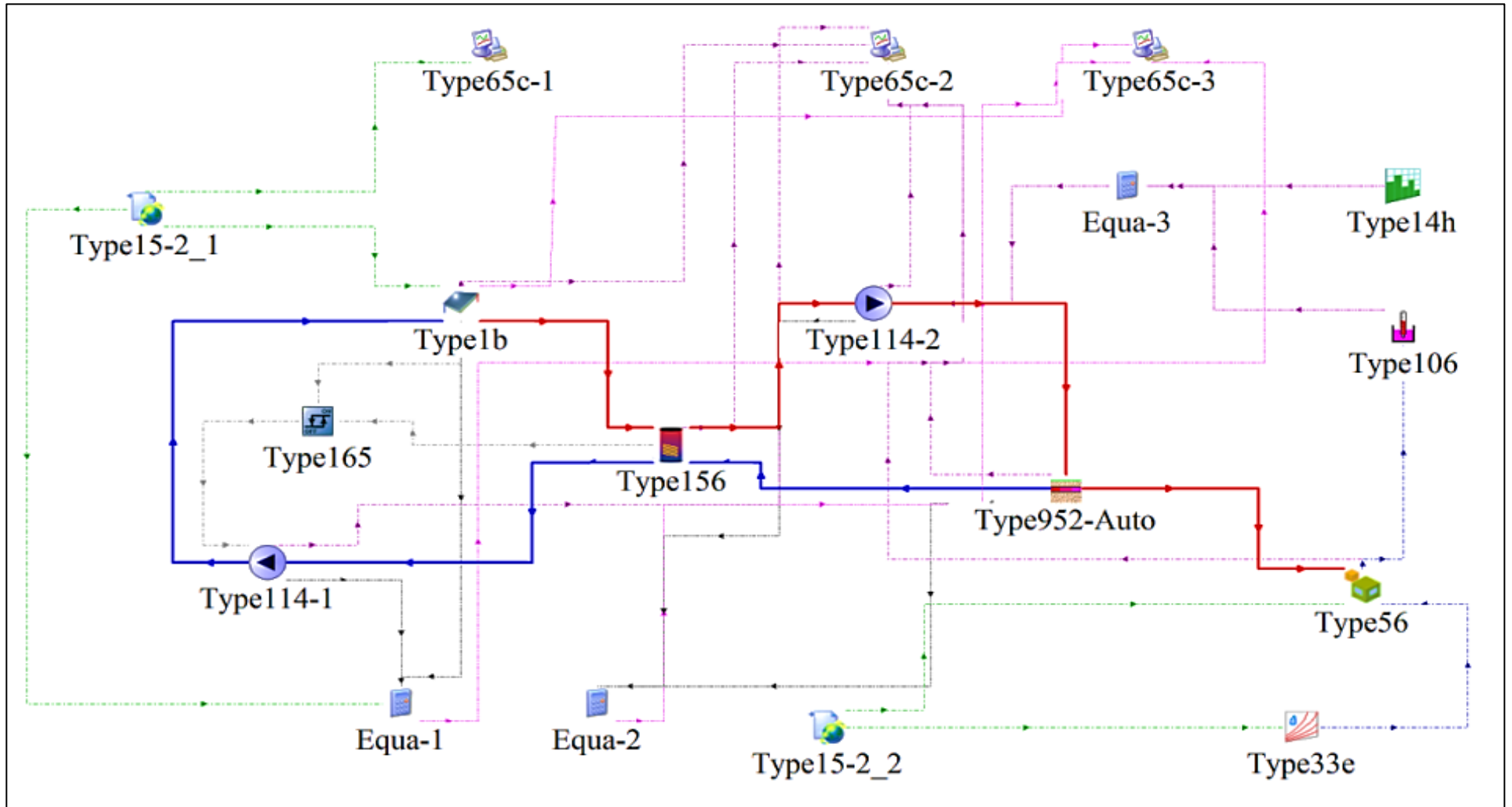


Figure 5.1 TRNSYS modeling of the SWHS.



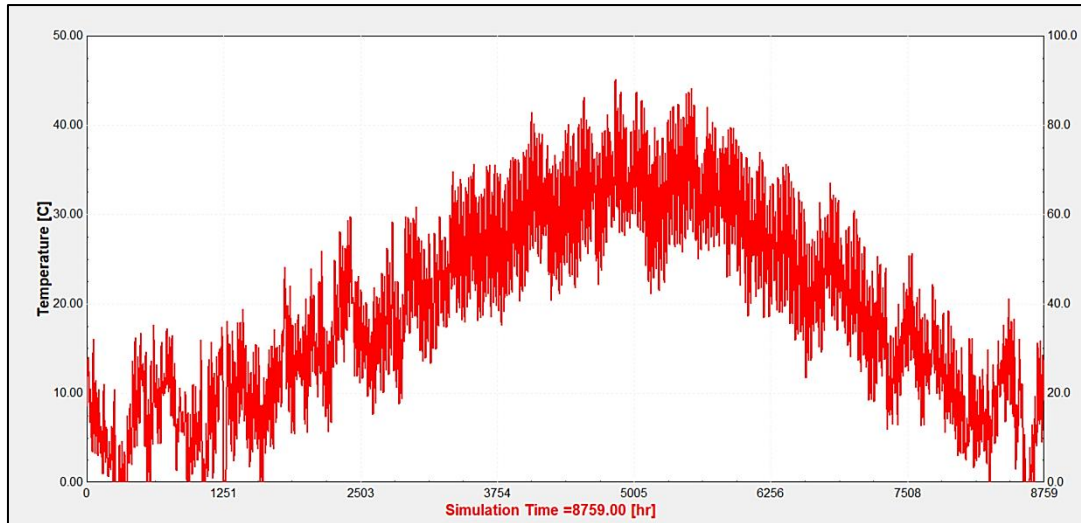


Figure 5.2 Yearly ambient temperatures for the city of Erbil.

### 5.2.3 Storage Tank (Type 156)

A stratified storage tank considering a constant volume with an immersed coiled-tube heat exchanger and volume equal to 1 m<sup>3</sup> and 2 m height was used in this study. To model the stratification found in storage tanks, the tank is subdivided into isothermal temperature nodes, and the user specifies the number of "nodes" to regulate the degree of stratification. The fluid in the storage tank and the fluid in the heat exchanger interact, and the heat is transferred from the heat exchanger to the water inside the tank. After that, the heat stored inside the tank will be pumped to the buried pipe Type 952.

### 5.2.4 Pump (Type 114)

This type depicts a pump with a single (constant) speed and a constant mass flow rate. This type uses its rated flow rate parameter and the current value of its control signal input to determine the downstream flow rate. In this work,

two pumps have been used to circulate the working fluid between the collector and the storage tank, and between the storage tank and the load.

### **5.2.5 Controller (Type 165)**

This is the on/off differential controller used to control the function of the circulating pump. The temperature differential specifies the control signals value between the upper ( $T_h$ ) and lower ( $T_l$ ) temperatures. The pump is activated when the collector outlet temperature become greater than the storage tank bottom temperature by  $2^\circ\text{C}$  (upper dead band temperature difference). Otherwise, the pump is turned off when this temperature difference drops below  $2^\circ\text{C}$  (lower dead band temperature difference).

### **5.2.6 Buried Pipe Model (Type 952)**

This type is used to simulate the thermal behavior of fluid flow in a buried pipe, and it is designed to replicate a horizontal insulated buried pipe. This type is linked to the building load and supplies heat from the storage tank to the load to estimate the room heating requirements at  $23^\circ\text{C}$ .

### **5.2.7 Building Load (Type 56)**

Type 56 requires a large amount of building data (e.g. geometrical data, wall construction data, etc.) and other variables (e.g. radiation, ambient temperature, humidity, building schedules, etc.) that influence the building to simulate the thermal behavior of the building. This type is used to model the greenhouse load. A 3-D sample building was enhanced through applying the graphical tools of SketchUp with a length of 5.25 meters, a width of 4.95 meters,

and a height of 3.6 meters. The geometry information is employed in a preprocessing step in TRNBuild, the building input description tool of TRNSYS and it is regarded as a single thermal zone. Moreover, a typical seasonal required heating rate is calculated using this building model.

#### **5.2.8 Forcing Function (Type 14h)**

The Type 14h generates a time-dependent pattern of predefined behavior that it may use for several activities. The forcing function was used to establish a hot water draw profile in this simulation by transmitting its output signal to the load component. The pattern of hot water draws was formed by entering data points at various times of the day. Each period of interest needed numerous data points to create step functions, which depend on linear interpolation between data points, the value specified for each period and the schedule is from 8:00 to 16:00.

#### **5.2.9 Psychrometrics (Type 33e)**

The dry-bulb temperature and humidity ratio of moist air are inputs for this component, which is called the TRNSYS Psychrometrics procedure, which returns the following properties of moist air: dry-bulb temperature, wet bulb temperature, dew point temperature, absolute humidity ratio, enthalpy, and relative humidity.

#### **5.2.10 Output (Type 65a)**

The online graphics component will show the specified system variables during the simulation. This component is highly recommended because it gives

users access to essential variable details and lets them quickly notice if the system is not working as expected. A new plot window will show the selected variables in its tab on the screen. In this case, the data given to the Type65a online plotter is automatically written to an external file that the user chooses once for each time step.

### **5.2.11 Equation Tool (Equa)**

Simple calculations may be performed using TRNSYS equation tool. Users may also use this tool to create and utilize parameters inside the simulation by referencing the parameter name. Model-specific parameters may be entered once and used in many models with the help of this tool. In the equation tool, a parameter may be identified and then set. Thus, the user may apply that parameter to such a component model by inputting a string input for each of the individual component parameters models.

## CHAPTER 6

### RESULTS AND DISCUSSIONS

#### 6.1 Introduction

After calibrating the instruments and installing the laboratory equipment, the experiments were done on sunny days. The experimental and TRNSYS simulation programs were utilized to investigate the collector's performance for greenhouse heating. These investigations were carried out over several days. Moreover, the data were collected every 15 minutes from 8:00 to 16:00. The collector's efficiency was evaluated in terms of working fluid concentration (water,  $\text{Al}_2\text{O}_3$ -nanofluid) under an extensive range of operating conditions.

#### 6.2 Experimental Results

The thermal performance of the FPSC for greenhouse heating systems with various working fluids has been studied via experimental observations and analysis. During the experiment, the inlet and outlet temperatures of the collector and greenhouse, ambient and room temperatures, volume flow rate, and global solar irradiance were measured. This section is divided into three parts. The first part of this section will examine the use of water as a working fluid. The second part gave the results of utilizing nanofluid. Finally, the third part illustrates the comparison between water and nanofluid as HTFs.

### 6.2.1 Water as Working Fluid

In the current investigation, the collector was first tested using water as the working fluid. Experiments were conducted on several clear-sky days on the 8<sup>th</sup>, 10<sup>th</sup>, 12<sup>th</sup>, 13<sup>th</sup>, 16<sup>th</sup>, 25<sup>th</sup>, and 28<sup>th</sup> of March.

In this part, the performance characteristics of the systems were determined by evaluating the results of the tests conducted during the heating period on 8<sup>th</sup> March. On the other hand, due to a similar tendency to the first day, comparisons between the different days are given in **Appendix D**.

In Figure 6.1 the inlet and outlet water temperatures of the solar collector are presented as a function of daytime with a water flow rate of 0.2 kg/s. As can be seen from the figure, due to an increase in solar radiation, the temperatures of the collector rise significantly in the morning, reaching a highest value at around 13:15 (local time). It can be observed that, during high solar radiation, the heat loss is negligible in comparison to the solar thermal energy absorbed by the fluids. Hence, the water temperature rises due to the most efficient heat transfer capacity. However, the temperature of the water falls until the evening as solar radiation declines. The highest and lowest observed outlet temperatures were 28.1°C and 69.7°C, respectively.

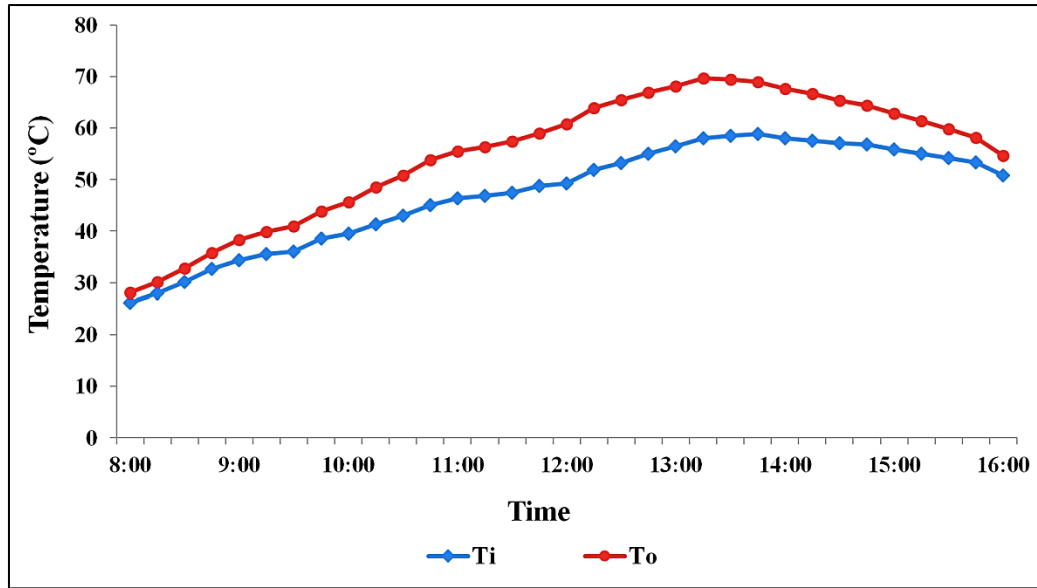


Figure 6.1 Inlet and the outlet collector water temperature of the FPSC on 8<sup>th</sup> March.

In order to evaluate the experimental investigation, the fluctuations of the flat plate solar collector energy efficiencies were investigated experimentally. Figure 6.2 shows how solar collector efficiency and solar irradiance change throughout the day time where Eq. (3.7) was used to figure out solar collector efficiency. Overall, these results indicate that, in the early morning, the collector efficiency rises with increasing incident solar radiation. The highest solar radiation absorbed by the collector occurs between 12:00 P.M. to 12:30 P.M. (local time). The collector efficiency continues to rise until it reaches its peak and then drops with the radiation until evening. Energy efficiency ranges from 31% to 67.9%, averaging 51.8%. As it is known, output temperature is one of the most influential characteristics that directly impact the energy efficiency of a flat plate solar collector. During the experiment, with the collector's maximum output water temperature, the collector's highest efficiency reached 67.9%.

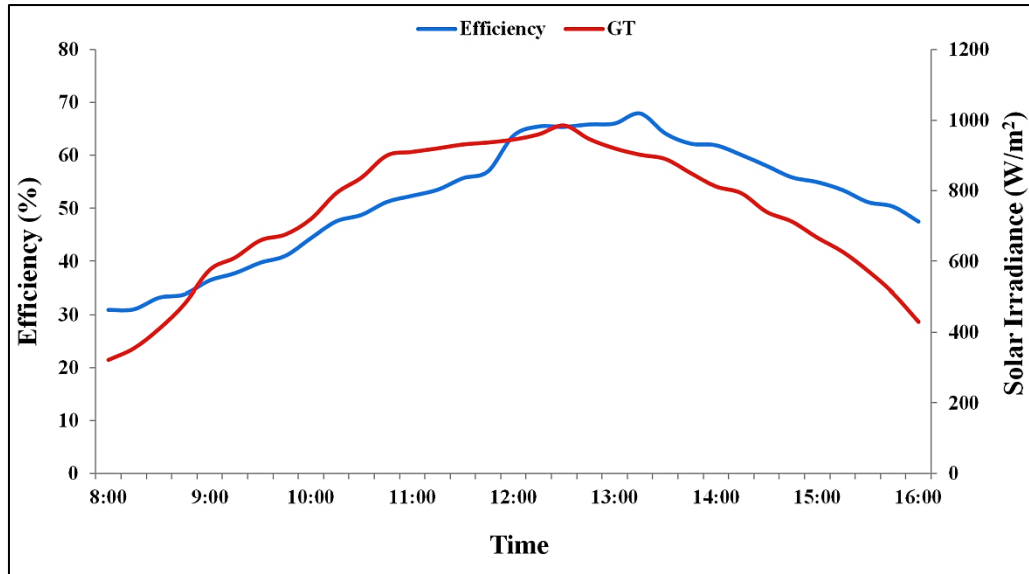


Figure 6.2 Efficiency of the collector and solar irradiance as a function of day times on 8<sup>th</sup> March.

The intercept of the line with the vertical axis absorbed energy parameter  $F_R(\tau\alpha)$ , and the slope of the line with the removed energy parameter ( $-F_R(U_L)$ ) are the two parameters of the efficiency line of the FPSC.  $F_R(\tau\alpha)$  indicates the highest collector efficiency at the temperature of the fluid entering the collector. At zero flow rates, the collector efficiency reaches zero at the intersection of the efficiency line with the horizontal axis, known as the stagnation point. The efficiency of solar collectors as a function of reduced temperature parameters  $\left(\frac{T_{Ci}-T_a}{G_T}\right)$  are shown in Figure 6.3. As visualized in this figure, the  $F_R(\tau\alpha)$  value was 0.675 and  $F_R(U_L)$  was -4.4667. Moreover, the root mean square error ( $R^2$ ) was found to be 0.9263, showing that the data points are close to a curve that can be fitted linearly.



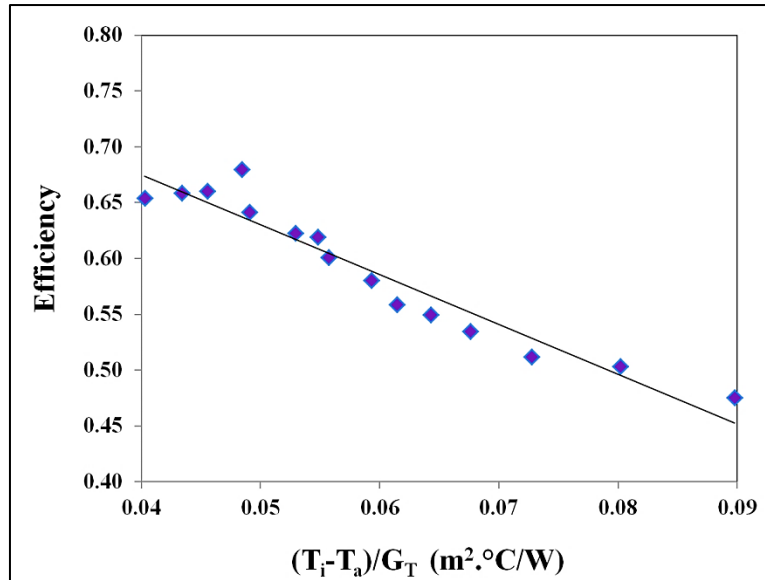


Figure 6.3 Efficiency of FPSC as a function of reduced temperature parameters on 8<sup>th</sup> March.

Figure 6.4 presents the variation of the useful energy with set point temperature and required energy as a function of day time. The greenhouse was heated using the solar system which was put in ran from 8:00 to 16:00, without using any auxiliary heating sources. As shown in the figure, the greenhouse heating load has the highest value at the beginning of the day, which was 9.98 kW, and this is expected because of large temperature difference between available and design room temperatures at the morning and because of low ambient temperature. In contrast, the heat supply from the collectors and the useful heat has the lowest value in the morning due to the sun's position. Also the figure illustrates that at 10:45 A.M, the temperature of the greenhouse reaches the set point temperature (23°C), and the system will automatically turn off. Further analysis showed that the greenhouse temperature gets lower than the set point temperature and the system will turn on again for about one hour, and after that no heating is needed in these periods. Overall, these results indicate that, with minimum and maximum ambient air temperatures of around 6.1°C and

14.8°C, the solar water heating system can overcome the greenhouse heating load for approximately four hours and store energy for the nighttime greenhouse heating requirement.

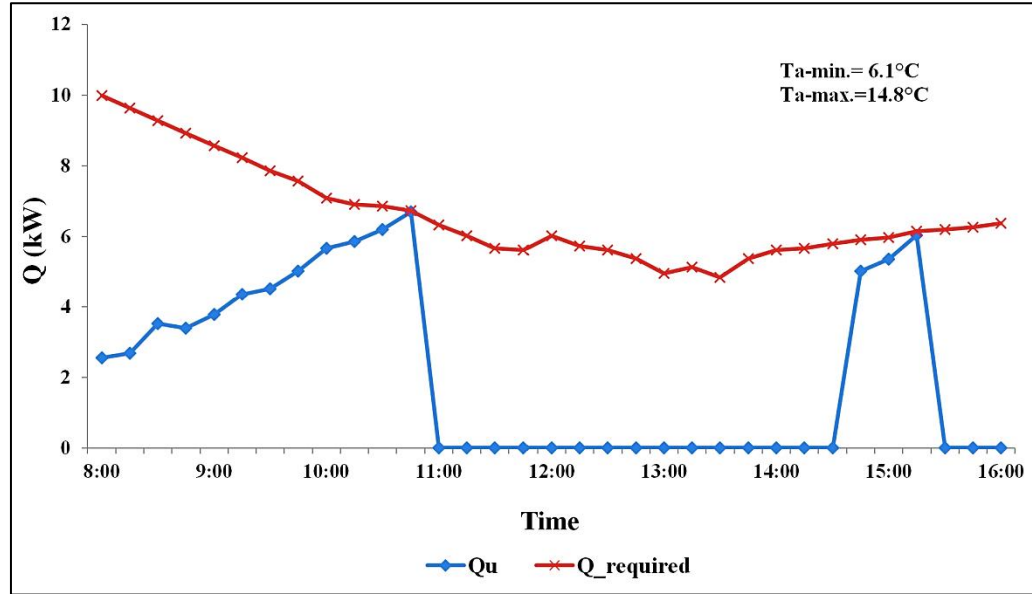


Figure 6.4 Greenhouse heating load versus energy provided (heat supply) during the day times on 8<sup>th</sup> March.

### 6.2.2 Nanofluid as Working Fluid

The nanofluid was prepared by dispersing  $\text{Al}_2\text{O}_3$  nanoparticles in distilled water (DW) at a concentration of 0.2wt.%. The study was conducted on two typical days of 29<sup>th</sup> March and 31<sup>st</sup> March with a mass flow rate of 0.2 kg/s.

The inlet and outlet temperatures throughout the testing duration are shown in Figures 6.5 and 6.6 for the two referred days. As seen in these figures, using nanofluid as a heat transfer fluid leads to a higher exit temperature, resulting in a higher temperature difference than in water cases. Adding nanoparticles to a base fluid can enhance thermal conductivity and heat transfer, resulting in a more active Brownian motion of nanoparticles, which depends on the fluid's temperature, which is the particular cause of the higher output temperature.

When nanoparticles are added to the base fluid, the effect of increased temperatures becomes more significant.

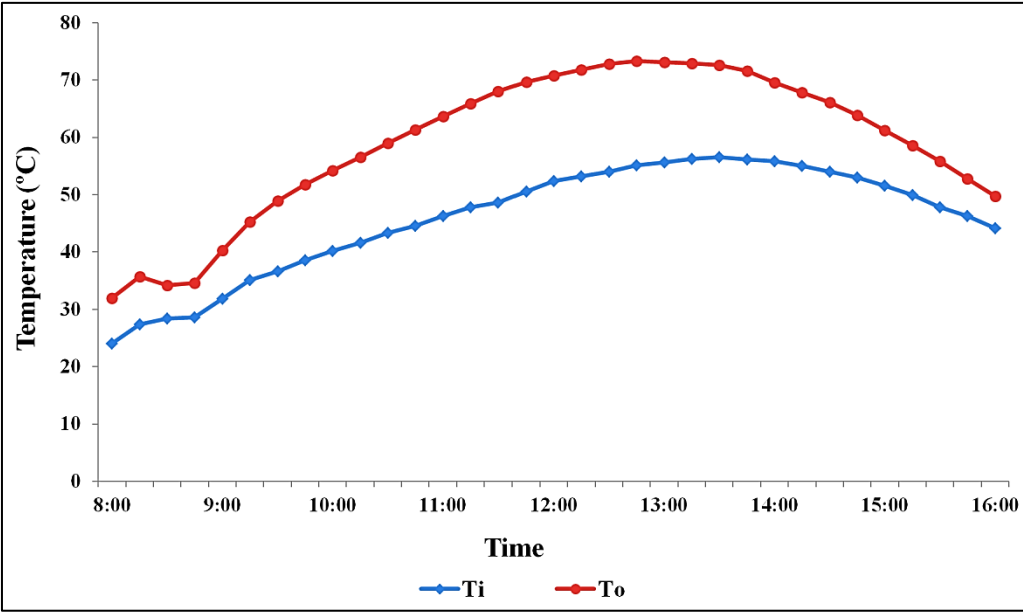


Figure 6.5 Inlet and outlet nanofluid temperature with respect to day time for 29<sup>th</sup> March.

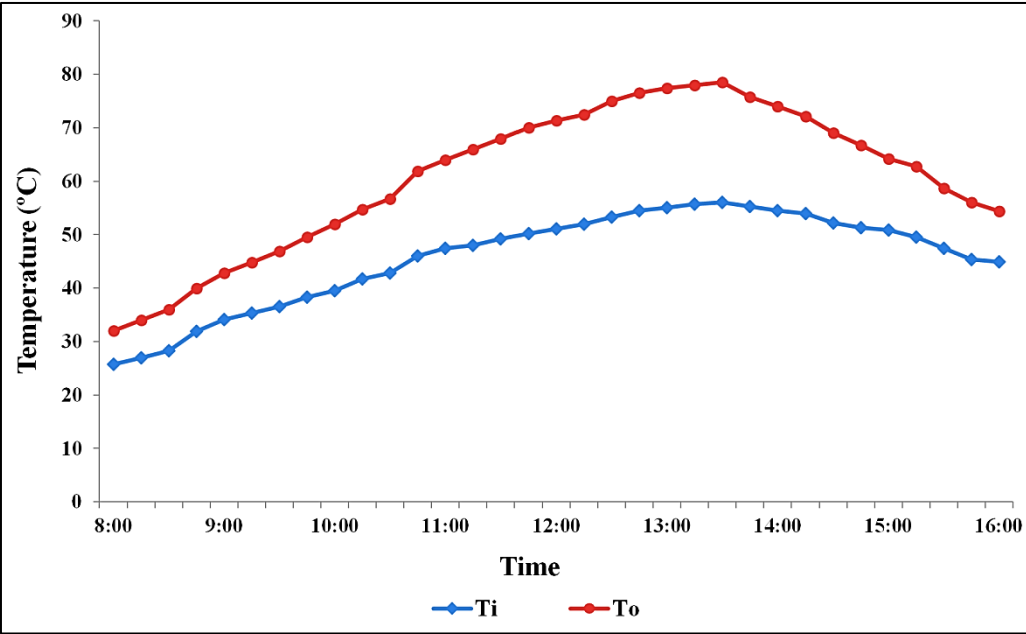


Figure 6.6 Inlet and outlet nanofluid temperature with respect to day time for 31<sup>st</sup> March.

Figures 6.7 and 6.8 illustrate the impact of utilizing nanofluid as an HTF on the collectors efficiency and the fluctuation of solar irradiance during the day. As demonstrated in these figures, FPSCs operating with  $\text{Al}_2\text{O}_3$ -water nanofluid have higher efficiency, owing to their higher output temperatures. As can be seen, adding nanoparticles to the base fluid raises the temperature difference, which leads to the output temperature rising and the collector efficiency increasing. The reason is that adding a nanoparticle improves the way heat moves through the tubes of the collectors by convection and conduction. As visualized in the figures below, the highest energy efficiency is about 73.9% and 74.3% for 29<sup>th</sup> and 31<sup>st</sup> of March, respectively. What is interesting about the results is that using nanofluid as the working fluid is a crucial part of enhancing the performance of flat plate solar collectors, and efficiency goes up even with a small concentration of nanoparticles.

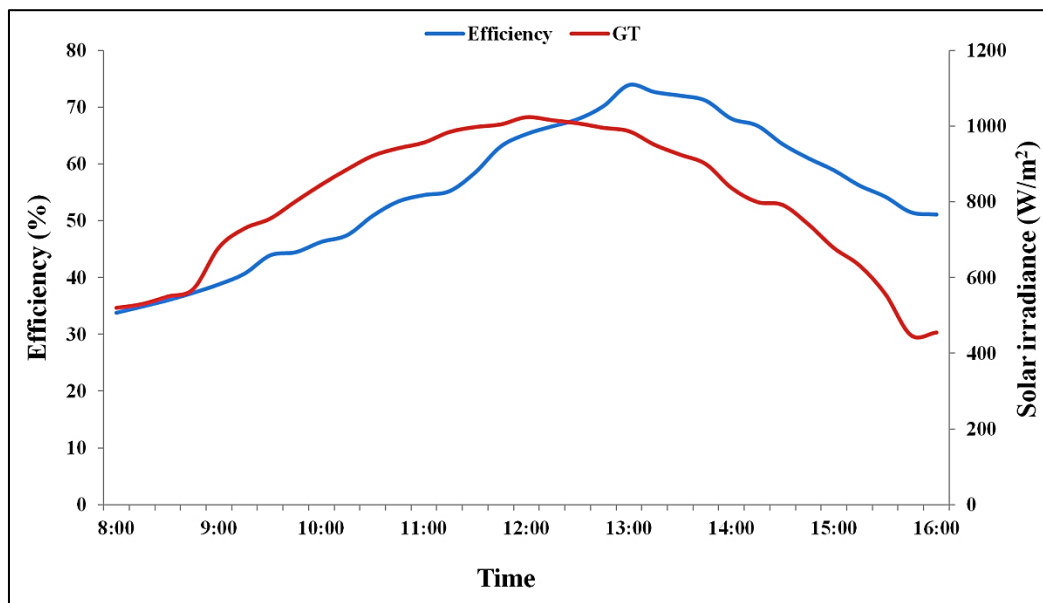


Figure 6.7 Collector efficiency and solar irradiance as a function of the day time for 29<sup>th</sup> March using  $\text{Al}_2\text{O}_3$  as nanofluid.

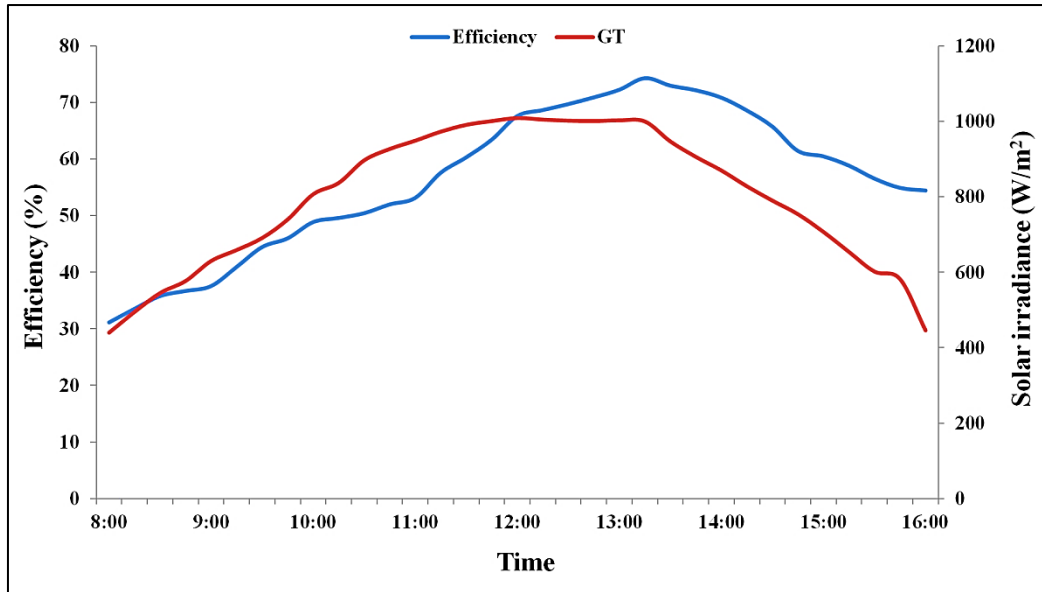


Figure 6.8 Collector efficiency and solar irradiance as a function of the day time for 31<sup>st</sup> March using Al<sub>2</sub>O<sub>3</sub> as nanofluid.

Figures 6.9 and 6.10 illustrate the collector's efficiency using nanofluids as a function of reduced temperature parameters  $\left(\frac{T_{Ci}-T_a}{G_T}\right)$  for a constant mass flow rate of 0.2 kg/s. The figures show that the absorbed energy parameter values for Al<sub>2</sub>O<sub>3</sub>-water nanofluid for 29<sup>th</sup> and 31<sup>st</sup> of March were 0.695% and 0.75%, respectively, which are greater than when using water as a working fluid. Although, due to the higher ambient temperature and solar irradiation on March 31<sup>st</sup>, the values of  $F_R(\tau\alpha)$  and  $F_R(U_L)$  are higher than that of the other days, as given in Table 6.1.

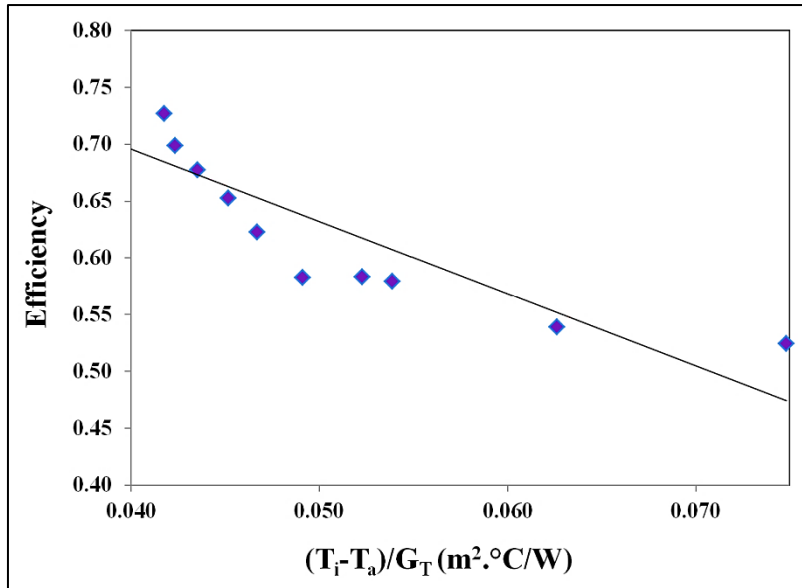


Figure 6.9 Efficiency of FPSC using  $Al_2O_3$ -water nanofluid for 29<sup>th</sup> March.

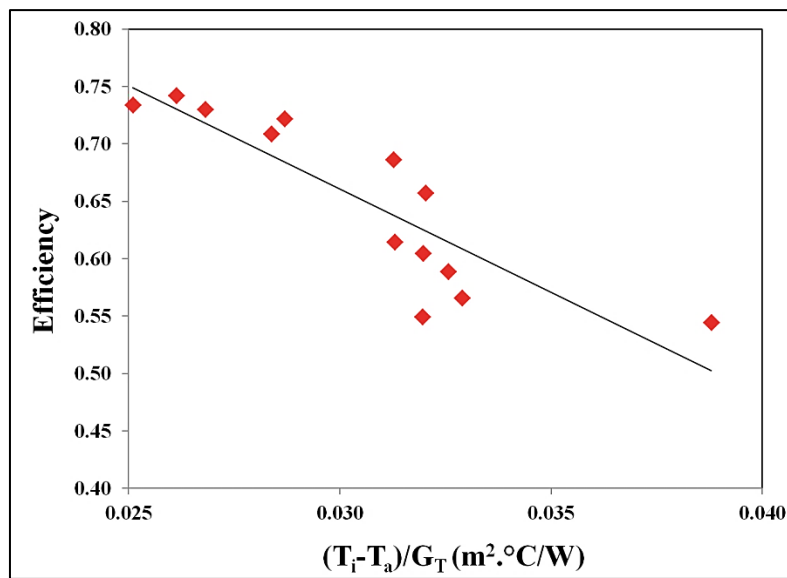


Figure 6.10 Efficiency of FPSC using  $Al_2O_3$ -water nanofluid for 31<sup>st</sup> March.

Table 6.1 Values of  $F_R(\tau\alpha)$  and  $F_R(U_L)$  for  $Al_2O_3$ -water nanofluid.

Day	$F_R(\tau\alpha)$	$F_R(U_L)$	$R^2$
29 <sup>th</sup> March	0.695	-6.3604	0.8141
31 <sup>st</sup> March	0.75	-18	0.7508

Figure 6.11 represents the hourly change of the greenhouse heating load required and heat supply for 29<sup>th</sup> March. In the first running hour, which is between 8:00 and 9:00 A.M., the inside air temperature (room temperature) is lower than the design temperature (which is 23°C), therefore the highest heating demand occurs at this time, and the system should supply a specific amount of heat to the greenhouse during this period. Meanwhile, when the heating load curve crosses the heat supply line, no heat supply is demand, where in this case the room temperature is equal or greater than the set point temperature (23°C). Another point to take into consideration is that, during the examination for 31<sup>st</sup> March, it was evident that the ambient temperature was similar to the design temperature at the starting time. Indeed, the ambient temperature rises during the daytime, ranging from 20.6°C to 26.9°C, and there is no need for heat supply to the greenhouse during this period.

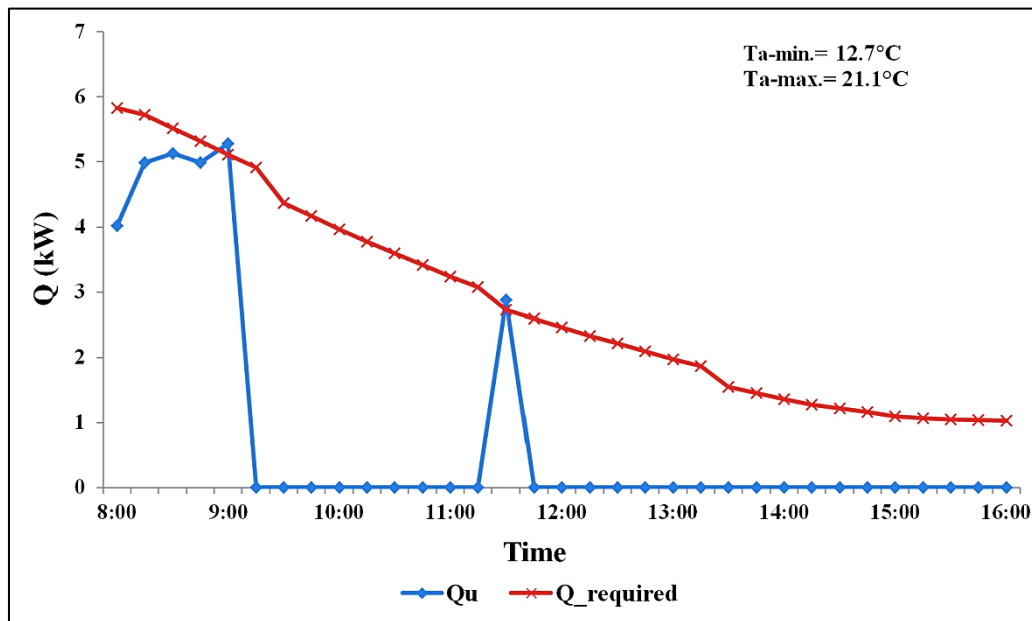


Figure 6.11 Greenhouse heating load versus energy provided (heat supply) as a function of day times for 29<sup>th</sup> March.

### 6.2.3 Comparisons between Different Working Fluids

Figures 6.12 and 6.13 illustrate the difference temperature and efficiency with various working fluids (water and nanofluid 0.2wt.%) as a function of day time. Experiments were conducted over two different days to determine how different HTFs affect flat plate solar collector efficiency (28<sup>th</sup> and 31<sup>st</sup> of March). The solar irradiance values for these two days are close to each other, ranging from (400-1010) W/m<sup>2</sup> on the 28<sup>th</sup> of March and (440-1001) W/m<sup>2</sup> on the 31<sup>st</sup> of March. Comparing the difference temperatures and efficiencies of two different working fluids indicates that the difference temperatures of the Al<sub>2</sub>O<sub>3</sub>-water nanofluid with 0.2wt.% are greater than those of the water case, which was expected because of the more active Brownian motion of the nanoparticles into the base fluid. Further, due to their higher output temperature, the collector has a higher efficiency than the water case when using nanofluid as a working fluid. The collector maximum difference temperature and efficiency were 16.5°C and 68.8% for water, respectively, and 22.4°C and 74.2% for Al<sub>2</sub>O<sub>3</sub>-water nanofluid, respectively. Interestingly, using the Al<sub>2</sub>O<sub>3</sub>-water nanofluid at a concentration of 0.2wt.% increases the efficiency of the flat plate solar collector by 7.9% compared to the water case.



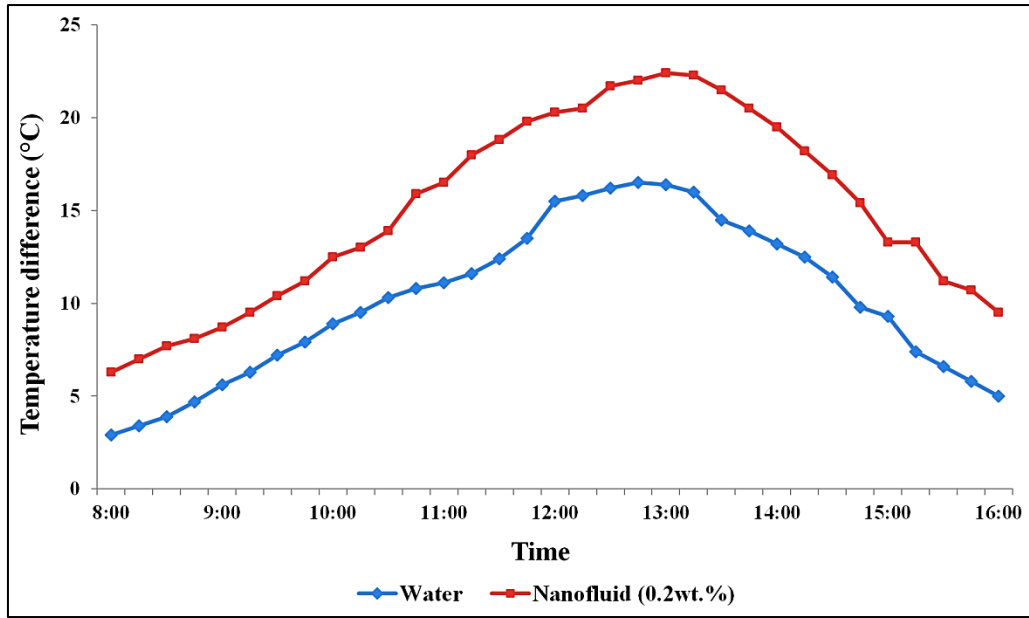


Figure 6.12 Collector difference temperature at different working fluids (DW and 0.2wt.%  $\text{Al}_2\text{O}_3$ -water nanofluid).

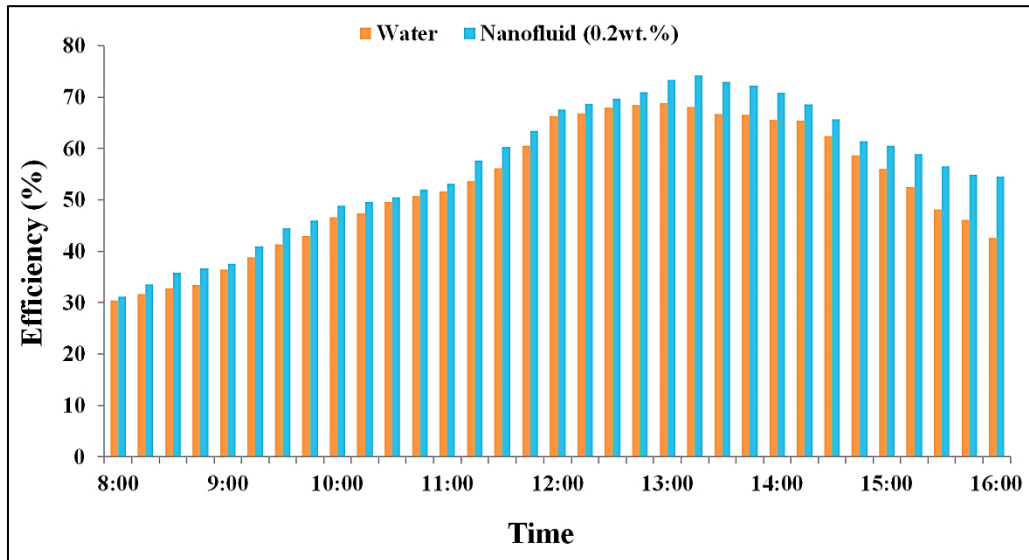


Figure 6.13 Collector efficiency at different working fluids (DW and 0.2wt.%  $\text{Al}_2\text{O}_3$ -water nanofluid).

### **6.3 Simulation Studies**

In this part, the results of a numerical simulation for the performance of a flat plate solar collector were presented to examine the influence of  $\text{Al}_2\text{O}_3$ -water nanofluid on the collectors' thermal performance. The TRNSYS simulation was developed and verified with the experimental results. In addition, the following sub-sections present numerical simulations comparing the two different working fluids (DW and  $\text{Al}_2\text{O}_3$ -water nanofluid) and the heat supply from the storage tank to the greenhouse.

#### **6.3.1 TRNSYS Model Validation**

The system was first tested using water as a working fluid, and then the water was replaced with  $\text{Al}_2\text{O}_3$ -water nanofluid for second stage. The experimental work and TRNSYS simulation program provide information on the fluctuations of the FPSCs inlet and outlet temperatures and the temperature difference between them for water as in Figure 6.14, and for  $\text{Al}_2\text{O}_3$ -water nanofluid with 0.2wt.% nanoparticle concentration as in Figure 6.15. The maximum percentage error between experimental and simulation results were 7.9% and 6.4% for inlet and outlet collector water temperature, respectively, while for  $\text{Al}_2\text{O}_3$ -water nanofluid were 6.8% and 4.5%, respectively. Additionally, the solar irradiance experimental measured data and predicted data using TRNSYS simulation program are presented in Figure 6.16 with approximately 10% maximum error.

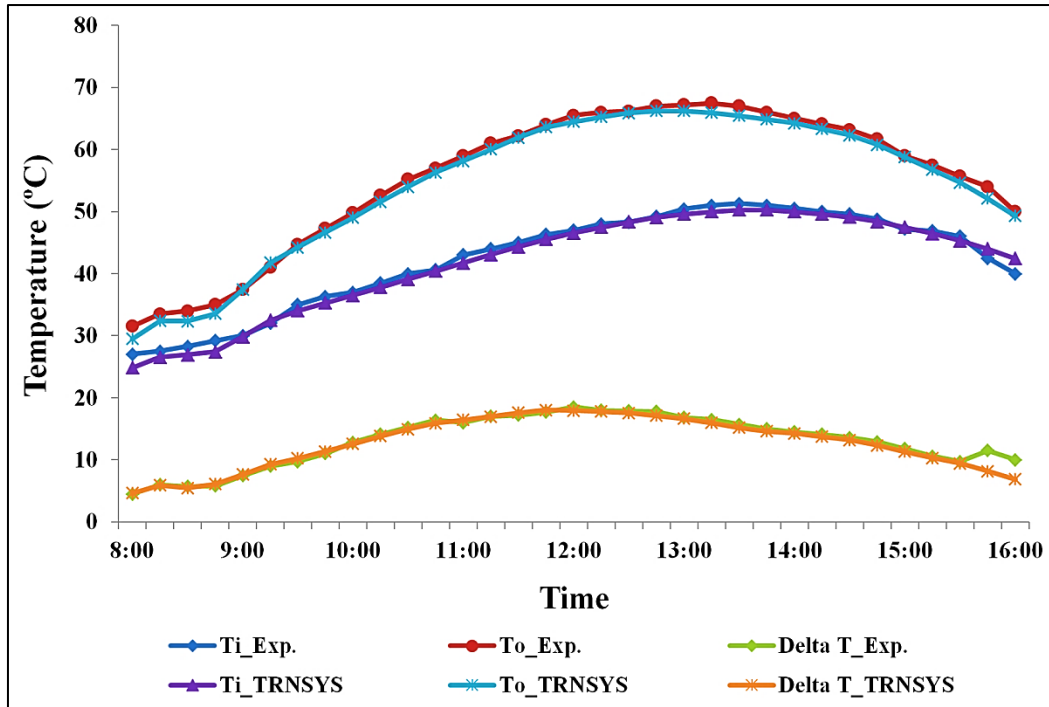


Figure 6.14 Comparison between the simulation and experimental results for FPSC water temperature.

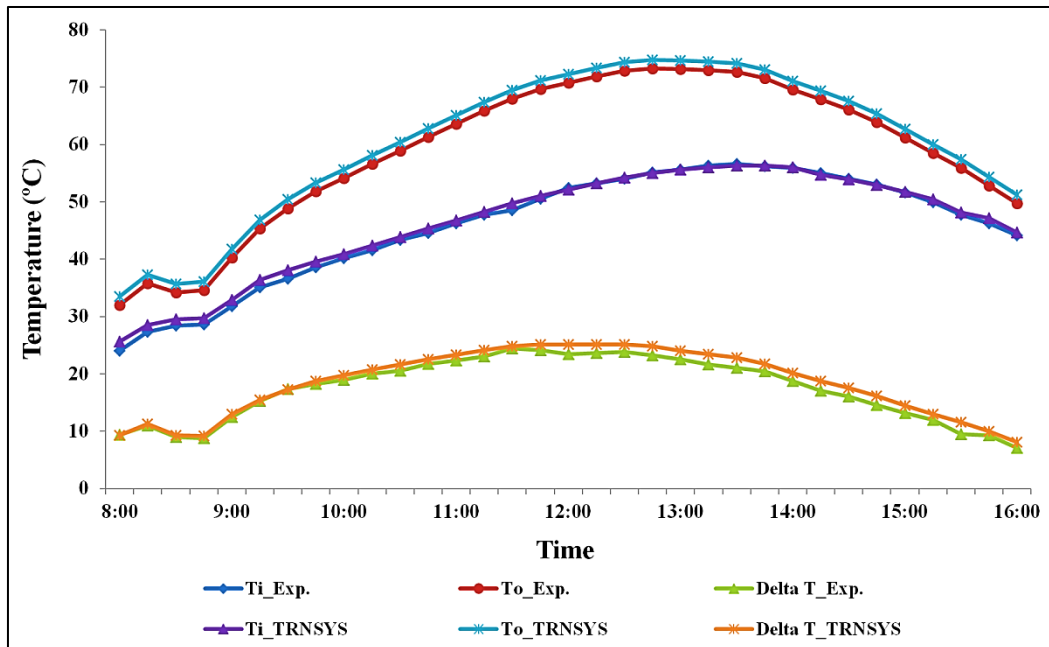


Figure 6.15 Comparison between experimental and simulation temperatures of the collectors nanofluid for 0.2wt.% concentration.

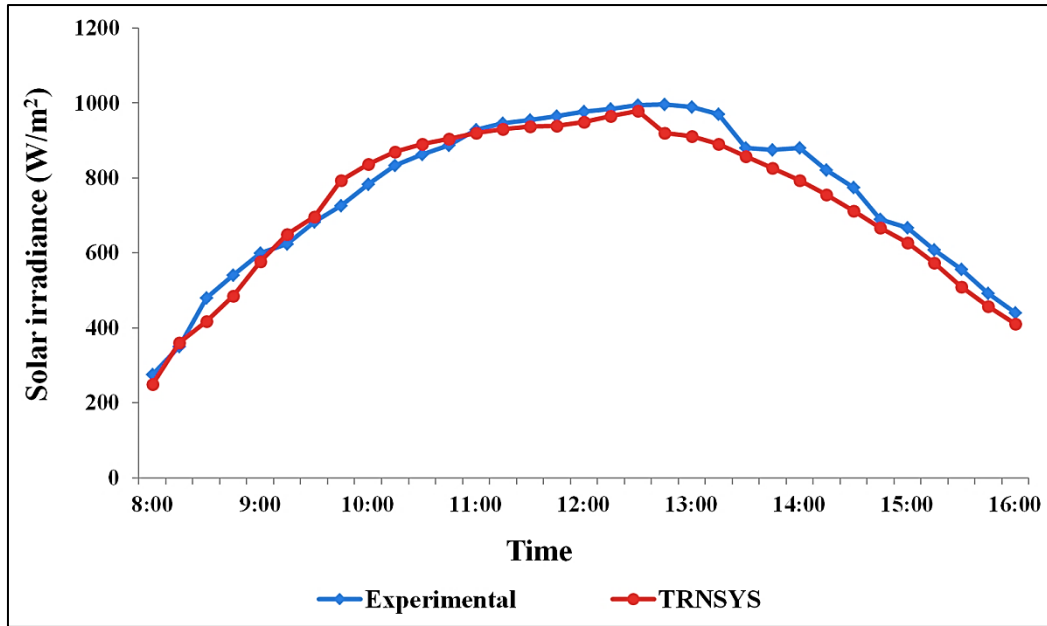


Figure 6.16 Solar irradiance verification between experimental and simulation results.

The verification results show a good agreement between experimental and simulation results that closely match with acceptable accuracy. From the figures above, it can be concluded that the TRNSYS simulation program is a useful tool that can be adopted for simulating the present solar water heating system.

### 6.3.2 Comparisons between the Working Fluids

Figure 6.17 shows the collector efficiency for different working fluids, where 0.2wt.%, 0.5wt.%, 1wt.%, and 1.5wt.%  $Al_2O_3$ -water nanofluid were used as the HTFs for a mass flow rate of 0.2 kg/s for one typical day of 18<sup>th</sup> February and for same boundary conditions. The figure indicates that the results for  $Al_2O_3$ -water nanofluid are higher than using water. When water was used as a working fluid in the FPSC the maximum collector efficiency was 66.3%. Moreover, when 0.2wt.%, 0.5wt.%, 1wt.%, and 1.5wt.%  $Al_2O_3$ -water nanofluid were used the maximum collector efficiency were 73.9%, 77.9%, 83.6%, and 81.1%, respectively. It is evident that optimum efficiency was reached for 1wt.% of

Al<sub>2</sub>O<sub>3</sub>-water nanofluid, which improved the efficiency of the collectors by 26.1% compared to the water case. Moreover, when the concentration of the Al<sub>2</sub>O<sub>3</sub>-water nanofluid was increased from 1wt.% to 1.5wt.%, the collector efficiency did not increase further; this is because as the nanoparticle concentration increases, the thermal conductivity also increases but the possibility of ensuring dispersion stability decreases. It was also found that, due to increased viscosity at higher concentrations, the frictional losses were also increased. Moreover, at higher concentrations, when particle agglomeration occurs, Brownian motion among nanoparticles and base fluid particles is slowed, resulting in decreased convective heat transfer between the base fluid and nanoparticles.

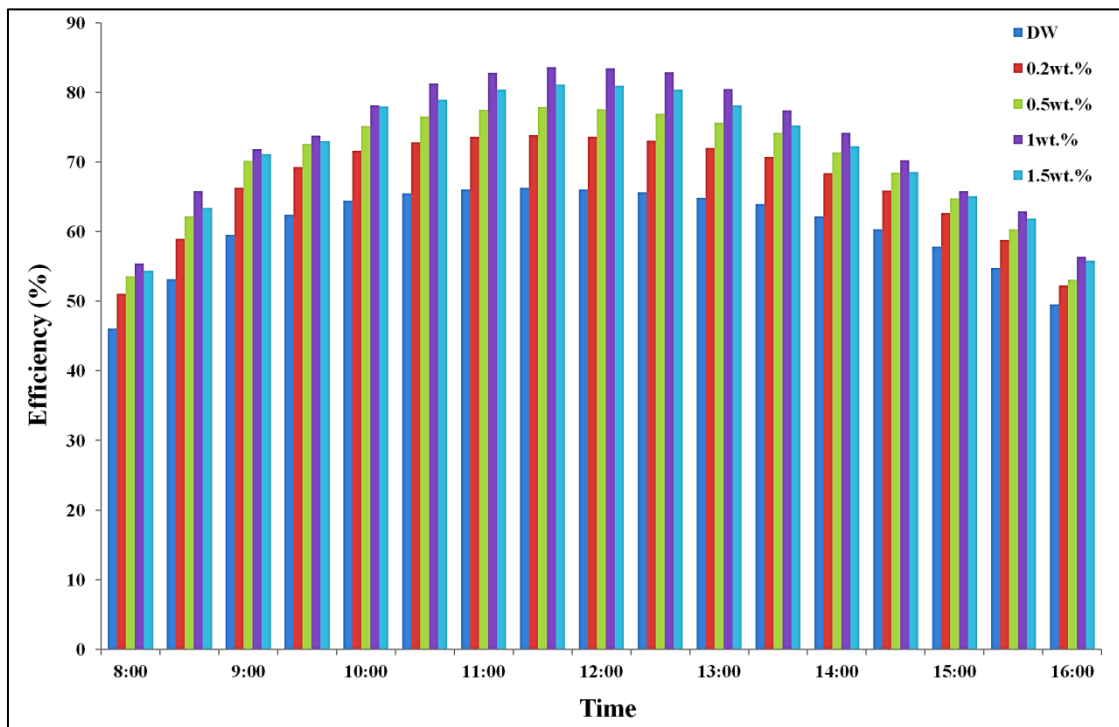


Figure 6.17 Collector efficiency at different working fluids DW and nanofluid with concentration of (0.2wt.%, 0.5wt.%, 1wt.%, and 1.5wt.%).

The pressure drop of Al<sub>2</sub>O<sub>3</sub>-water nanofluid in the system is also a significant factor influencing efficiency. Figures 6.18 and 6.19 illustrate the pressure drops and pumping power of working fluid flows as a function of nanofluid concentration. As predicted, the nanofluid density and viscosity will increase as the concentration rises and causing increase in the pressure drop. It is also important to know that the nanoparticles Brownian motions, dispersion, and fluctuation will increase their momentum exchange rates, and this momentum exchange may amplify the axial pressure drop (Kahani, Heris and Mousavi, 2013). The results showed that when water was used, the highest pressure drop in the system was 2.09 kPa. In addition, when 0.2wt.%, 0.5wt.%, 1wt.%, and 1.5wt.% of Al<sub>2</sub>O<sub>3</sub>-water nanofluid were used, the highest pressure drop were 2.104 kPa, 2.122 kPa, 2.152 kPa, and 2.183 kPa, respectively. However, raising the nanoparticle concentration with 1wt.% raises the pressure drop by 2.97% compared with the water case. Regardless, this percentage is observable; the effect of this value on pump power can be considered negligible when compared to the improvement in heat transfer characteristics and the increase in outlet temperature of the nanofluids. Additionally, the performance of the solar collector was not significantly affected.

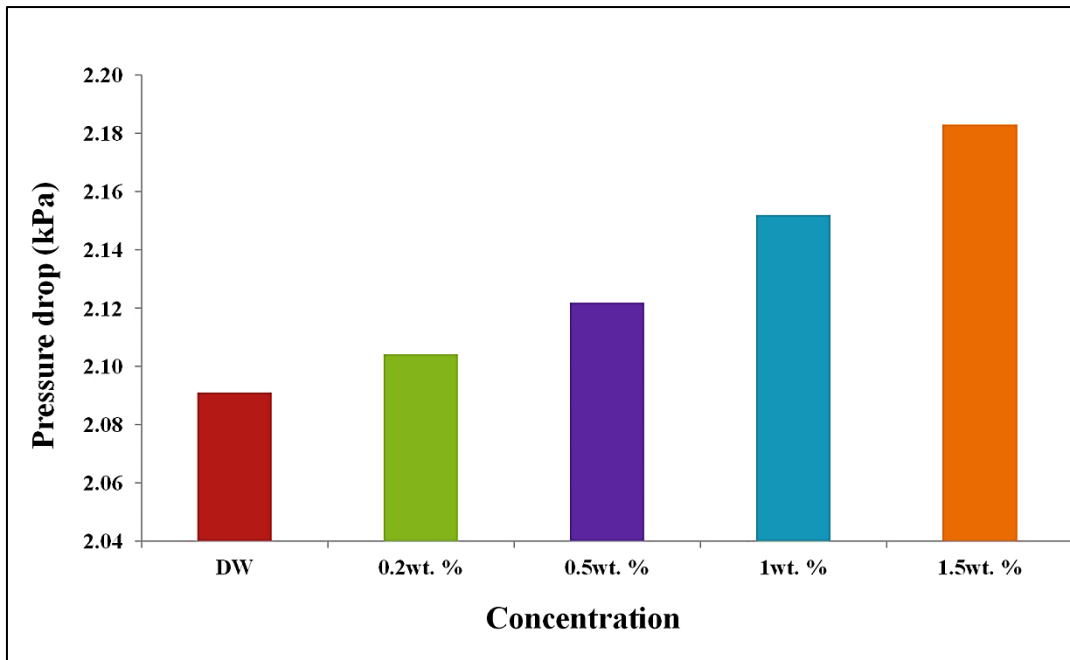


Figure 6.18 System pressure drop for water and different concentration of  $\text{Al}_2\text{O}_3$ -water nanofluid.

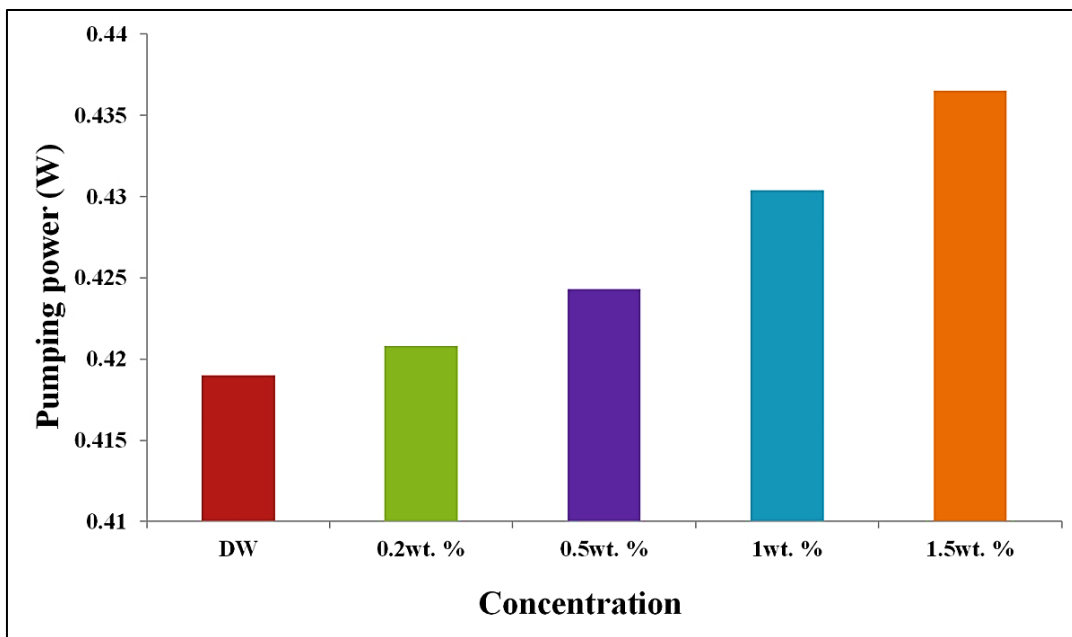


Figure 6.19 Pump power for water and different concentration of  $\text{Al}_2\text{O}_3$ -water nanofluid.

Figure 6.20 shows the variation of the FPSC efficiency with solar irradiance for two working fluids (i) DW, and (ii) Al<sub>2</sub>O<sub>3</sub>-water nanofluids with three nanoparticle concentrations of 0.2wt.% and 0.5wt.%, and 1wt.%. From this figure, note that as the solar irradiation increases, the collector performance goes up at the beginning of the day, reaching its highest point at noon and then declines till sunset with the solar irradiation.

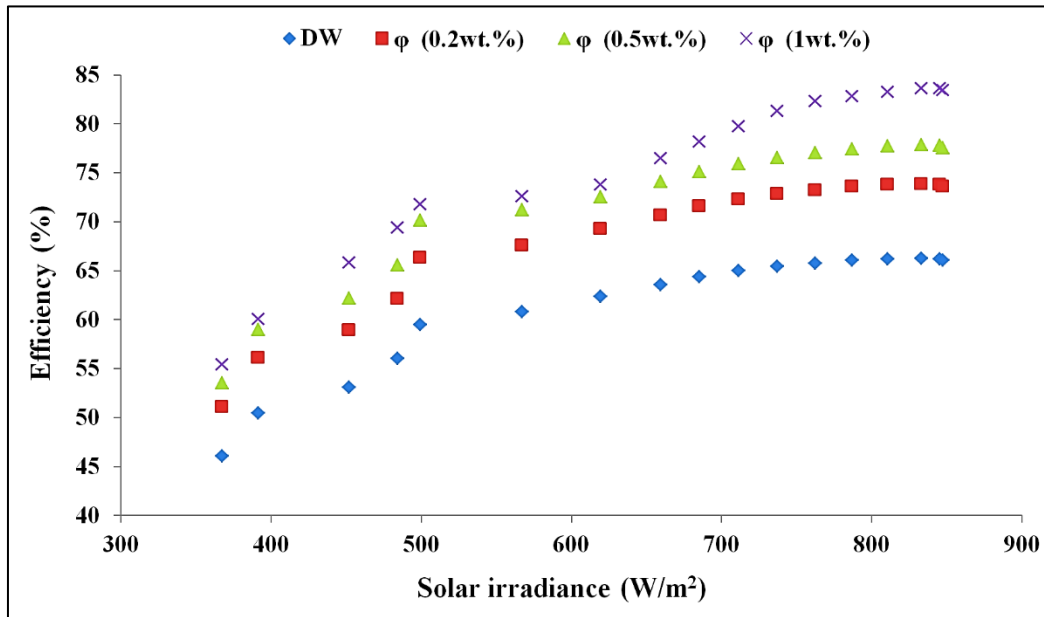


Figure 6.20 Efficiency versus solar irradiance for DW and for nanofluid with different concentration.

Figure 6.21 depicts the efficiency of solar collectors as a function of reduced temperature parameters  $\left(\frac{T_{Ci}-T_a}{G_T}\right)$  for DW and for Al<sub>2</sub>O<sub>3</sub>-water nanofluid with different concentration. The values of the absorbed energy parameter  $F_R(\tau\alpha)$  and removed energy parameter  $F_R(U_L)$  for FPSC are listed in Table 6.2 for different working fluids. The results showed that the value of  $F_R(\tau\alpha)$  for water is 0.654; however, for Al<sub>2</sub>O<sub>3</sub>-water nanofluid are 0.752, 0.785, and 0.876 for 0.2wt.%, 0.5wt.%, and 1wt.% particle concentration, respectively.



Additionally,  $F_R(U_L)$  values for  $Al_2O_3$ -nanofluid and water are relatively close to each other since the slopes of models are negative. It can be observed that the value of  $F_R(\tau\alpha)$  for nanofluid is higher than water for all involved concentrations. Moreover, this value was about 34% greater for nanofluid with 1wt.% concentration than that of water.

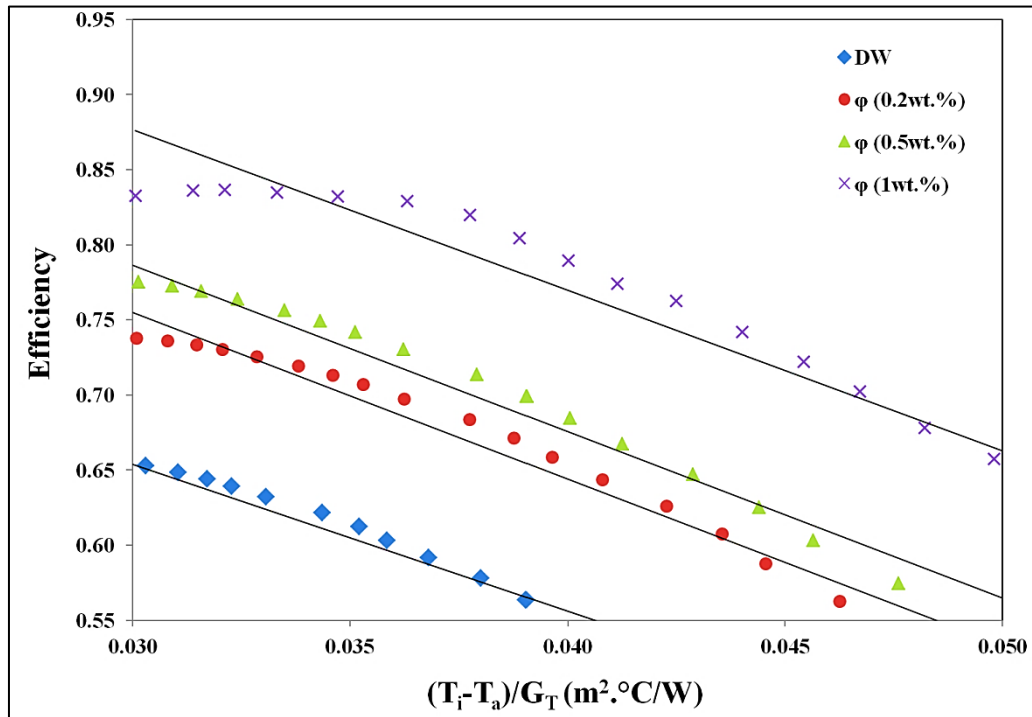


Figure 6.21 FPSC efficiency for DW and for  $Al_2O_3$ -water nanofluid with different concentrations.

Table 6.2 Values of  $F_R(\tau\alpha)$  and  $F_R(U_L)$  for different working fluids.

Base fluid type	$F_R(\tau\alpha)$	$F_R(U_L)$	$R^2$
Water	0.654	-9.7765	0.9614
0.2wt.% $Al_2O_3$ -nanofluid	0.752	-10.429	0.9642
0.5wt.% $Al_2O_3$ -nanofluid	0.785	-10.822	0.9672
1wt.% $Al_2O_3$ -nanofluid	0.876	-10.69	0.9375

The pump enhanced the collisions between liquid molecules and solid particles by increasing the random motion of the particles. The thermal conductivity of the nanofluid is greater than that of DW, and this is because of the Brownian motion, which plays an essential factor in this improvement. It is also worth noting that in this study, the turbulent fluid flow has been attained. This is because the convective heat transfer coefficient and the efficiency of the FPSC by using nanofluid were greater than using water, and this variation is demonstrated in Eq. (3.7).

The variation of collector outlet temperature with respect to time is illustrated in Figure 6.22 for two different working fluids, water and nanofluid (0.2wt.%, 0.5wt.%, 1wt.%). According to the findings, the outcomes are higher for Al<sub>2</sub>O<sub>3</sub>-water nanofluid than for water. This is to be expected since Brownian motion increases the nanoparticles conduction and convection heat transfer (Moravej *et al.*, 2020). Moreover, by comparing the collector outlet temperature using nanofluids with three different concentrations, it showed that the maximum outlet temperature could be achieved for 1wt.% which was about 113°C. Consequently, it can be concluded that the addition of nanoparticles to the base fluid increases the amount of temperature rise.

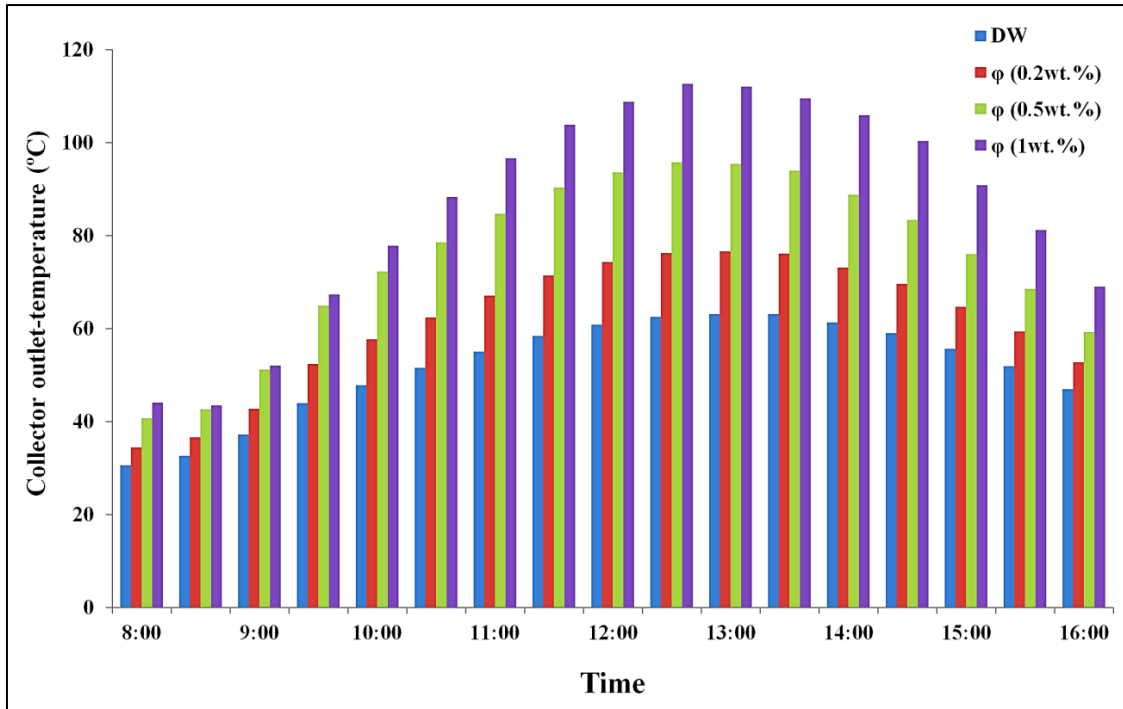


Figure 6.22 Collector outlet temperatures for different working fluids.

Furthermore, the average outlet temperature from solar collector for DW and for  $\text{Al}_2\text{O}_3$ -water nanofluid with three different concentrations (0.2wt.%, 0.5wt.%, and 1wt.%) from November to April are shown in Figures 6.23 to 6.28, respectively.

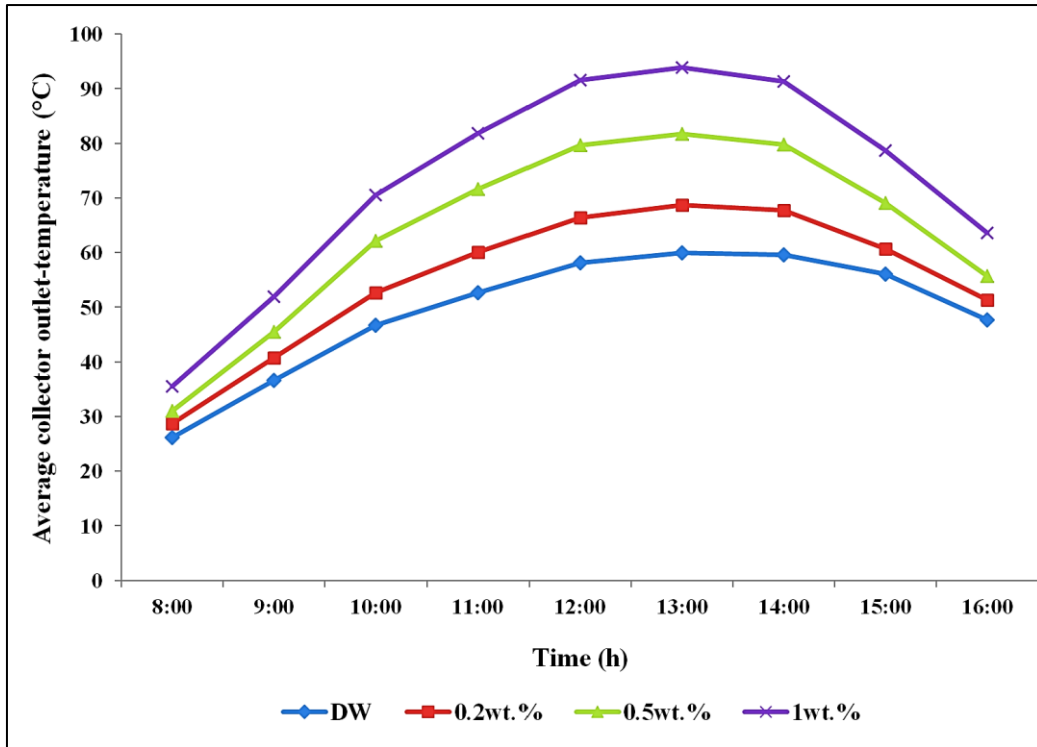


Figure 6.23 Average collector outlet temperatures for different working fluid for November.

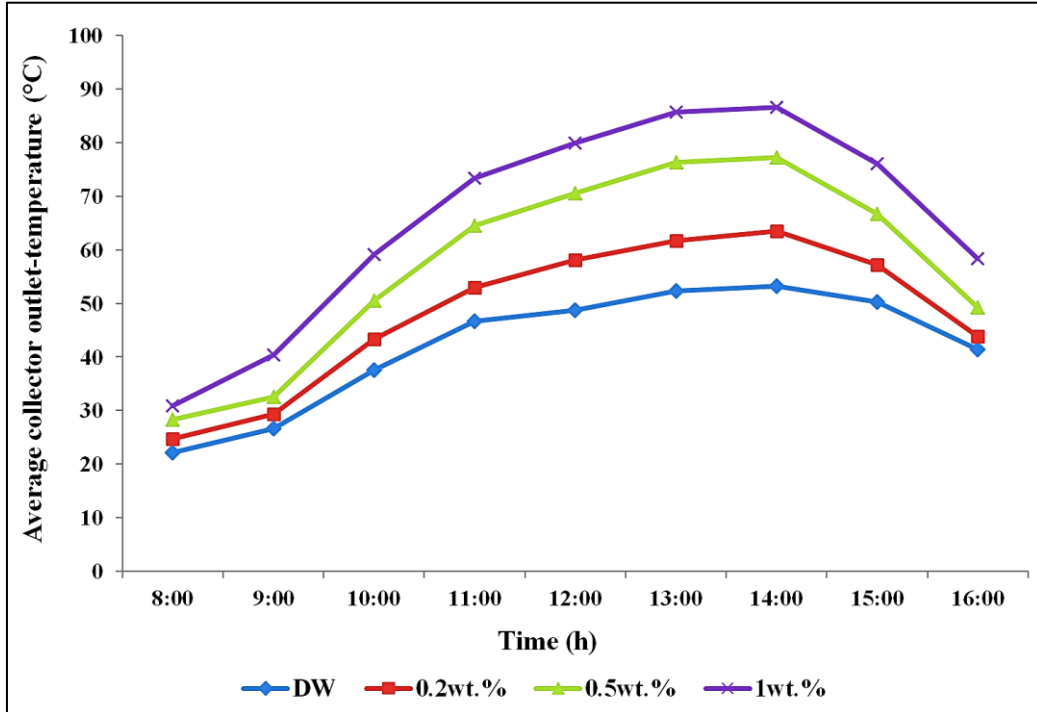


Figure 6.24 Average collector outlet temperatures for different working fluid for December.

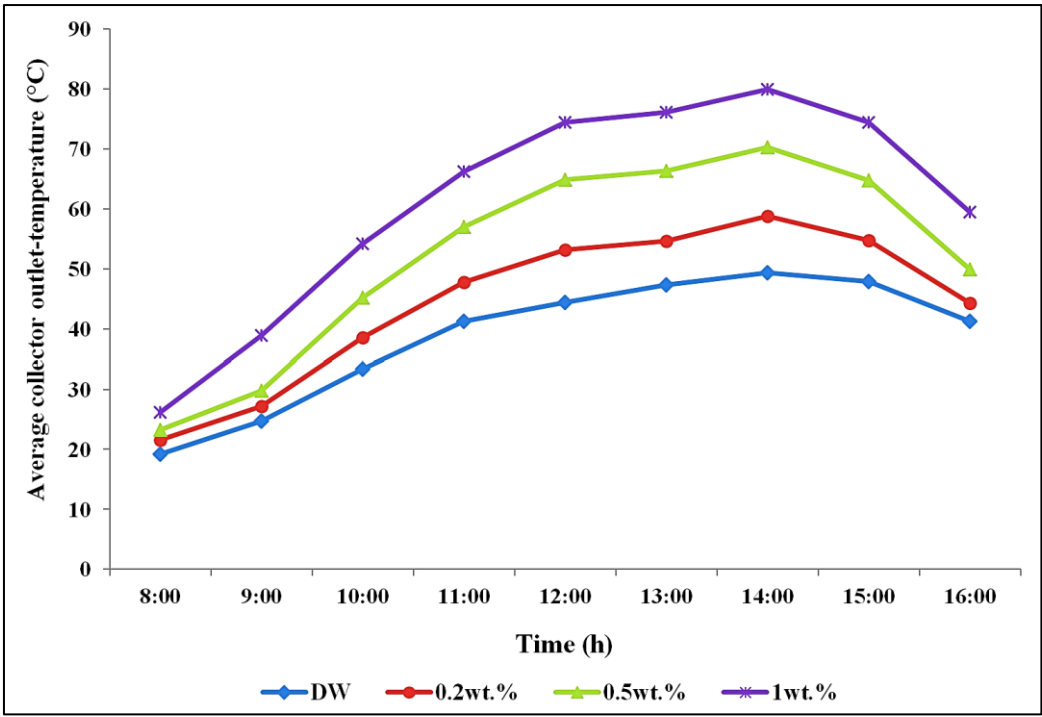


Figure 6.25 Average collector outlet temperatures for different working fluid for January.

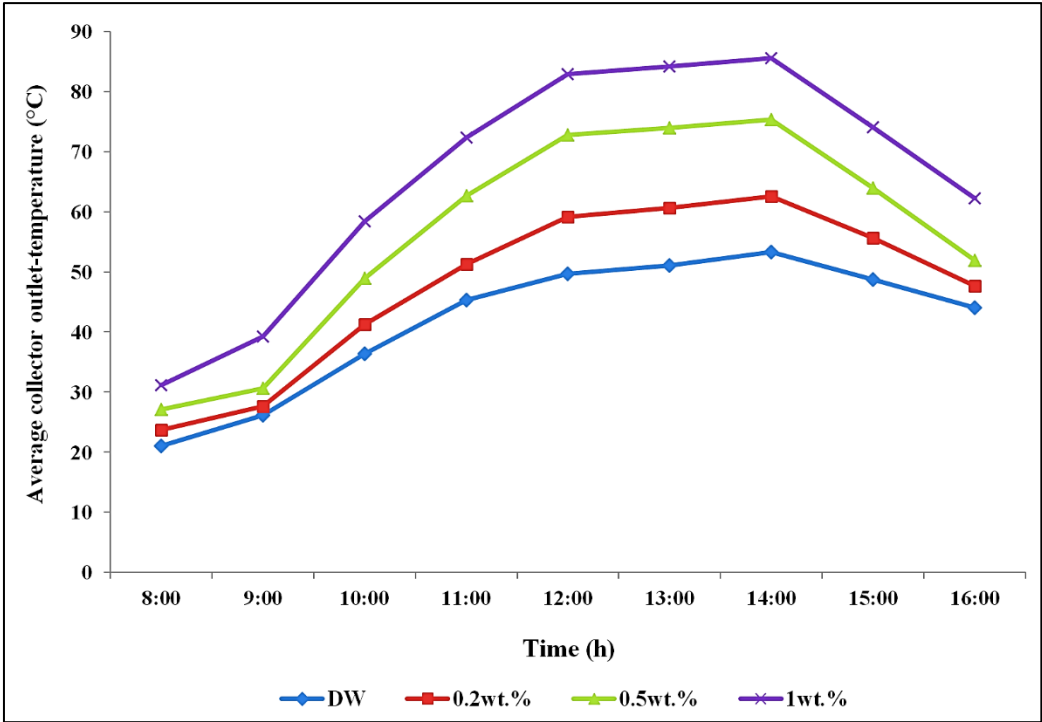


Figure 6.26 Average collector outlet temperatures for different working fluid for February.

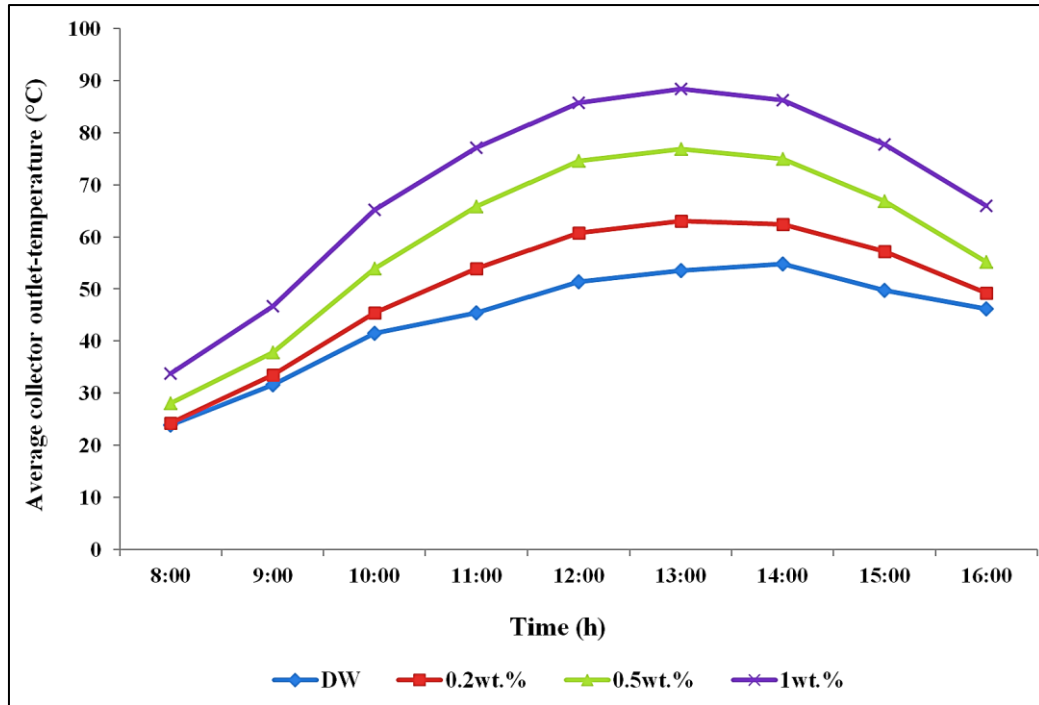


Figure 6.27 Average collector outlet temperatures for different working fluid for March.

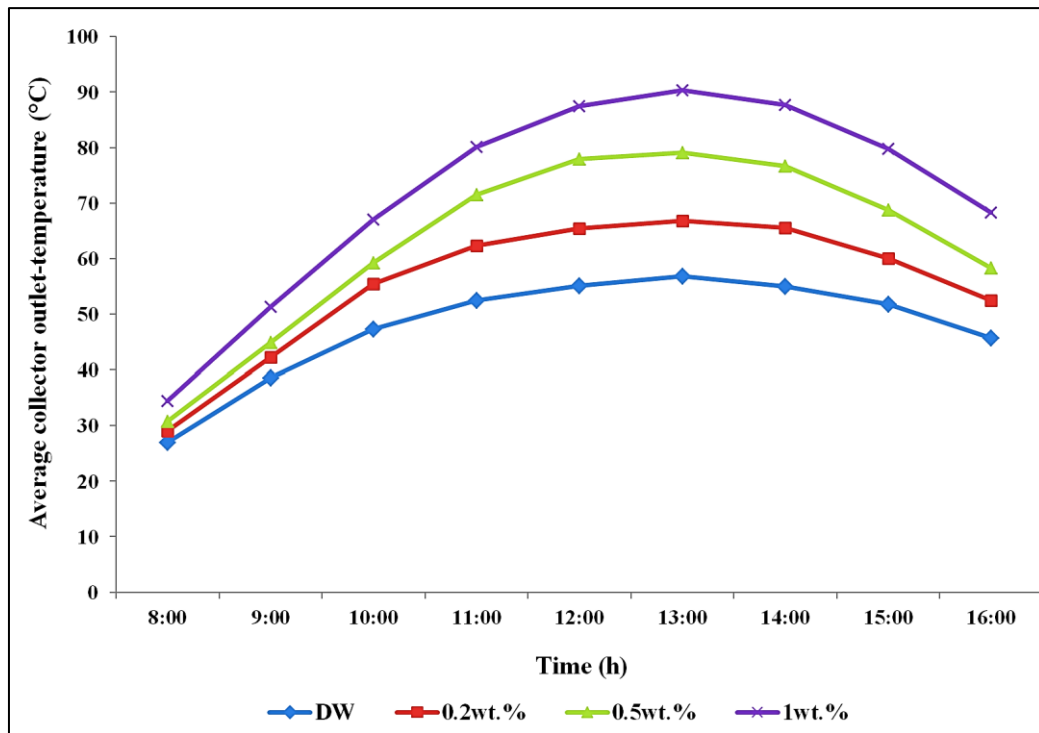


Figure 6.28 Average collector outlet temperatures for different working fluid for April.

### 6.3.3 Greenhouse Heating Load

The greenhouse heating load is calculated using Eq. (3.1). The maximum estimated value was 12.8 kW, which was obtained during the coldest day of the winter season, (12<sup>th</sup> January 2022), where the minimum ambient air temperature recorded was 0°C according to the Erbil's weather data. Therefore, as illustrated in Figure 6.29, the primary heat loss from the greenhouse happens during the night hours.

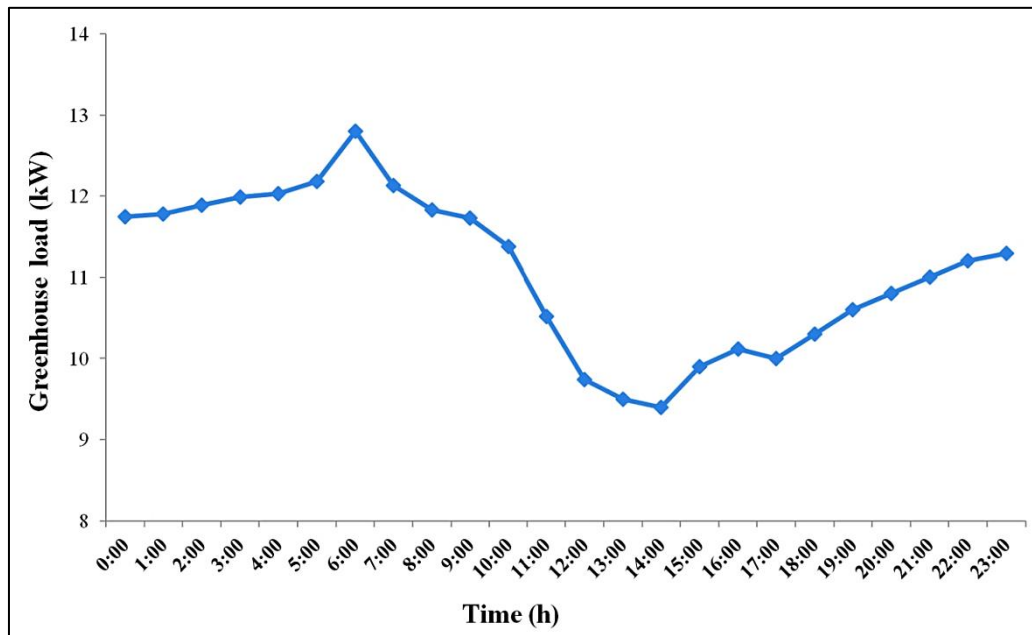


Figure 6.29 Greenhouse heating load value on 12<sup>th</sup> January.

Energy is provided to the greenhouse if the inside air temperature obtained from the dynamic model is less than the design temperature set at 23°C. Figures 6.30 and 6.31 show that the greenhouse supplied useful heat for winter's coldest day (12<sup>th</sup> January) without set temperature and with set point temperature, respectively. The results showed the heat supply to the greenhouse with different working fluids of DW and Al<sub>2</sub>O<sub>3</sub>-water nanofluid. As shown in the mentioned figures, the required heating load of the greenhouse has the highest value at the

beginning of the day, which is 11.83kW. In contrast, the supply heat from the collectors and the useful heat from the storage tank have the lowest value in the morning due to the sun's position and the highest value after solar noon, as illustrated in Figure 6.30. The maximum useful heat from the system continuously without any setting temperature were 9.29 kW, 10.14 kW, 10.55 kW, and 11.49 kW for water, and nanofluid (0.2wt.%, 0.5wt.%, and 1wt.%), respectively.

Moreover, Figure 6.31 observed that when the greenhouse temperature reaches the set point temperature, the system is automatically turned off until the greenhouse temperature gets down the set point temperature. The results showed that the required temperature of the greenhouse could not be reached when water was used as the working fluid for this typical day. Further analysis showed that when different nanofluid concentrations are used, the system produces more useful heat than water, and the set point temperature was reached in the greenhouse. On the other hand, it is worth noting that the solar system may produce more heat for heating the greenhouse as ambient temperatures rise, which would reduce greenhouse heating demand.



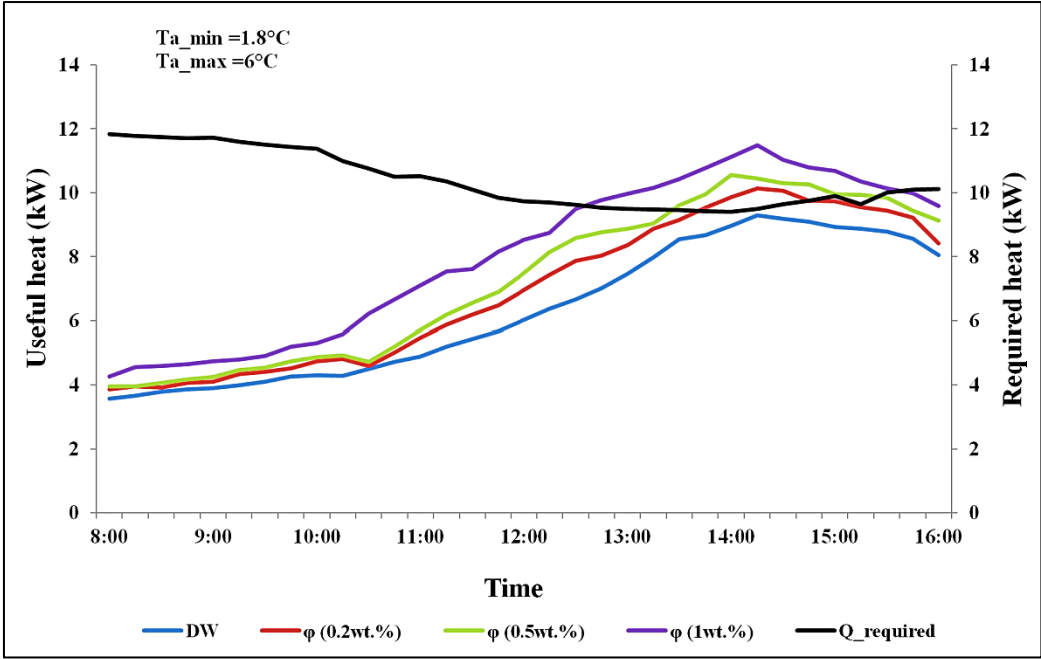


Figure 6.30 Greenhouse heating load required and energy provided (heat supply) with non-set-point temperature for 12<sup>th</sup> January.

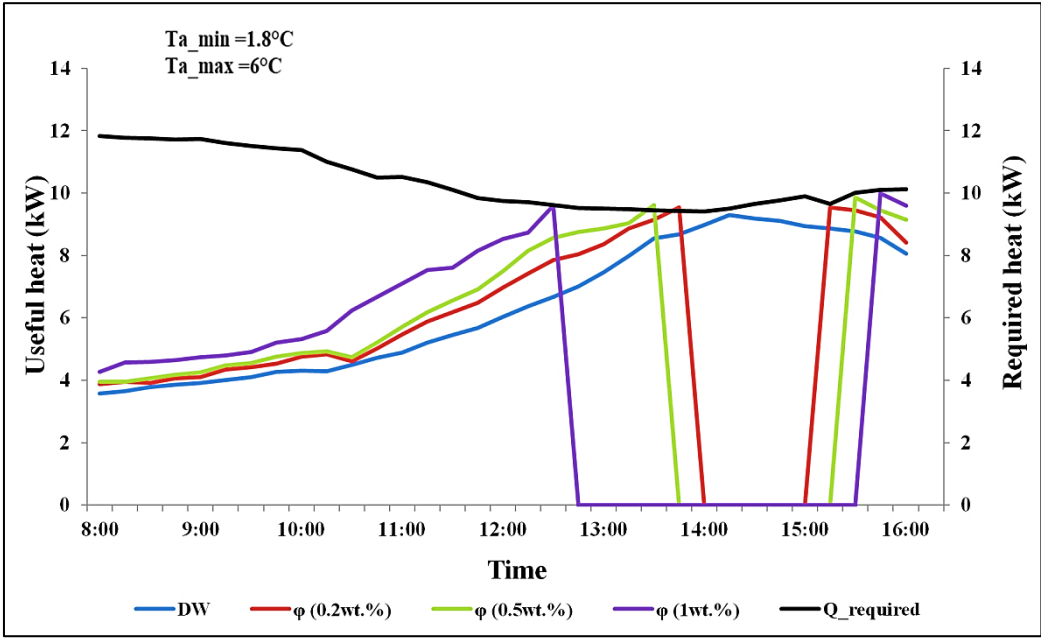


Figure 6.31 Greenhouse heating load required and energy provided (heat supply) with set-point temperature for 12<sup>th</sup> January.

Further, Figures 6.32 to 6.36 provide the greenhouse useful heat supply for non-set point temperature and for coldest day of November, December, February, March, and April, respectively, for two different HTFs, DW and nanofluid (0.2wt.%, 0.5wt.%, and 1wt.%). Additionally, same results were conducted but with greenhouse set point temperature, as illustrated in Figures 6.37 to 6.41.

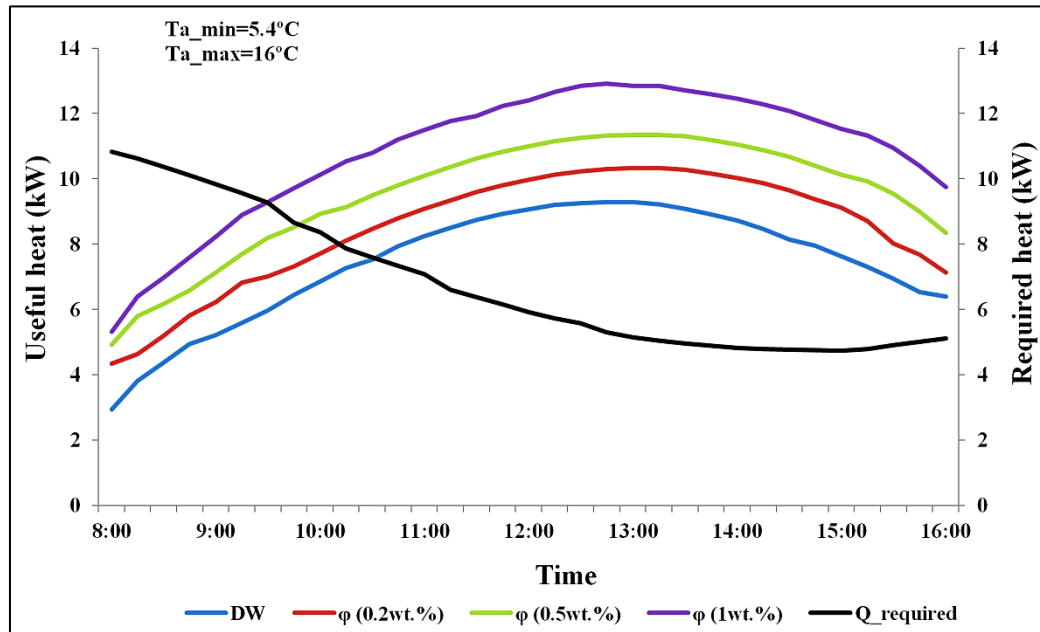


Figure 6.32 Greenhouse heating load required and energy provided (heat supply) with non-set-point temperature for 30<sup>th</sup> November.

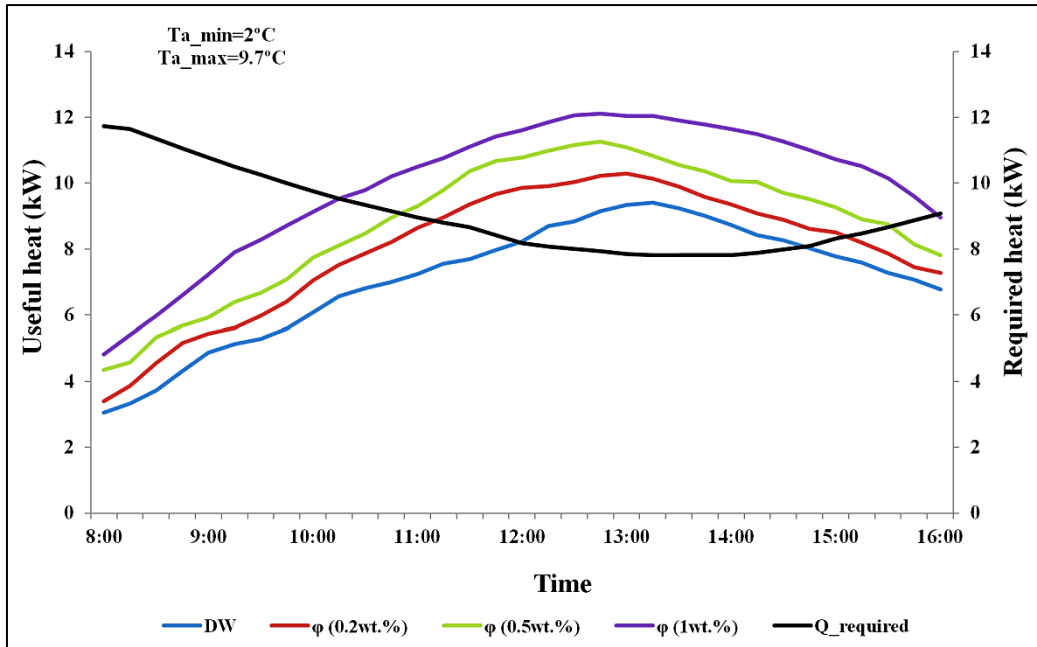


Figure 6.33 Greenhouse heating load required and energy provided (heat supply) with non-set-point temperature for 28<sup>th</sup> December.

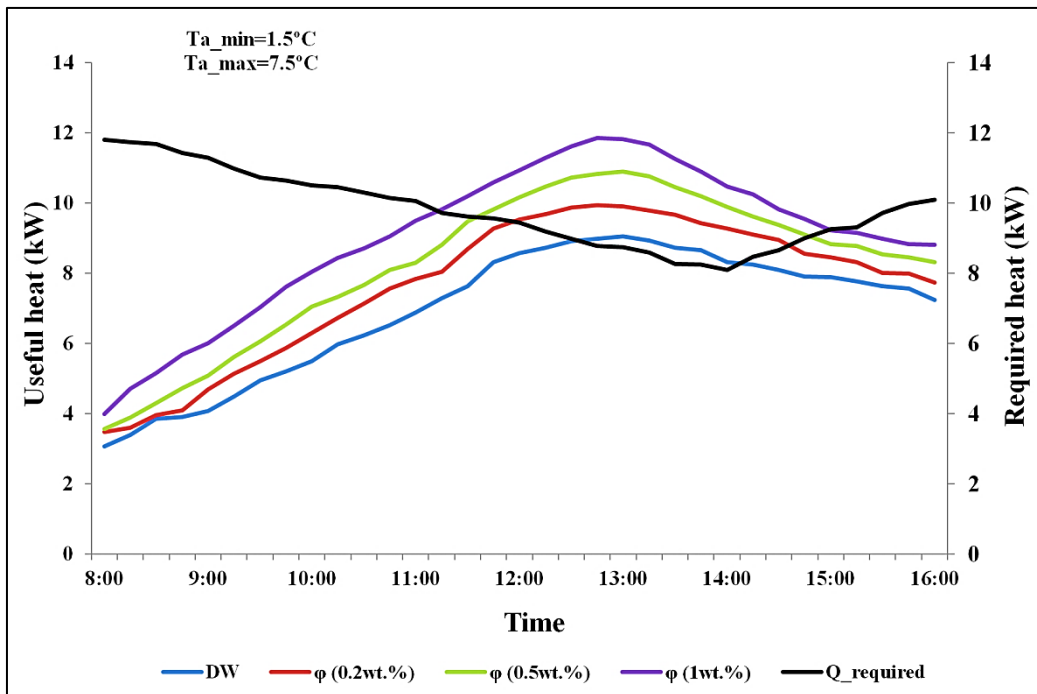


Figure 6.34 Greenhouse heating load required and energy provided (heat supply) with non-set-point temperature for 4<sup>th</sup> February.

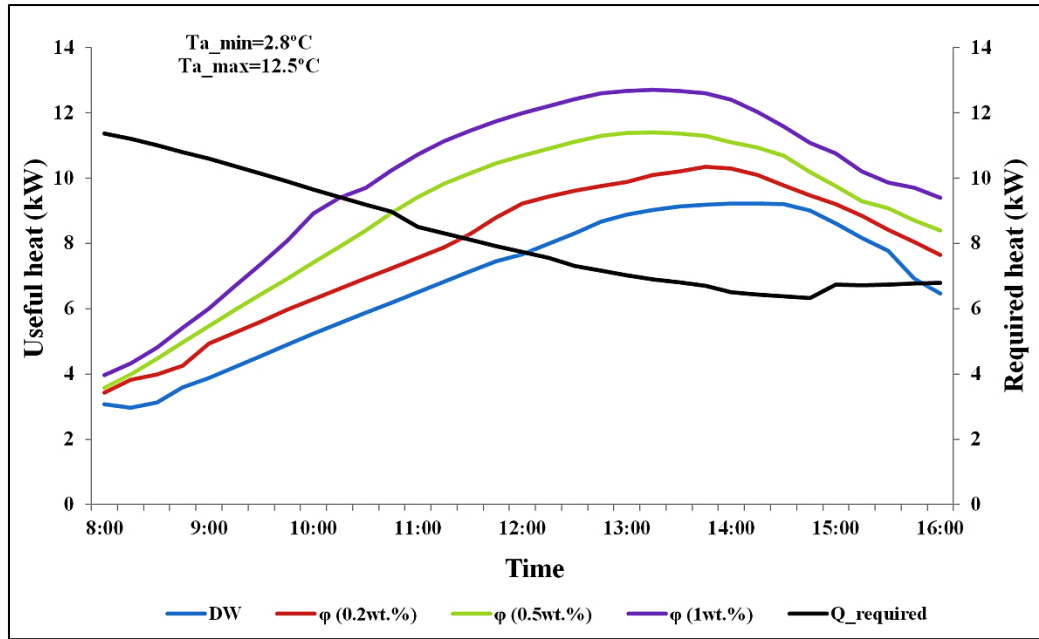


Figure 6.35 Greenhouse heating load required and energy provided (heat supply) with non-set-point temperature for 4<sup>th</sup> March.

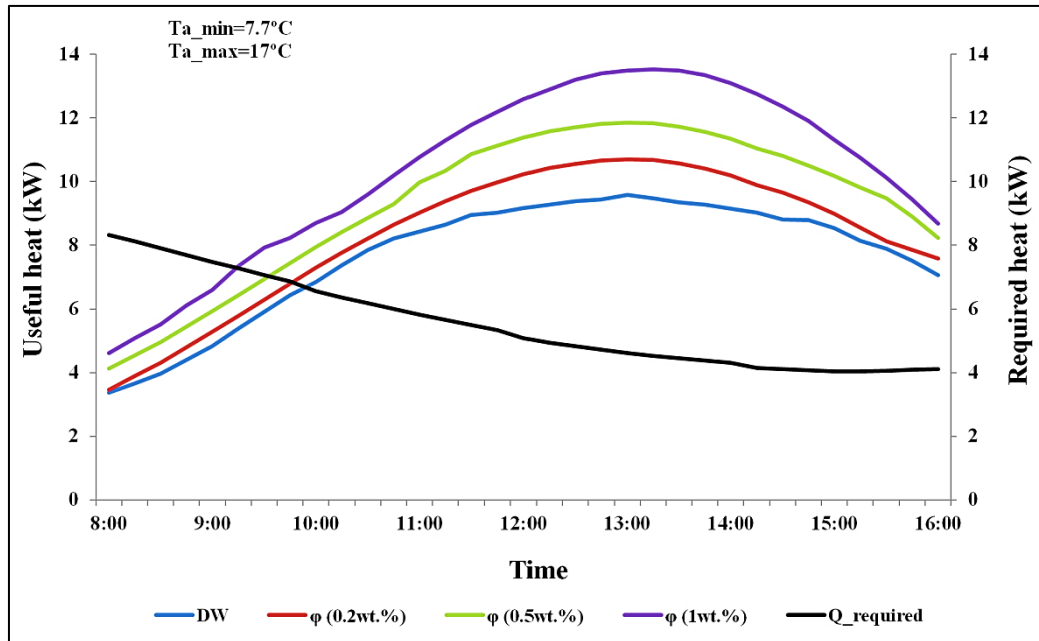


Figure 6.36 Greenhouse heating load required and energy provided (heat supply) with non-set-point temperature for 3<sup>th</sup> April.

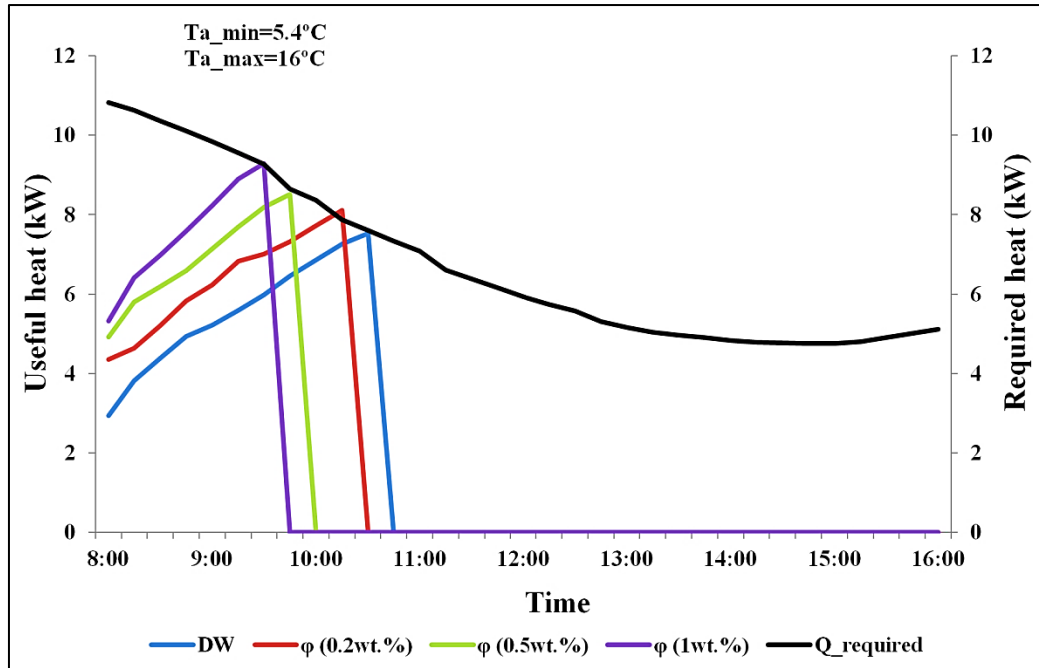


Figure 6.37 Greenhouse heating load required and energy provided (heat supply) with set-point temperature for 30<sup>th</sup> November.

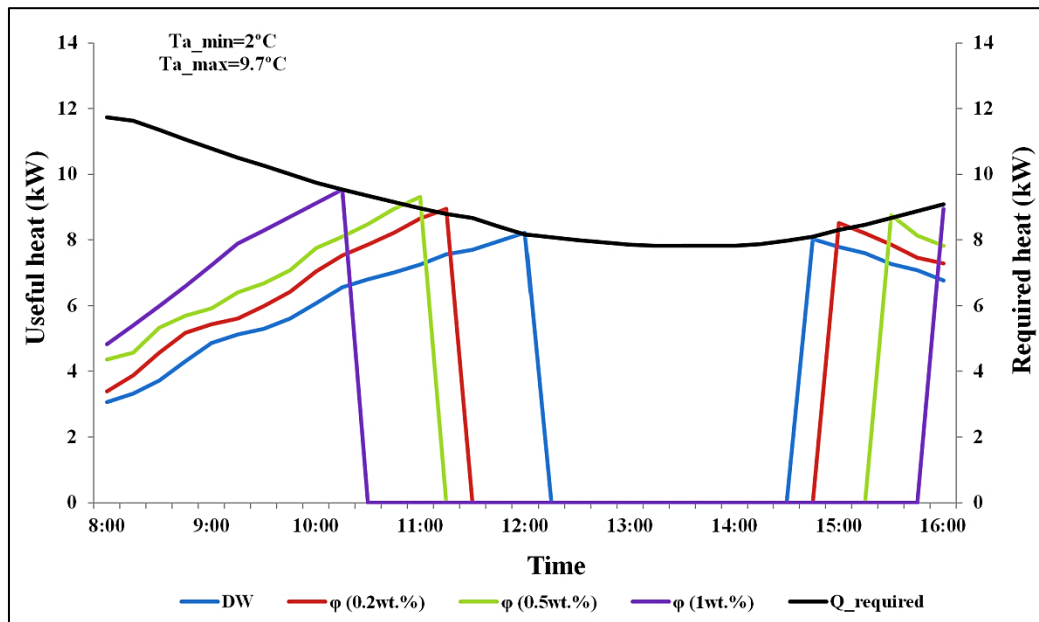


Figure 6.38 Greenhouse heating load required and energy provided (heat supply) with set-point temperature for 28<sup>th</sup> December.

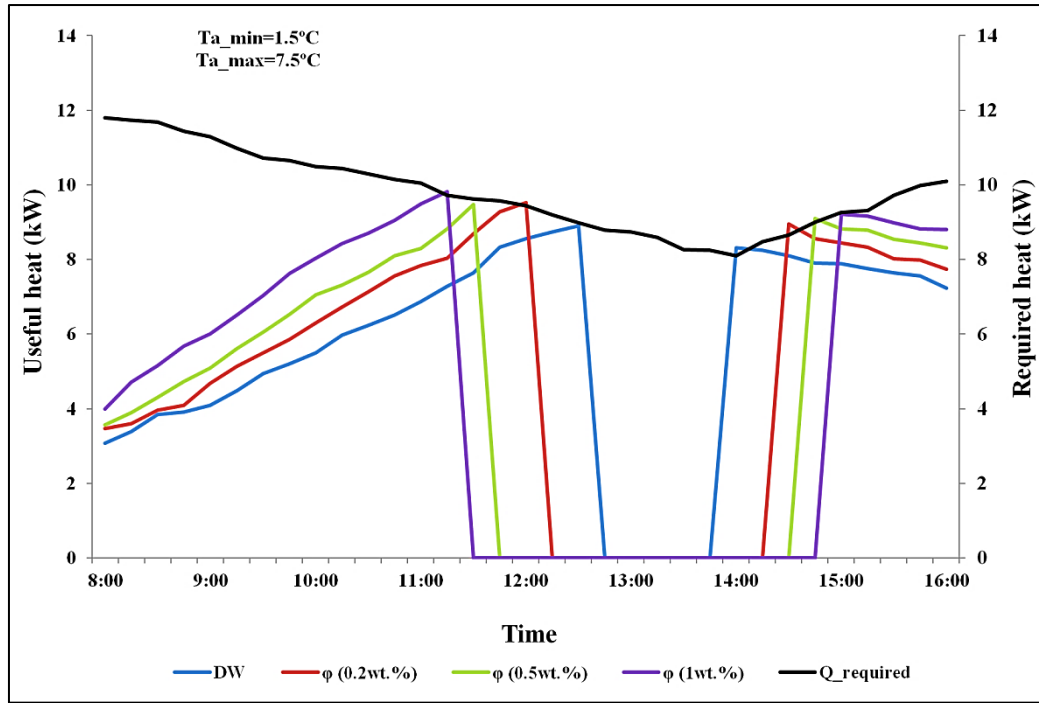


Figure 6.39 Greenhouse heating load required and energy provided (heat supply) with set-point temperature for 4<sup>th</sup> February.

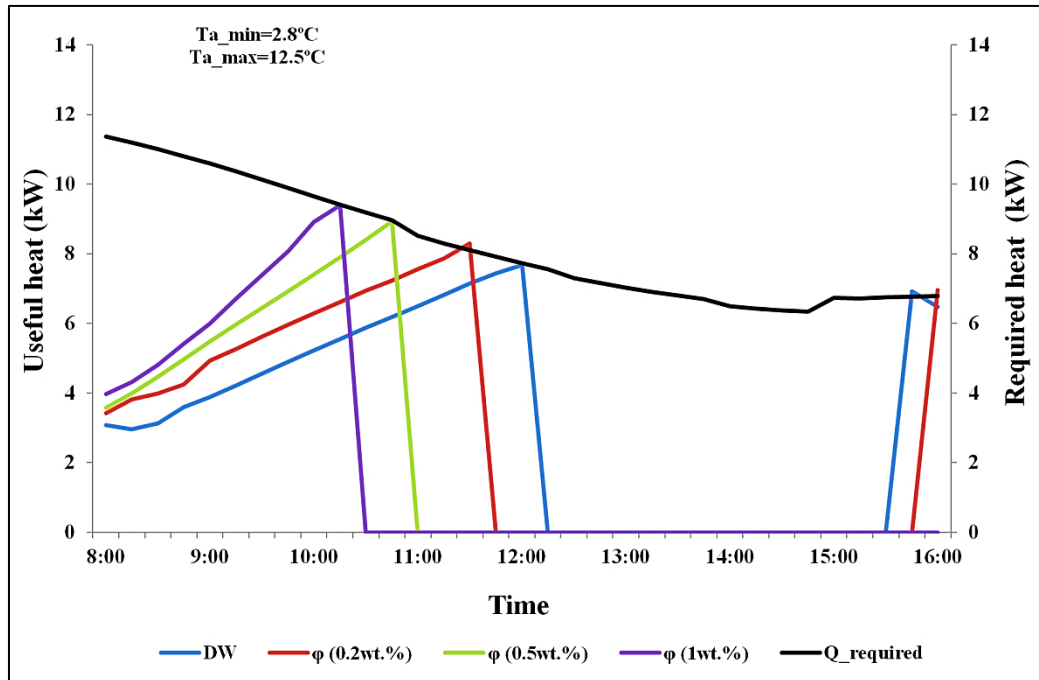


Figure 6.40 Greenhouse heating load required and energy provided (heat supply) with non-set-point temperature for 4<sup>th</sup> March.

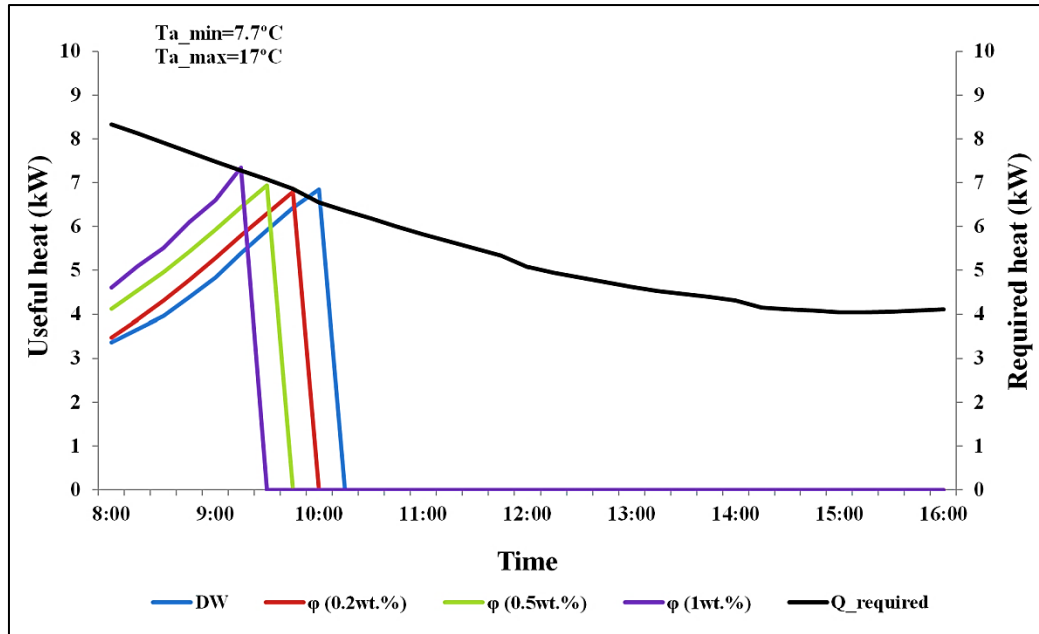


Figure 6.41 Greenhouse heating load required and energy provided (heat supply) with set-point temperature for 3<sup>th</sup> April.

Finally, Table 6.3 illustrates the greenhouse average monthly useful heat supply in kWh during November, December, January, February, March, and April. It was observed that the maximum useful heat supply to the greenhouse was during November, which was (2715.9, 3213.1, 3378.7, and 3608.4) kWh for DW and 0.2wt.%, 0.5wt.%, and 1wt.%  $\text{Al}_2\text{O}_3$ -water nanofluid, respectively. In contrast, Figure 6.42 shows the average monthly solar irradiance during these six months.

Table 6.3: Average monthly greenhouse useful heat in (kWh).

Month	Water	Al <sub>2</sub> O <sub>3</sub> -water nanofluid		
		(0.2 wt. %)	(0.5 wt. %)	(1 wt. %)
November	2715.90	3213.1	3378.7	3608.4
December	2580.68	2880.8	2979.7	3178.7
January	2288.13	2793.99	2889.60	2998.2
February	2451.37	2913.26	3003.53	3218.6
March	2643.92	3168.71	3212.20	3428.7
April	2662.77	3187.48	3289.42	3598.8

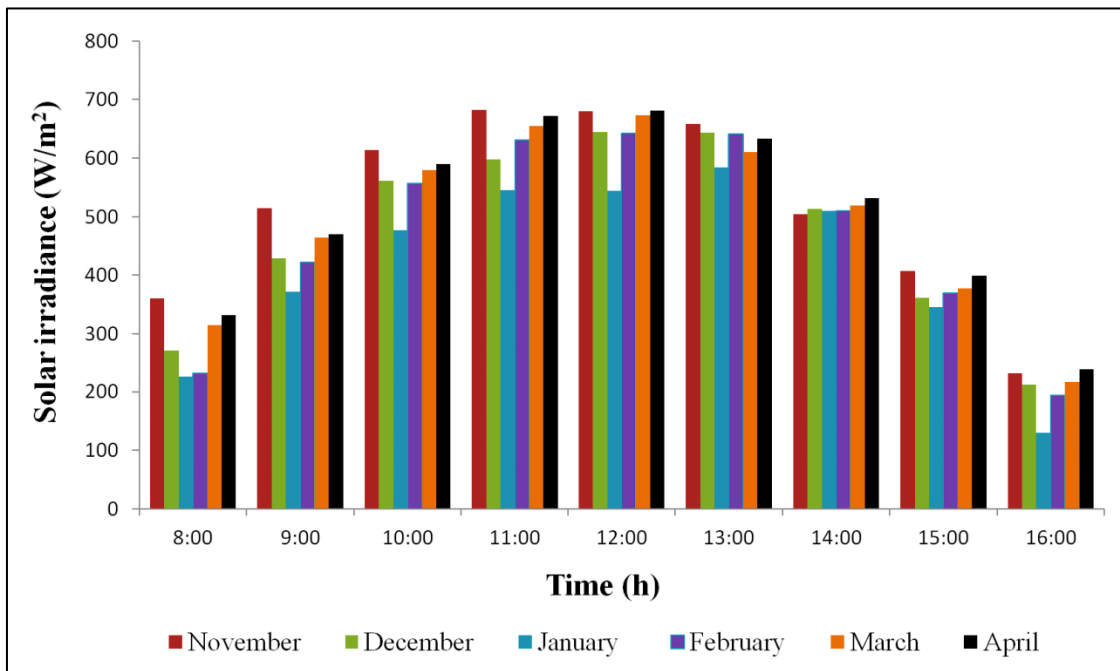


Figure 6.42 Monthly average solar irradiance.



## CHAPTER 7

### CONCLUSION AND RECOMMENDATIONS

#### 7.1 Summary

This research aimed to evaluate the viability of utilizing SWHS for greenhouse heating systems using  $\text{Al}_2\text{O}_3$ -water nanofluid as the working fluid in the Kurdistan Region of Iraq. The project aimed to maximize energy saving and enhance the collector's performance. This study used the experimental and TRNSYS simulation programs to determine how well the collector works for heating greenhouses. This study focused on using nanofluids with improved thermo-physical properties of the base fluid to enhance solar collector performance and increase the collector efficiency compared to distilled water. As a first step, water was used as the working fluid in this work, and then replaced by  $\text{Al}_2\text{O}_3$ -water nanofluids as a second step.

#### 7.2 Conclusion

A flat plate solar water heating system was assigned to greenhouse heating using different working fluids experimentally and numerically, and the following points were concluded in this work:

1. The experimental results illustrated that using  $\text{Al}_2\text{O}_3$ -water nanofluid at a concentration of 0.2wt.% increase the collector efficiency by 7.9% compared to water.
2. Verification findings demonstrate that the experimental and simulation results are in excellent agreement with acceptable accuracy.

3. The simulation results indicate that the maximum efficiency of the collector was achieved, when 1wt.% nanofluid was used, which increased the collector efficiency by 26.1% over the water case. Any further increase in the percentage of nanoparticles reduces collector efficiency.
4. Increasing the nanoparticle percentage in the nanofluid to 1wt.% increased the pressure drop by 2.97% compared with the water, which does not adversely affect the collector's thermal performance.
5. The absorbed energy parameter  $F_R(\tau\alpha)$  values of  $\text{Al}_2\text{O}_3$ -water nanofluid for all applied concentrations were higher than utilizing water. Moreover, when a nanoparticle concentration of 1wt.% was used, there will be a 34% increase in this factor compared to using water only.
6. The maximum estimated value of the greenhouse heating load was 12.8 kW. In summary, these results show that the maximum heat supply to the greenhouse was during November, which was (2715.9, 3213.1, 3378.7, and 3608.4) kWh for DW and 0.2wt.%, 0.5wt.%, and 1wt.%  $\text{Al}_2\text{O}_3$ -water nanofluid, respectively.
7. Adding nanofluid to the system as HTFs, could produce and store more energy, which in turn, increase energy produced by about 22% over the case of using water only.
8. Using nanofluid instead of water as a working fluid yields significant economic results, where the system payback period is about 6 years compared to 7 years for water.

### 7.3 Recommendation for Further Study

Considerably, the following suggestions have been identified for future scope of work:

- The experiment can be repeated using a surfactant and a higher concentration of nanofluids.
- Using nanofluid in the circulation between the storage tank and the greenhouse instead of between the storage tank and the collectors.
- During nanofluid preparation, the experiment can be repeated with various base fluids. It is possible to use base fluids such as ethylene glycol, or transformer oil and compare their effects.
- Using hybrid nanofluids to investigate the FPSCs performance. In FPSCs, a profitable HTF is a mixture of two or more different nanoparticles dispersed in the base fluid.
- Experiments may be carried out using varying volume flow rates and also different nanoparticle sizes.
- Adding electrical heaters to the storage tanks to investigate the amount of energy required in addition to the SWHS energy and to calculate the solar fraction of the system, which indicates whether the system is entirely powered by solar collectors or needs to be powered by electrical heaters to overcome the greenhouse heating load.
- The experiment can be conducted with PV-T hybrid collectors.

## REFERENCES

- Ahmed, K., Mustafa, J. and Hasan, M. (2013) 'Cooling and Heating a Greenhouse in Baghdad by a Solar Assisted Desiccant System', *Journal of Engineering*, 19(8), pp. 933–951.
- Alim, M. A. et al. (2013) 'Analyses of Entropy Generation and Pressure Drop for a Conventional Flat Plate Solar Collector Using Different Types of Metal Oxide Nanofluids', *Energy and Buildings*, 66, pp. 289–296. doi: 10.1016/j.enbuild.2013.07.027.
- Angayarkanni, S. A. and Philip, J. (2015) 'Review on Thermal Properties of Nanofluids: Recent Developments', *Advances in Colloid and Interface Science*, 225, pp. 146–176. doi: 10.1016/j.cis.2015.08.014.
- Arthur, O. and Karim, M. A. (2016) 'An Investigation into the Thermophysical and Rheological Properties of Nanofluids for Solar Thermal Applications', *Renewable and Sustainable Energy Reviews*, 55, pp. 739–755. doi: 10.1016/j.rser.2015.10.065.
- Attar, I. et al. (2013) 'Parametric and Numerical Study of a Solar System for Heating a Greenhouse Equipped With a Buried Exchanger', *Energy Conversion and Management*, 70, pp. 163–173. doi: 10.1016/j.enconman.2013.02.017.
- Bazgaou, A. et al. (2021) 'Effect of Active Solar Heating System on Microclimate, Development, Yield and Fruit Quality in Greenhouse Tomato Production', *Renewable Energy*, 165, pp. 237–250. doi: 10.1016/j.renene.2020.11.007.
- Bellos, E., Said, Z. and Tzivanidis, C. (2018) 'The Use of Nanofluids in Solar Concentrating Technologies: A Comprehensive Review', *Journal of Cleaner Production*, 196, pp. 84–99. doi: 10.1016/j.jclepro.2018.06.048.

- Bezaatpour, M. and Rostamzadeh, H. (2021) 'Simultaneous Energy Storage Enhancement and Pressure Drop Reduction in Flat Plate Solar Collectors Using Rotary Pipes With Nanofluid', *Energy and Buildings*, 239, p. 110855. doi: 10.1016/j.enbuild.2021.110855.
- Bhowmik, H. and Amin, R. (2017) 'Efficiency Improvement of Flat Plate Solar Collector Using Reflector', *Energy Reports*, 3, pp. 119–123. doi: 10.1016/j.egyr.2017.08.002.
- Buonomo, B. et al. (2018) 'Application of Nanofluids in Solar Cooling System: Dynamic Simulation by Means of TRNSYS Software', *Modelling, Measurement and Control B*, 87(3), pp. 143–150. doi: 10.18280/mmc-b.870305.
- Chau, J. et al. (2009) 'Economic Sensitivity of Wood Biomass Utilization for Greenhouse Heating Application', *Applied Energy*, 86(5), pp. 616–621. doi: 10.1016/j.apenergy.2008.11.005.
- Cuce, E., Harjunowibowo, D. and Cuce, P. M. (2016) 'Renewable and Sustainable Energy Saving Strategies for Greenhouse Systems: A Comprehensive Review', *Renewable and Sustainable Energy Reviews*, 64, pp. 34–59. doi: 10.1016/j.rser.2016.05.077.
- Das, S. K., Choi, S. U. S. and Patel, H. E. (2006) 'Heat Transfer in Nanofluids - A Review', *Heat Transfer Engineering*, 27(10), pp. 3–19. doi: 10.1080/01457630600904593.
- Deceased, J. A. D. and Beckman, W. A. (1982) *Solar Engineering of Thermal Processes, Design Studies*. doi: 10.1016/0142-694x(82)90016-3.
- Dincer, I. (2000) 'Renewable Energy and Sustainable Development: A Crucial Review', *Renewable & sustainable energy reviews*, 4(2), pp. 157–175. doi: 10.1016/S1364-0321(99)00011-8.

- Esen, M. and Yuksel, T. (2013) 'Experimental Evaluation of Using Various Renewable Energy Sources for Heating a Greenhouse', *Energy and Buildings*, 65, pp. 340–351. doi: 10.1016/j.enbuild.2013.06.018.
- Faizal, M. et al. (2013) 'Energy, Economic and Environmental Analysis of Metal Oxides Nanofluid for Flat-Plate Solar Collector', *Energy Conversion and Management*, 76, pp. 162–168. doi: 10.1016/j.enconman.2013.07.038.
- Florschuetz, L. W. (1979) 'Extension of the Hottel-Whillier Model to the Analysis of Combined Photovoltaic/Thermal Flat Plate Collectors', *Solar Energy*, 22(4), pp. 361–366. doi: 10.1016/0038-092X(79)90190-7.
- Ganvir, R. B., Walke, P. V. and Kriplani, V. M. (2017) 'Heat Transfer Characteristics in Nanofluid—A Review', *Renewable and Sustainable Energy Reviews*, 75(November), pp. 451–460. doi: 10.1016/j.rser.2016.11.010.
- Giovannetti, F. et al. (2014) 'High Transmittance, Low Emissivity Glass Covers for Flat Plate Collectors: Applications and Performance', *Solar Energy*, 104, pp. 52–59. doi: 10.1016/j.solener.2013.10.006.
- Hawwash, A. A. et al. (2018) 'Numerical Investigation and Experimental Verification of Performance Enhancement of Flat Plate Solar Collector Using Nanofluids', *Applied Thermal Engineering*, 130, pp. 363–374. doi: 10.1016/j.applthermaleng.2017.11.027.
- Hawwash, A. A. et al. (2021) 'Thermal Analysis of Flat Plate Solar Collector Using Different Nanofluids and Nanoparticles Percentages', *IEEE Access*, 9, pp. 52053–52066. doi: 10.1109/ACCESS.2021.3060004.

- He, Q., Zeng, S. and Wang, S. (2014) 'Experimental Investigation on the Efficiency of Flat-Plate Solar Collectors With Nanofluids', *Applied Thermal Engineering*, 88, pp. 165–171. doi: 10.1016/j.applthermaleng.2014.09.053.
- Holman, V. (1999) 'Introduction', *Visual Resources*, 15(3), pp. ix–x. doi: 10.1080/01973762.1999.9658510.
- Jamar, A. et al. (2016) 'A Review of Water Heating System for Solar Energy Applications', *International Communications in Heat and Mass Transfer*, 76, pp. 178–187. doi: 10.1016/j.icheatmasstransfer.2016.05.028.
- Jani, D. B. et al. (2020) 'A Review on Use of TRNSYS as Simulation Tool in Performance Prediction of Desiccant Cooling Cycle', *Journal of Thermal Analysis and Calorimetry*, 140(5), pp. 2011–2031. doi: 10.1007/s10973-019-08968-1.
- Joardder, M. U. H. et al. (2017) *Solar Pyrolysis: Converting Waste into Asset Using Solar Energy, Clean Energy for Sustainable Development: Comparisons and Contrasts of New Approaches*. Elsevier Inc. doi: 10.1016/B978-0-12-805423-9.00008-9.
- Joudi, K. A. and Farhan, A. A. (2014) 'Greenhouse Heating by Solar Air Heaters on the Roof', *Renewable Energy*, 72, pp. 406–414. doi: 10.1016/j.renene.2014.07.025.
- Kalogirou, S. A. (2001) 'Use a TRNSYS for Modelling and Simulation of a Hybrid Pv-Thermal Solar System for Cyprus', *Renewable Energy*, 23(2), pp. 247–260. doi: 10.1016/S0960-1481(00)00176-2.
- Kannan, N. and Vakeesan, D. (2016) 'Solar Energy for Future World: - A Review', *Renewable and Sustainable Energy Reviews*, 62, pp. 1092–1105. doi: 10.1016/j.rser.2016.05.022.

- Kiliç, F., Menlik, T. and Sözen, A. (2018) 'Effect of Titanium Dioxide/Water Nanofluid Use on Thermal Performance of the Flat Plate Solar Collector', *Solar Energy*, 164(April 2017), pp. 101–108. doi: 10.1016/j.solener.2018.02.002.
- Kober, T. et al. (2020) 'Global Energy Perspectives to 2060 – WEC's World Energy Scenarios 2019', *Energy Strategy Reviews*, 31(June), p. 100523. doi: 10.1016/j.esr.2020.100523.
- Li, S. et al. (2017) 'Comparative Study on the Performance of a New Solar Air Collector With Different Surface Shapes', *Applied Thermal Engineering*, 114, pp. 639–644. doi: 10.1016/j.applthermaleng.2016.12.026.
- Michael Joseph Stalin, P. et al. (2020) 'Energy, Economic and Environmental Investigation of a Flat plate Solar Collector With CeO<sub>2</sub>/Water Nanofluid', *Journal of Thermal Analysis and Calorimetry*, 139(5), pp. 3219–3233. doi: 10.1007/s10973-019-08670-2.
- Moghadam, A. J. et al. (2014) 'Effects of CuO/Water Nanofluid on the Efficiency of a Flat-Plate Solar Collector', *Experimental Thermal and Fluid Science*, 58, pp. 9–14. doi: 10.1016/j.expthermflusci.2014.06.014.
- Morad, D. H. (2018) 'The Potential and Social Acceptability of Renewable Energy Sources in North Iraq: Kurdistan Region', *Academic Journal of Nawroz University*, 7(4), p. 93. doi: 10.25007/ajnu.v7n4a276.
- Moravej, M. et al. (2020) 'Enhancing the Efficiency of a Symmetric Flat-Plate Solar Collector via the Use of Rutile TiO<sub>2</sub>-Water Nanofluids', *Sustainable Energy Technologies and Assessments*, 40(October 2019). doi: 10.1016/j.seta.2020.100783.
- Muhammad, M. J. et al. (2016) 'The Use of Nanofluids for Enhancing the Thermal Performance of Stationary Solar Collectors: A Review', *Renewable and Sustainable Energy Reviews*, 63, pp. 226–236. doi: 10.1016/j.rser.2016.05.063.



- Mukherjee, S. et al. (2020) 'Transient Heat Transfer Characteristics and Process Intensification with Al<sub>2</sub>O<sub>3</sub>-Water and TiO<sub>2</sub>-Water Nanofluids: An Experimental Investigation', *Chemical Engineering and Processing - Process Intensification*, 150(February), p. 107887. doi: 10.1016/j.cep.2020.107887.
- Naderi, M. (2016) 'Nano Fluid in Water as Base Fluid in Flat-Plate Solar Collectors With an Emphasis on Heat Transfer', *Indian Journal of Science and Technology*, 9(31). doi: 10.17485/ijst/2016/v9i31/90341.
- Pandya, H. and Behura, A. K. (2017) 'Experimental Study of V-Through Solar Water Heater for Tilt Angle and Glass Transmissivity', *Energy Procedia*, 109(November 2016), pp. 377–384. doi: 10.1016/j.egypro.2017.03.034.
- Raj, P. and Subudhi, S. (2018) 'A Review of Studies Using Nanofluids in Flat-Plate and Direct Absorption Solar Collectors', *Renewable and Sustainable Energy Reviews*, 84(August 2017), pp. 54–74. doi: 10.1016/j.rser.2017.10.012.
- Resources, T. and All, L. L. C. (2012) 'Reductions in Energy Consumption and CO<sub>2</sub> Emissions for Greenhouses Heated With Heat Pumps', 28(3), pp. 401–406.
- Saffarian, M. R., Moravej, M. and Doranehgard, M. H. (2020) 'Heat Transfer Enhancement in a Flat Plate Solar Collector With Different Flow Path Shapes Using Nanofluid', *Renewable Energy*, 146, pp. 2316–2329. doi: 10.1016/j.renene.2019.08.081.
- Said, Z., Sabiha, M. A., et al. (2015) 'Performance Enhancement of a Flat Plate Solar Collector Using Titanium Dioxide Nanofluid and Polyethylene Glycol Dispersant', *Journal of Cleaner Production*, 92, pp. 343–353. doi: 10.1016/j.jclepro.2015.01.007.
- Salavati Meibodi, S. et al. (2015) 'Experimental Investigation on the Thermal Efficiency and Performance Characteristics of a Flat Plate Solar Collector Using SiO<sub>2</sub>/EG-Water

- Nanofluids', *International Communications in Heat and Mass Transfer*, 65, pp. 71–75.  
doi: 10.1016/j.icheatmasstransfer.2015.02.011.
- Sarkar, J. (2011) 'A critical Review on Convective Heat Transfer Correlations of Nanofluids', *Renewable and Sustainable Energy Reviews*, 15(6), pp. 3271–3277. doi: 10.1016/j.rser.2011.04.025.
- Sharafeldin, M. A. and Gróf, G. (2018) 'Experimental Investigation of Flat Plate Solar Collector Using CeO<sub>2</sub>-Water Nanofluid', *Energy Conversion and Management*, 155(October 2017), pp. 32–41. doi: 10.1016/j.enconman.2017.10.070.
- Shukla, R. et al. (2013) 'Recent Advances in the Solar Water Heating Systems: A Review', *Renewable and Sustainable Energy Reviews*, 19, pp. 173–190. doi: 10.1016/j.rser.2012.10.048.
- Sint, N. K. C. et al. (2017) 'Theoretical Analysis to Determine the Efficiency of a CuO-Water Nanofluid Based-Flat Plate Solar Collector for Domestic Solar Water Heating System in Myanmar', *Solar Energy*, 155, pp. 608–619. doi: 10.1016/j.solener.2017.06.055.
- Suman, S., Khan, M. K. and Pathak, M. (2015) 'Performance Enhancement of Solar Collectors - A Review', *Renewable and Sustainable Energy Reviews*, 49, pp. 192–210. doi: 10.1016/j.rser.2015.04.087.
- Taki, M., Rohani, A. and Rahmati-Joneidabad, M. (2018) 'Solar Thermal Simulation and Applications in Greenhouse', *Information Processing in Agriculture*, 5(1), pp. 83–113. doi: 10.1016/j.inpa.2017.10.003.
- Tong, Y. et al. (2019) 'Energy and Exergy Comparison of a Flat-Plate Solar Collector Using Water, Al<sub>2</sub>O<sub>3</sub> Nanofluid, and CuO Nanofluid', *Applied Thermal Engineering*, 159(October 2018), p. 113959. doi: 10.1016/j.applthermaleng.2019.113959.

- Verma, S. K., Tiwari, A. K. and Chauhan, D. S. (2016) 'Performance Augmentation in Flat Plate Solar Collector Using MgO/Water Nanofluid', *Energy Conversion and Management*, 124, pp. 607–617. doi: 10.1016/j.enconman.2016.07.007.
- Xu, W., Song, W. and Ma, C. (2020) 'Performance of a Water-Circulating Solar Heat Collection and Release System for Greenhouse Heating using an Indoor Collector Constructed of Hollow Polycarbonate Sheets', *Journal of Cleaner Production*, 253, p. 119918. doi: 10.1016/j.jclepro.2019.119918.
- Xuan, Y. and Roetzel, W. (2000) 'Conceptions for Heat Transfer Correlation of Nanofluids', *International Journal of Heat and Mass Transfer*, 43(19), pp. 3701–3707. doi: 10.1016/S0017-9310(99)00369-5.
- Yousefi, T. et al. (2012) 'An Experimental Investigation on the Effect of Al<sub>2</sub>O<sub>3</sub>-H<sub>2</sub>O Nanofluid on the Efficiency of Flat-Plate Solar Collectors', *Renewable Energy*, 39(1), pp. 293–298. doi: 10.1016/j.renene.2011.08.056.
- Yu, W. and Choi, S. U. S. (2003) 'The Role of Interfacial Layers in the Enhanced Thermal Conductivity of Nanofluids: A Renovated Maxwell Model', *Journal of Nanoparticle Research*, 5(1–2), pp. 167–171. doi: 10.1023/A:1024438603801.
- Zayed, M. E. et al. (2019) 'Factors Affecting the Thermal Performance of the Flat Plate Solar Collector Using Nanofluids: A Review', *Solar Energy*, 182(November 2018), pp. 382–396. doi: 10.1016/j.solener.2019.02.054.
- Zhou, L., Wang, Y. and Huang, Q. (2019) 'Parametric Analysis on the Performance of Flat Plate Collector With Transparent Insulation Material', *Energy*, 174, pp. 534–542. doi: 10.1016/j.energy.2019.02.168.

Zhu, Y. et al. (2017) 'A Superhydrophobic Solar Selective Absorber Used in a Flat Plate Solar Collector', RSC Advances, 7(54), pp. 34125–34130. doi: 10.1039/c7ra04238h.

## APPENDIX (A)

### SAMPLE OF CALCULATIONS

The first section of this appendix provides a sample of calculations for determining the greenhouses overall thermal losses during the coldest day of the winter season.

In the subsequent sections of the appendix, a similar discussion for the determination of the FPSCs efficiency, the amount of heat supply from the storage tank to the greenhouse, the amount of pressure drop, and pumping power for two different working fluids (water, and  $\text{Al}_2\text{O}_3$ -water nanofluid with a concentration of 0.2wt.%) were presented. In addition, the entire findings of the associated investigations are shown in the results chapter.

#### A.1 Greenhouse Heating Load Calculation

In this section, the maximum required heating load is estimated using Eq. (3.1), (3.2), and (3.3), based on the lowest ambient air temperature on the coldest day of the year (12<sup>th</sup> January, 2022). The greenhouse-required heating load can be calculated as follows:

- Zoon inside design temperature  $T_r$  (23 °C)
- Outside temperature  $T_a$  (0 °C)
- Inside unconditioned space  $T_s$  (7 °C)

Specification of the greenhouse:

- Length (base) ( $b$ ) =5.25 m
- Width ( $w_i$ ) =4.95 m

- Triangular high ( $h_b$ ) = 0.3 m
- Side wall high ( $h_s$ ) = 3.3 m
- Top to bottom high ( $h$ ) = 3.6 m
- Glass thickness ( $th$ ) = 0.01 m [Single glass]
- $h_i$  = 8.32 W/m<sup>2</sup>.°C
- $h_o$  = 34.1 W/m<sup>2</sup>.°C
- $k_m$  = 0.96 W/m.°C

**East and West side:**

Both sides have the same area, and can be estimated as follows:

$$Area_1 = \frac{1}{2} b h_b$$

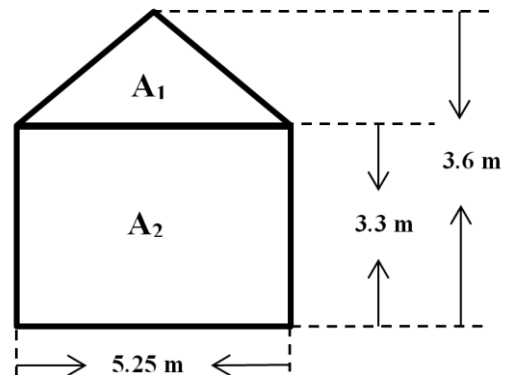
$$= \frac{1}{2} \times 5.25 \times 0.3 = 0.78 m^2$$

$$Area_2 = b \times h_s$$

$$= 5.25 \times 3.3 = 17.33 m^2$$

$$Area_{total} = Area_1 + Area_2$$

$$= 0.78 + 17.33 = 18 m^2$$



$$R_{total} = \frac{1}{h_i} + \frac{x}{k_m} + \frac{1}{h_o}$$

$$= \frac{1}{8.32} + \frac{0.01}{0.96} + \frac{1}{34.1} = 0.16 \text{ } ^\circ\text{C}/W$$

$$U = \frac{1}{R_{total}}$$

$$= \frac{1}{0.16} = 6.25 \text{ } W/m^2 \cdot ^\circ\text{C}$$

$$\begin{aligned}
 Q_{Gloss(East)} &= U A_G (T_r - T_a) \\
 &= 6.25 \times 17.94 \times (23 - 0) \\
 &= 2578.88 \text{ W} = 2.579 \text{ kW}
 \end{aligned}$$

$$\begin{aligned}
 Q_{Gloss(West)} &= U A_G (T_r - T_s) \\
 &= 6.25 \times 17.94 \times (23 - 7) \\
 &= 1794 \text{ W} = 1.794 \text{ kW}
 \end{aligned}$$

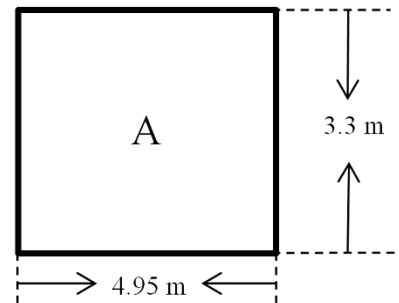
**North and South side:**

Both sides have the same area, and the heating load, and can be determined as follows:

$$Area = w_i \times h_s$$

$$= 4.95 \times 3.3 = 16.34 \text{ m}^2$$

$$\begin{aligned}
 R_{total} &= \frac{1}{h_i} + \frac{x}{k_m} + \frac{1}{h_o} \\
 &= \frac{1}{8.32} + \frac{0.01}{0.96} + \frac{1}{34.1} = 0.16 \text{ } ^\circ\text{C/W}
 \end{aligned}$$



$$\begin{aligned}
 U &= \frac{1}{R_{total}} \\
 &= \frac{1}{0.16} = 6.25 \text{ W/m}^2 \cdot ^\circ\text{C}
 \end{aligned}$$

$$\begin{aligned}
 Q_{Gloss(North)} &= U A_G (T_r - T_a) \\
 &= 6.25 \times 16.34 \times (23 - 0) \\
 &= 2348.88 \text{ W} = 2.349 \text{ kW}
 \end{aligned}$$

Additionally,

$$Q_{Gloss(South)} = 2.349 \text{ kW}$$

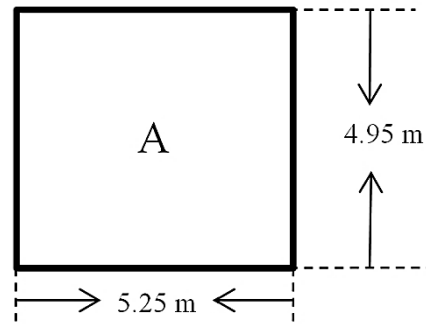
**Top side:**

$$Area = w_i \times b$$

$$= 4.95 \times 5.25 = 25.99 \text{ m}^2$$

$$R_{total} = \frac{1}{h_i} + \frac{x}{k_m} + \frac{1}{h_o}$$
$$= \frac{1}{8.32} + \frac{0.01}{0.96} + \frac{1}{34.1} = 0.16 \text{ }^\circ\text{C/W}$$

$$U = \frac{1}{R_{total}}$$
$$= \frac{1}{0.16} = 6.25 \text{ W/m}^2 \cdot ^\circ\text{C}$$



$$Q_{Gloss(Top)} = U A_G (T_r - T_a)$$
$$= 6.25 \times 25.99 \times (23 - 0)$$
$$= 3736.06 \text{ W} = 3.736 \text{ kW}$$

**Total Heating Load:**

$$Q_{Gloss(total)} = Q_{Gloss(East)} + Q_{Gloss(West)} + Q_{Gloss(North)} + Q_{Gloss(South)}$$
$$+ Q_{Gloss(Tope)}$$
$$= 2.579 + 1.794 + 2.349 + 2.349 + 3.736 = 12.8 \text{ kW}$$



## A.2 Water Case

In this sample calculation, the FPSCs efficiency, the amount of heat supplied from the storage tank to the greenhouse, the amount of pressure drop, and the pumping power are all estimated using water as the working fluid with a water flow rate of 0.2 kg/s for 28<sup>th</sup> March.

### A.2.1 Thermal Performance Analysis of the FPSC

Calculating the collector efficiency at 13:00, as follows:

$$\dot{m}_c = 0.2 \text{ kg/s}$$

$$C_p = 4.19 \text{ kJ/kg.k}$$

$$T_{Co} = 67 \text{ }^\circ\text{C}$$

$$T_{Ci} = 50.6 \text{ }^\circ\text{C}$$

$$G_T = 999 \text{ W/m}^2$$

$$A_c = 20 \text{ m}^2$$

$$\begin{aligned} Q_{Cu} &= \dot{m}_c C_p (T_{Co} - T_{Ci}) \\ &= 0.2 \times 4.19 \times (67 - 50.6) = 13.74 \text{ kW} = 13743.2 \text{ Watt} \end{aligned}$$

$$\begin{aligned} \eta_{th} &= \frac{Q_{Cu}}{G_T A_c} \\ &= \frac{13743.2}{999 \times 20} \times 100 = 68.78 \% \end{aligned}$$

### A.2.2 Calculation of Heat Supply

A sample calculation for the amount of heat supply from the storage tank to the greenhouse was presented at 9:30 A.M. because at 13:00 the system was turned off.

$$\dot{m}_H = 0.08 \text{ kg/s}$$

$$C_p = 4.19 \text{ kJ/kg.k}$$

$$T_{Hi} = 39 \text{ }^\circ\text{C}$$

$$T_{Ho} = 22.6 \text{ }^\circ\text{C}$$

$$\begin{aligned} Q_{Hu} &= \dot{m}_H C_p (T_{Hi} - T_{Ho}) \\ &= 0.08 \times 4.19 \times (39 - 22.6) = 5.49 \text{ kW} \end{aligned}$$

### A.2.3 Pressure Drop and Pumping Power Analysis

In this instance, the pressure drop and pumping power value for water are calculated as follows:

$$\Delta l = 35 \text{ m}$$

$$D_i = 0.0254 \text{ m}$$

$$\dot{V} = 0.0002 \text{ m}^3/\text{s}$$

$$A_p = 5.06 \times 10^{-4} \text{ m}^2$$

$$\sum K_l = 16.18$$

$$\dot{m} = 0.2 \text{ kg/s}$$

$$\rho_{bf} = 997.1 \text{ kg/m}^3$$

$$\mu_{bf} = 0.89 \text{ mPa.s} = 0.00089 \text{ Pa.s}$$

$$V = \frac{\dot{V}}{A_p} = \frac{0.0002}{5.05 \times 10^{-4}} = 0.396 \text{ m/s}$$

$$Re = \frac{\rho V D_i}{\mu} = \frac{997.1 \times 0.396 \times 0.0254}{0.00089} = 11268.798 > 4000 \text{ \{Turbulent flow\}}$$

$$f = \frac{0.079}{(Re)^{1/4}} = \frac{0.079}{(11268.798)^{1/4}} = 7.667 \times 10^{-3}$$

The total pressure drop is determined by applying Eq. (3.13):

$$\begin{aligned} \Delta P &= f \frac{\rho V^2 \Delta l}{2 D_i} + \sum K_l \frac{\rho V^2}{2} \\ &= 7.667 \times 10^{-3} \left( \frac{997.1 \times 0.396^2}{2} \times \frac{35}{0.0254} \right) + 16.18 \left( \frac{997.1 \times 0.396^2}{2} \right) \\ &= 2091 \text{ Pa} = 2.091 \text{ kPa} \end{aligned}$$

Finally, the pumping power is calculated utilizing Eq. (3.18):

$$\begin{aligned} \text{pumping power} &= \dot{V} \times \Delta P \\ &= 0.0002 \times 2091 = 0.419 \text{ Watt} \end{aligned}$$

### A.3 Al<sub>2</sub>O<sub>3</sub>-Water Nanofluid

To achieve the appropriate calculation, the nanofluids thermal conductivity, density, specific heat, and viscosity must be calculated. Additionally, in this section, the efficiency of FPSC, the amount of pressure drop, and pumping power are determined using Al<sub>2</sub>O<sub>3</sub>-water nanofluid at a

concentration of 0.2wt.% with a mass flow rate of 0.2 kg/s for 31<sup>st</sup> March. The nanofluid is estimated to contain 50 nm-diameter spherical particles.

### A.3.1 Calculation of Thermophysical Properties

An example calculation for determining the thermophysical properties of Al<sub>2</sub>O<sub>3</sub>-water nanofluids at a concentration of 0.2wt.% are provided in this section.

The mixture's thermal conductivity ( $k$ ) can be calculated using Eq. (3.9):

$$\varphi = 0.2 \text{ wt. \%} = 0.002 \text{ wt.}$$

$$k_{bf} = 0.605 \text{ W/m.k}$$

$$k_p = 40 \text{ W/m.k}$$

$$\begin{aligned} k_{nf} &= k_{bf} \left[ \frac{k_p + 2k_{bf} - 2\varphi(k_{bf} - k_p)}{k_p + 2k_{bf} + \varphi(k_{bf} - k_p)} \right] \\ &= 0.605 \left[ \frac{40 + 2(0.605) - 2(0.002)(0.605 - 40)}{40 + 2(0.605) + (0.002)(0.605 - 40)} \right] = 0.6085 \text{ W/m.k} \end{aligned}$$

The density ( $\rho$ ) of the nanofluid can be determined using Eq. (3.10):

$$\rho_{bf} = 997.1 \text{ kg/m}^3$$

$$\rho_{np} = 3960 \text{ kg/m}^3$$

$$\rho_{nf} = (1 - \varphi)\rho_{bf} + \varphi\rho_{np}$$

$$= (1 - 0.002)997.1 + (0.002)3960 = 1003.026 \text{ kg/m}^3$$

The nanofluid's heat capacity ( $C_p$ ) can be determined applying Eq. (3.11):

$$C_{p,bf} = 4179 \text{ j/kg.k}$$

$$C_{p,np} = 773 \text{ j/kg.k}$$

$$\begin{aligned} C_{p,nf} &= \frac{(C_p\rho)_{bf}(1 - \varphi) + (C_p\rho)_{np}(\varphi)}{\rho_{nf}} \\ &= \frac{(4179 \times 997.1)(1 - 0.002) + (773 \times 3690)0.002}{1003.026} \\ &= 4152.105 \text{ j/kg.k} = 4.152 \text{ kj/kg.k} \end{aligned}$$

The viscosity ( $\mu$ ) of the nanofluid is found applying Eq. (3.12):

$$\mu_{bf} = 0.89 \text{ mPa.s}$$

$$\begin{aligned} \mu_{nf} &= \mu_{bf}(1 + 2.5\varphi) \\ &= 0.89(1 + 2.5(.002)) = 0.895 \text{ mPa.s} \end{aligned}$$

### A.3.2 Thermal Performance Analysis of the FPSC

Calculating the collector efficiency at 13:13, as follows:

$$\dot{m}_c = 0.2 \text{ kg/s}$$

$$C_{p,nf} = 4.152 \text{ kj/kg.k}$$

$$T_{Co} = 76.9 \text{ }^\circ\text{C}$$

$$T_{Ci} = 59 \text{ }^\circ\text{C}$$

$$G_T = 1000 \text{ W/m}^2$$

$$A_c = 20 \text{ m}^2$$

$$\begin{aligned} Q_{cu} &= \dot{m}_c C_p (T_{Co} - T_{Ci}) \\ &= 0.2 \times 4.152 \times (76.9 - 59) = 14.8642 \text{ kW} = 14864.2 \text{ Watt} \end{aligned}$$

$$\eta_{th} = \frac{Q_{Cu}}{G_T A_c}$$

$$= \frac{14864.2}{1000 \times 20} \times 100 = 74.3\%$$

### A.3.3 Pressure Drop and Pumping Power Analysis

In this example, the pressure drop and the pumping power value for the concentration of 0.2wt.% Al<sub>2</sub>O<sub>3</sub>-water nanofluid were calculated.

$$\Delta l = 35 \text{ m}$$

$$D_i = 0.0254 \text{ m}$$

$$\dot{V} = 0.0002 \text{ m}^3/\text{s}$$

$$A_p = 5.06 \times 10^{-4} \text{ m}^2$$

$$\sum K_l = 16.18$$

$$\dot{m} = 0.2 \text{ kg/s}$$

$$\rho_{nf} = 1003.026 \text{ kg/m}^3$$

$$\mu_{nf} = 0.895 \text{ mPa.s} = 0.000895 \text{ Pa}$$

$$V = \frac{\dot{V}}{A_p} = \frac{0.0002}{5.05 \times 10^{-4}} = 0.396 \text{ m/s}$$

$$Re = \frac{\rho V D_i}{\mu} = \frac{1003.026 \times 0.396 \times 0.0254}{0.000895} = 11272.443 > 4000 \text{ \{Turbulent flow\}}$$

$$f = \frac{0.079}{(Re)^{1/4}} = \frac{0.079}{(11272.443)^{1/4}} = 7.6669 \times 10^{-3}$$

The total pressure drop is determined by applying Eq. (3.13):

$$\Delta P = f \frac{\rho V^2 \Delta l}{2 D_i} + \sum K_l \frac{\rho V^2}{2}$$

$$\begin{aligned} &= 7.666 \times 10^{-3} \left( \frac{1003.026 \times 0.396^2}{2} \times \frac{35}{0.0254} \right) + 16.18 \left( \frac{1003.26 \times 0.396^2}{2} \right) \\ &= 2104 \text{ Pa} = 2.104 \text{ kPa} \end{aligned}$$

Finally, the pumping power is calculated using Eq. (3.18):

$$\begin{aligned} \text{pumping power} &= \dot{V} \times \Delta P \\ &= 0.0002 \times 2104 = 0.4208 \text{ Watt} \end{aligned}$$

## APPENDIX (B)

### TECHNICAL SPECIFICATION AND CALIBRATION

#### B.1 Temperature Sensors

##### B.1.1 Technical Specification of Temperature Sensors

Type	Content	Description
<b>QAP21.2</b>	Measuring range	(-30 to +180) °C
	Measurement accuracy at (-30 to +180) °C	±1.65 K
	Cable length	1.5 m
	Sensing element	LG-Ni1000
	Time constant	Without protection pocket: 20 s
	Degree of protection	IP67
<b>QAE26.9</b>	Measuring range	(-50 to +180) °C
	Measurement accuracy at (-50 to +180) °C	±1.75 K
	Cable length	2 m
	Sensing element	LG-Ni1000
	Time constant	<2.5 s
	Nominal pressure PN class	PN 16
	Immersion length	15 to 65 mm
<b>QAA25</b>	Measuring range	(0 to 50) °C
	Setpoint setting range	(5 to 35) °C
	Connection, electrical	Screw terminals
	Sensing element	LG-Ni1000
	Time constant	420 s
	Degree of protection	IP30



## B.2 Flow Meter

### B.2.1 Technical Specification of Flow Meter

Content	Description
Measuring range	1.8-32 l/min
Max. pressure at medium temperature during life	12 bar at 40 °C 6 bar at 100 °C
Measuring accuracy at < 50% FS (water) at > 50% FS (water)	<1% FS (Full Scale) <2% measured value
Nominal width diameter	DN10 mm

### B.2.2 Calibration of Flow Meter Type QVE3100

Calibrated flow rate (Lit/min)	Measured flow rate (Lit/min)	Delta
6.7	8.7	2
8.3	10.1	1.8
11.1	12	0.9
14.3	15.5	1.2
15.4	16	0.6

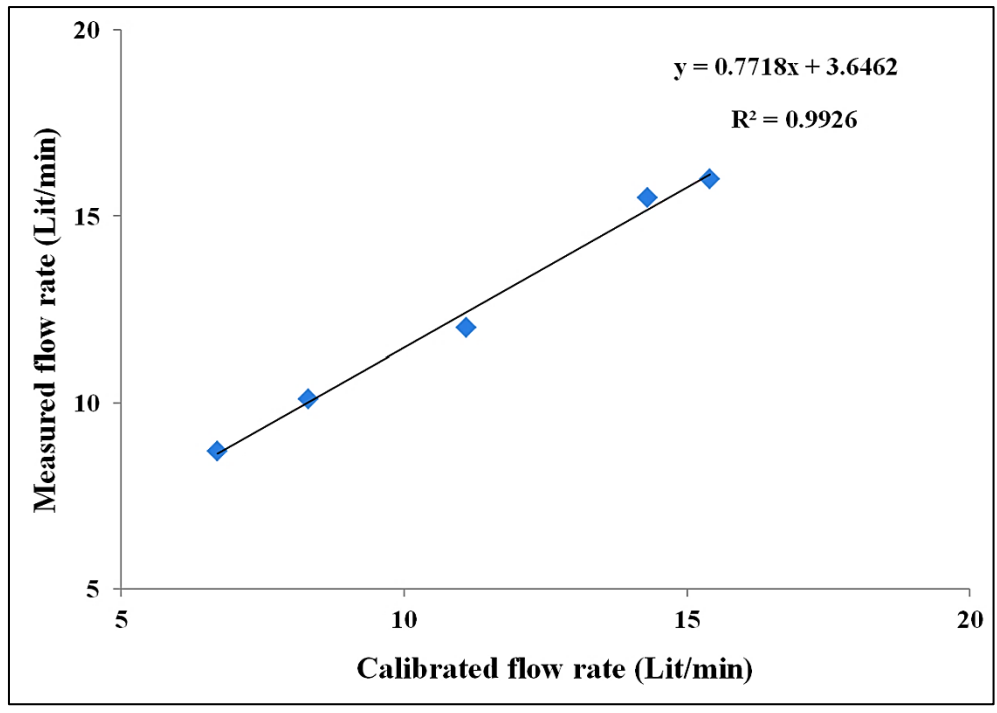


Figure B.1 Calibration curve for flow meter type QVE3100.

## APPENDIX (C)

### SAMPLE OF TRNSYS SIMULATION RESULTS

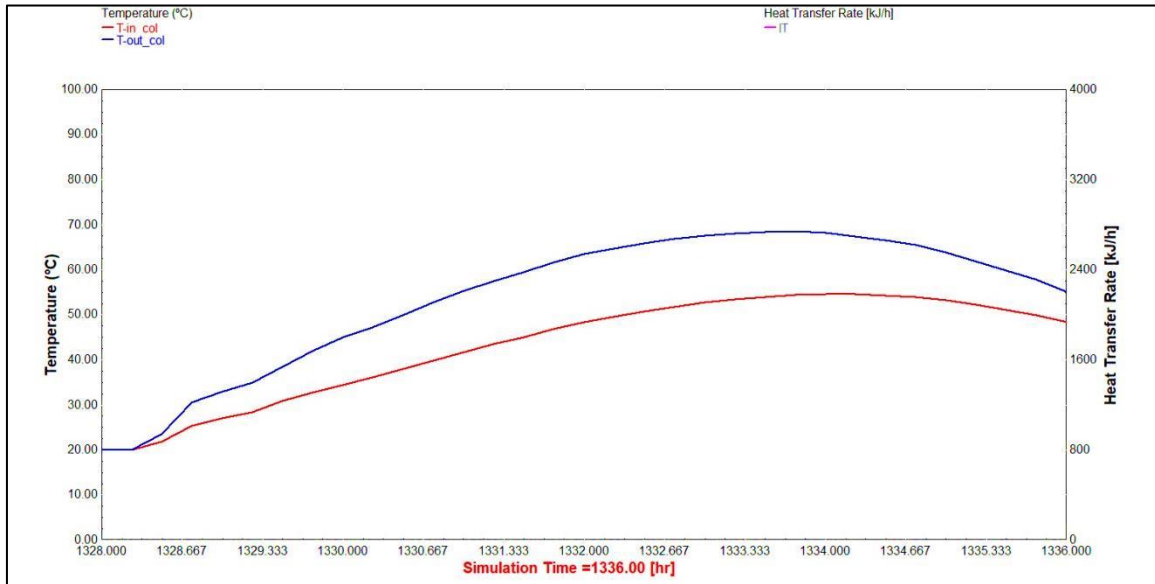


Figure C.1 TRNSYS inlet and the outlet collector water temperature of the FPSC.

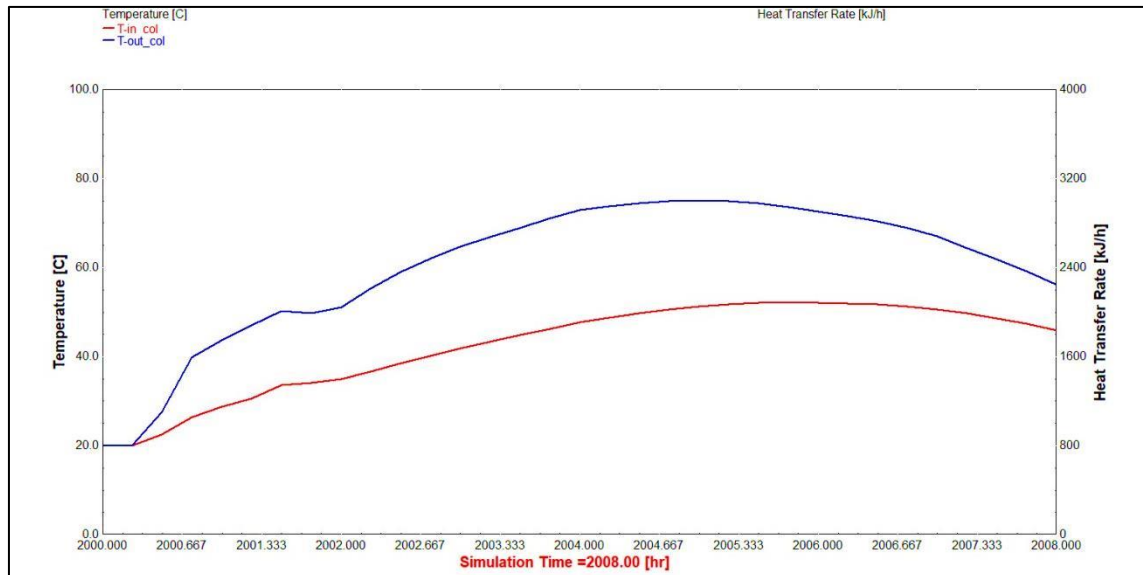


Figure C.2 TRNSYS inlet and the outlet collector Al<sub>2</sub>O<sub>3</sub> nanofluid temperature of the FPSC.

## APPENDIX (D)

### EXPERIMENTAL RESULTS

#### C.1 Inlet and Outlet Temperature (°C) of the FPSC

Time	10 <sup>th</sup> March		12 <sup>th</sup> March		15 <sup>th</sup> March		16 <sup>th</sup> March		26 <sup>th</sup> March		28 <sup>th</sup> March	
	Ti	To	Ti	To	Ti	To	Ti	To	Ti	To	Ti	To
8:00	21	23.1	21.0	23.1	21.3	23.8	26.4	28.8	27.0	31.5	29.0	31.9
8:15	23	25.4	22.0	24.5	24.0	26.9	27.6	30.4	27.5	33.5	31.0	34.4
8:30	25	27.8	23.4	26.5	27.8	31.3	29.8	33.2	28.3	34.0	32.0	35.9
8:45	27.5	30.9	27.2	31.0	31.7	35.6	30.1	34.0	29.2	35.0	34.0	38.7
9:00	29.3	33.2	31.7	36.1	34.7	39.3	32.8	37.4	30.0	37.4	35.8	41.4
9:15	31	35.1	34.7	39.6	36.2	41.5	33.0	38.2	32.0	41.0	36.7	43.0
9:30	32.8	37.4	35.0	40.5	38.3	44.0	35.2	41.0	35.0	44.7	37.3	44.5
9:45	35	40.2	35.9	42.0	39.7	46.1	39.1	45.2	36.3	47.3	38.2	46.1
10:00	36	42	36.4	43.2	40.2	47.7	39.8	46.3	37.0	49.8	39.4	48.3
10:15	37.9	44.8	38.0	45.3	41.3	49.8	40.9	47.7	38.5	52.6	40.5	50.0
10:30	40	47.5	40.0	48.5	42.8	52.0	41.3	49.0	40.0	55.2	41.9	52.2
10:45	41	49	41.9	51.1	44.2	54.1	42.8	50.8	40.6	57.0	43.1	53.9
11:00	42.9	51.3	43.5	53.4	45.5	56.0	44.0	52.5	43.0	59.0	44.0	55.1
11:15	44.9	54.1	44.3	54.8	46.8	58.2	45.8	55.0	44.0	61.0	45.2	56.8
11:30	45.5	55.5	46.5	58.0	48.5	60.2	47.0	57.0	45.0	62.2	46.0	58.4
11:45	45.6	56.7	48.3	60.4	49.6	61.5	48.4	58.8	46.3	64.0	46.5	60.0
12:00	48	59.4	49.6	62.5	50.7	63.2	50.0	61.1	47.0	65.5	47.0	62.5
12:15	50	61.8	50.7	64.2	51.5	64.5	52.1	63.6	48.0	66.0	48.0	63.8
12:30	51.5	63.9	51.3	65.5	53.1	66.4	54.0	66.0	48.3	66.2	48.5	64.7
12:45	53	65.2	52.8	67.5	54.3	67.9	55.8	68.5	49.2	67.0	49.5	66.0
13:00	54	66.2	53.4	68.2	55.0	69.1	57.0	69.7	50.4	67.2	50.6	67.0
13:15	55	66	54.0	68.5	56.1	70.2	57.5	69.0	51.0	67.5	51.5	67.5
13:30	55.5	65.5	54.4	68.4	55.9	69.1	56.0	67.0	51.3	67.0	52.0	66.5
13:45	56	65.7	54.5	68.0	55.0	67.3	55.5	65.3	51.0	66.0	51.6	65.5
14:00	56.2	65	54.6	67.4	52.5	64.2	53.1	62.0	50.5	65.0	51.0	64.2
14:15	55.6	63.9	54.0	66.2	50.1	61.3	51.5	60.0	50.0	64.1	49.5	62.0
14:30	53.2	60.9	53.2	64.5	49.6	59.5	50.0	58.0	49.6	63.2	49.0	60.4
14:45	51.3	57.7	52.5	63.0	48.7	57.9	48.2	55.7	48.8	61.7	48.0	57.8
15:00	49.9	55.4	51.2	60.8	47.8	55.6	46.1	52.8	47.2	59.0	46.8	56.1
15:15	49	53.4	50.0	58.7	46.7	53.9	44.8	50.7	46.9	57.5	45.0	52.4
15:30	48.3	52.1	48.5	55.2	45.6	51.6	43.5	48.7	46.0	55.7	43.0	49.6
15:45	48	51	46.5	52.4	44.1	49.3	42.1	46.6	42.5	54.0	40.0	45.8
16:00	46	48.5	44.7	49.0	42.5	47.0	40.5	44.6	40.0	50.0	39.4	44.4

C.2 Efficiency (%) of the collector and solar irradiance ( $W/m^2$ )

Time	10 <sup>th</sup> March		12 <sup>th</sup> March		15 <sup>th</sup> March		16 <sup>th</sup> March		26 <sup>th</sup> March		28 <sup>th</sup> March	
	$\eta_{th}$	$G_T$	$\eta_{th}$	$G_T$	$\eta_{th}$	$G_T$	$\eta_{th}$	$G_T$	$\eta_{th}$	$G_T$	$\eta_{th}$	$G_T$
8:00	29.3	375	29.3	300	29.6	354	26.1	385	30.9	275	30.4	400
8:15	30.7	410	29.9	350	32.0	380	27.9	420	32.3	350	31.7	450
8:30	31.9	460	31.9	407	35.8	410	28.5	499	34.8	480	32.7	499
8:45	34.9	510	34.6	460	37.6	435	30.8	530	35.6	540	33.4	589
9:00	36.5	560	36.9	499	38.6	499	32.2	598	36.3	600	36.4	644
9:15	37.7	570	38.2	537	39.7	560	33.8	645	39.3	624	38.8	680
9:30	40.8	590	39.4	585	41.0	582	35.8	678	41.7	683	41.3	730
9:45	42.6	640	41.2	620	43.3	620	37	690	44.4	726	42.9	771
10:00	46.2	680	42.7	667	45.5	691	38	717	47.9	783	46.6	800
10:15	48.8	740	43.1	710	47.1	756	38.5	740	48.6	833	47.4	840
10:30	49.9	787	45.6	781	48.4	797	40.9	788	49.8	863	49.6	870
10:45	50.8	825	46.3	833	50.3	824	41.9	800	50.3	888	50.8	891
11:00	51.1	861	47.6	872	52.0	846	43.4	820	52.4	928	51.7	900
11:15	53.1	908	49.2	894	53.9	886	46.2	835	56.5	946	53.6	907
11:30	54.6	960	51.3	940	54.7	896	49.5	847	56.6	955	56.2	925
11:45	59.1	983.	53.4	949	55.4	900	50.7	860	57.6	965	60.6	934
12:00	59.7	1000	55.8	969	56.8	922	52.3	890	59.5	977	66.3	980
12:15	62.0	997	57.4	985	57.3	950	53.5	900	61.3	985	66.9	990
12:30	65.4	993	61.3	971.3	57.7	965	54.7	920	62.2	995	67.9	999
12:45	65.6	974	63.6	967.7	58.1	980	57.2	930	63.2	997	68.5	1010
13:00	67.3	950	64.7	958.2	59.4	995	58.5	910	64	990	68.8	999
13:15	63.7	904	64.0	948.8	62.9	940	55.4	870	64.8	971	68.1	985
13:30	59.5	880	62.9	932.4	63.8	867	54	853	62.8	880	66.7	911
13:45	58.2	873	62.2	909.1	63.2	815	53.7	764.8	57.8	875	66.6	875
14:00	55.9	824	61.1	877.9	62.1	790	50.5	737.8	54.5	880	65.6	843
14:15	55.3	786	60.6	843.8	61.7	761	49.6	717.5	53.9	822	65.5	800
14:30	54.4	742	58.2	812.9	59.0	703	47.7	702.9	51.5	774	62.4	765
14:45	50.2	668	57.3	768	58.1	664	47.6	660.6	50.2	689	58.7	700
15:00	48.0	600	56.6	711.1	57.0	573	47.1	594.6	48.2	667	56.1	695
15:15	42.3	545	55.0	662.8	56.6	533	46	535.7	46.4	608	52.6	590
15:30	37.9	525	52.0	540	52.2	482	45.3	483.5	43.8	557	48.2	574
15:45	32.7	481	51.0	485	51.8	421	43.8	434.7	41.5	493	46.1	527
16:00	31	422	45	400	48.5	389	44	388.6	40	440	42.6	492

### C.3 Greenhouse Heating Load (kW) and Heat Supply (kW)

Time	10 <sup>th</sup> March		12 <sup>th</sup> March		15 <sup>th</sup> March		16 <sup>th</sup> March		26 <sup>th</sup> March		28 <sup>th</sup> March	
	Qu	QR	Qu	QR	Qu	QR	Qu	QR	Qu	QR	Qu	QR
8:00	2.0	9.7	2.6	9.3	3.2	8.9	3.8	8.3	3.7	7.9	4.1	7.2
8:15	2.3	9.4	3.0	9.1	3.4	8.6	4.0	8.2	3.9	7.5	4.4	6.9
8:30	3.0	9.2	3.5	8.8	4.4	8.3	4.4	8.2	4.0	7.2	4.7	6.6
8:45	3.8	9.0	4.5	8.5	5.4	8.1	4.7	8.1	4.4	6.9	5.3	6.3
9:00	4.4	8.5	5.3	8.2	6.0	7.8	5.2	8.0	4.5	6.3	5.3	6.0
9:15	5.0	8.3	6.0	7.9	6.7	7.5	5.4	7.9	5.1	6.0	5.4	5.7
9:30	5.5	8.1	6.4	7.4	6.5	7.3	5.6	7.8	5.4	5.7	5.4	5.4
9:45	5.9	7.9	6.5	7.1	6.5	6.5	6.7	7.6	5.4	5.4	0.0	5.2
10:00	6.4	7.7	6.9	6.8	0.0	6.3	6.9	7.5	0.0	5.1	0.0	4.9
10:15	6.6	7.5	0.0	6.5	0.0	6.0	7.0	7.4	0.0	4.4	0.0	4.3
10:30	6.9	7.3	0.0	6.2	0.0	5.8	7.2	7.2	0.0	4.2	0.0	4.1
10:45	6.7	7.2	0.0	5.9	0.0	5.5	0.0	6.6	0.0	3.9	0.0	3.9
11:00	6.8	7.0	0.0	5.6	0.0	5.3	0.0	6.5	0.0	3.7	0.0	3.7
11:15	6.5	6.9	0.0	5.3	0.0	5.1	0.0	6.4	0.0	3.4	0.0	3.5
11:30	6.4	6.8	0.0	5.0	0.0	4.9	0.0	6.2	0.0	3.2	0.0	3.3
11:45	6.7	6.7	0.0	4.8	0.0	4.4	0.0	6.0	0.0	2.8	0.0	3.2
12:00	0.0	6.6	0.0	4.5	0.0	4.2	5.3	5.9	0.0	2.6	0.0	3.1
12:15	0.0	6.5	0.0	4.3	0.0	4.0	5.6	5.7	0.0	2.4	0.0	2.7
12:30	0.0	6.4	0.0	4.1	0.0	3.9	5.7	5.5	0.0	2.3	0.0	2.6
12:45	0.0	6.4	0.0	4.0	3.4	3.8	0.0	5.0	0.0	2.1	0.0	2.6
13:00	0.0	6.3	0.0	3.9	3.5	3.7	0.0	4.9	0.0	1.9	0.0	2.5
13:15	0.0	6.3	0.0	3.7	3.7	3.6	0.0	4.7	0.0	1.8	0.0	2.4
13:30	0.0	6.3	0.0	3.6	0.0	3.4	0.0	4.5	0.0	1.7	0.0	2.3
13:45	0.0	6.3	3.4	3.6	0.0	3.3	0.0	4.4	0.0	1.6	0.0	2.3
14:00	0.0	6.3	3.7	3.5	0.0	3.2	0.0	4.2	0.0	1.5	0.0	2.3
14:15	5.4	6.3	0.0	3.5	0.0	3.1	0.0	4.1	0.0	1.5	0.0	2.3
14:30	5.7	6.4	0.0	3.4	0.0	3.1	0.0	4.0	0.0	1.4	0.0	2.3
14:45	6.4	6.5	0.0	3.5	0.0	3.1	0.0	3.8	0.0	1.4	0.0	2.3
15:00	6.7	6.6	0.0	3.5	0.0	3.1	0.0	3.7	0.0	1.4	0.0	2.4
15:15	0.0	6.7	0.0	3.6	0.0	3.1	0.0	3.6	0.0	1.4	0.0	2.4
15:30	0.0	6.8	0.0	3.7	0.0	3.2	0.0	3.5	0.0	1.4	0.0	2.5
15:45	0.0	6.9	0.0	3.8	0.0	3.2	0.0	3.4	0.0	1.5	0.0	2.6
16:00	0.0	7.0	0.0	4.0	0.0	3.3	0.0	3.3	0.0	1.6	0.0	2.7

C.4 Values of  $F_R(\tau\alpha)$ ,  $F_R(U_L)$ , and  $R^2$

Day	$F_R(\tau\alpha)$	$F_R(U_L)$	$R^2$
10 <sup>th</sup> March	0.668	-8.5656	0.9569
12 <sup>th</sup> March	0.621	-5.722	0.9628
15 <sup>th</sup> March	0.622	-6.0321	0.8907
16 <sup>th</sup> March	0.551	-8.107	0.5604
26 <sup>th</sup> March	0.65	-15.176	0.894
28 <sup>th</sup> March	0.679	-11.02	0.4816



**زانكۆی پۆلیتیه كنیکی ههولیر**  
**ERBIL POLYTECHNIC UNIVERSITY**

**شیکاری توانای گهرمی پلیتی ته ختی کوکهرهوهی ووزهی خور بو سیستمی گهرم کردنی ژوریکی**

**کشتوکائی به به کارهینانی شلهی نانۆ**

تیزیکه

پیشکەشی ئەنجومەنی کۆلیژی ئەندازیاری تەکنیکی ههولیر کراوه له زانکۆی پۆلیتیه كنیکی ههولیر له بهشیکي جیهه جیکردنی مهرجهکان بو پروانامهی ماستەر له ئەندازیاری میکانیک و ووزه

□ له لایهن

□ ژيان فائق حسن

به کالۆریۆس له ئەندازیاری سارد کردنهوه و ههواسازی

به سههه پهریشتاری

**د. بانپالانو یعقوب**

□ ههولیر- کوردیستان

ئەیلوول ۲۰۲۲



## پوخته

بهره‌مه رووه‌کيه‌کان له ژوره کشتوکالیه‌کان ده‌چینرین بو به‌رزکردنه‌وهی کوالیتی و پاراستنیا ن له کاریگه‌ریه‌کانی ژینگه‌ی سروشتی وهک سه‌رما و با و باران. له که‌شوه‌ه‌وای مامناوه‌نددا، ووزه زۆرتیرین تیچووی سه‌ره‌کیه له به‌ره‌مه‌هینانی به‌ره‌مه‌ی ژوره کشتوکالیه‌کان. هه‌روه‌ها تیچووی سووته‌مه‌نی به‌ردینی و به‌شه‌کانی تری وزه‌ی باو به‌رده‌وام له به‌رزبوونه‌وه‌دایه. سیسته‌میکی گه‌رم‌که‌روه‌ی گونجاو به‌ نرخیکی گونجاو زۆر گرنگه بو گه‌رم‌کردنی ژوره کشتوکالیه‌کان وه بو دا‌بین‌کردنی بارودۆخیکی گونجاو به‌ درێزایی مانگه سارده‌کان. پلیتی ته‌ختی کوکه‌روه‌ی ووزه‌ی خوژ یه‌کیکه له باشترین چاره‌سه‌ره‌کانی گه‌رم‌کردنه‌وه که ژینگه‌ی دوستتیرینه وه ووزه به‌کارده‌هینیت. له‌م کاردا، شیکاری توانای گه‌رمی پلیتی ته‌ختی کوکه‌روه‌ی ووزه‌ی خوژ بو سیسته‌می گه‌رم‌کردنی ژوریکی کشتوکالی به‌ به‌کارهینانی شله‌ی ناو به‌ شیوه‌ی کرداری و تیوری لیکۆلینه‌وه‌ی له‌سه‌ر کراوه، یه‌که‌م هه‌نگاو به‌ به‌کارهینانی ناو وهک شله‌ی کارکردن و دووه‌م هه‌نگاو به‌کارهینانی ناووشله‌ی ناوی  $Al_2O_3$  به‌ چیری جیاوازی ناوگه‌ردیله‌ی (0.2wt.%, 0.5wt.%, 1wt.%, 1.5wt.%) به‌ تیره‌ی 50 ناوومه‌تر. مۆدیلی هاوشیوه‌کردن به‌ به‌کارهینانی TRNSYS 18 نه‌جام‌دراوه. ده‌ره‌نه‌جامه‌که‌ی به‌ نه‌جامی تاقیکاری پشت‌راسته‌کرایه‌وه. هه‌موو پیکهاته‌کان به‌ ته‌واوی له‌ پرۆگرامی TRNSYS مۆدیل کراون، وه تاقیکردنه‌وه کرداریه‌کان زانیاریه‌کانی نه‌رمه‌کالای مۆدیلیان هه‌لسه‌نگاند. وهک هه‌نگاوی یه‌که‌م، توێژینه‌ومه‌که زۆرتیرین بری وزه‌ی پیویست ده‌خه‌ملینیت که 12.8 کیلووات بووه له ساردترین رۆژی زستاندا (12<sup>th</sup> January 2022)، بو ژوریکی کشتوکالی که ده‌که‌ویته‌ ناوه‌ندی توێژینه‌وه‌ی زانستی له شاری هه‌ولێر، عێراق. پله‌ی گه‌رمی 23 پله‌ی سه‌دی وهک پله‌ی گه‌رمی خالی دیاریکراو له ژوره‌که‌دا هه‌لبژێردرا، که نه‌مه‌ش زۆر گرنگه بو نه‌و تاقیکردنه‌وانه که پیویستن بو په‌ره‌پیدانی زۆربه‌ی رووه‌که‌کان. نه‌م لیکۆلینه‌وه‌یه ستانداردی ASHRAE په‌یره‌و کردوه. سه‌رنجراکیشتیرین دۆزینه‌وه نه‌وه بوو که کاتیک ناووشله‌کان وهک شله‌ی کارکردن به‌کارهینا، زیادبوونی کارایی گه‌ورمه‌تر بوو له به‌کارهینانی ته‌نها ناو، ته‌نانه‌ت به‌ چیریکی که‌می ناوگه‌ردیله‌کان. نه‌جامه تاقیکاریه‌کان ده‌ریانخست که به‌کارهینانی

نانوشلهی ئاوی  $Al_2O_3$  به چربی 0.2wt.% توانای کۆکهرهوهی به ریزهی 9.9% زیاد دهکات به بهراورد به ئاو. سههرهرای ئهوه، ئهنجامهکانی هاوشیوهکردن ئاماژه بهوه دهکمن که زۆرتین کارایی کۆکهرهوه بهدهست هاتوه، که 83.6% بوو، کاتیک 1wt.% نانوشله له FPSC بهکارهات، که کارایی کۆکهرهوهی به ریزهی 26.1% زیادیکرد به بهراورد به کهیسی ئاو. ههر زیادبوونیکی زیاده له ریزهی سهدی نانۆگهردیلهکان توانای کۆکهرهوه کهمهکاتهوه. به کورتی، ئهنجامهکان دهریدهخن که له ساردترین مانگهکانی سالد، سیستهمهکه دهتوانیت پلهی گهرمی ههواي ناوهوهی ژوره که بهرز بکاتهوه، که ئهمهش گونجاوه بۆ بهکارهینانی کشتوکال و ژینگه پیس ناکات. ههروهها دهرکهوت که بهکارهینانی نانوشله شلهیهکی کارکردنی قازانج بهخشه که تیچووی سیستهمی گهرمکردنهوه کهمهکاتهوه. سههرهرای ئهوهش، به زیادکردنی شلهی نانۆ وهک شلهی کارکردن سیستهمهکه دهتوانیت وزهی زیاتر بهرهم بهینیت و ههلیبگریت.

